

1 FLUXNET-CH4: A global, multi-ecosystem dataset and analysis 2 of methane seasonality from freshwater wetlands

3

4 Kyle B. Delwiche¹, Sara Helen Knox², Avni Malhotra¹, Etienne Fluet-Chouinard¹, Gavin
5 McNicol¹, Sarah Feron^{1,3}, Zutao Ouyang¹, Dario Papale^{4,5}, Carlo Trotta⁵, Eleonora Canfora⁵,
6 You-Wei Cheah⁶, Danielle Christianson⁶, MMa. Carmelita R. Alberto⁷, Pavel Alekseychik⁸,
7 Mika Aurela⁹, Dennis Baldocchi¹⁰ Baldocchi¹, Sheel Bansal¹¹, David P. Billesbach¹², Gil
8 Bohrer¹³

9 Rosvel Bracho¹⁴, Nina Buchmann¹⁵, David I. Campbell¹⁶, Gerardo Celis¹⁷, Jiquan Chen¹⁸,
10 Weinan Chen¹⁹, Housen Chu²⁰ Chu², Higo J. Dalmagro²¹, Sigrid Dengel⁶, Ankur R. Desai²²,
11 Matteo Detto²³, Han Dolman²⁴, Elke Eichelmann²⁵, Eugenie Euskirchen²⁶, Daniela Famulari²⁷,
12 Thomas Friberg²⁸, Kathrin Fuehs²⁹ Fuehs²⁸, Mathias Goeckede³⁰ Goeckede²⁹, Sébastien
13 Gogo³¹ Gogo³, Mangaliso J. Gondwe³² Gondwe³¹, Jordan P. Goodrich¹⁶, Pia
14 Gottschalk³³ Gottschalk³², Scott L. Graham³⁴ Graham³³, Martin Heimann³⁰ Heimann²⁹, Manuel
15 Helbig^{35,36} Helbig^{34,35}, Carole Helfter³⁷ Helfter³⁶, Kyle S. Hemes^{10,38} Hemes^{1,37}, Takashi
16 Hirano³⁹ Hirano³⁸, David Hollinger⁴⁰ Hollinger³⁹, Lukas Hörtnagl¹⁵, Hiroki Iwata⁴¹ Iwata⁴, Adrien
17 Jacotot³¹, Joachim Jansen⁴² Jacotot³, Gerald Jurasinski⁴³ Jurasinski⁴¹, Minseok Kang⁴⁴ Kang⁴²,
18 Kuno Kasak⁴⁵ Kasak⁴³, John King⁴⁶ King⁴⁴, Janina Klatt⁴⁷ Klatt⁴⁵, Franziska Koebse⁴³ Koebse⁴¹,
19 Ken W. Krauss⁴⁸ Krauss⁴⁶, Derrick Y.F. Lai⁴⁹ Lai⁴⁷, Annalea Lohila^{9,48}, Ivan
20 Mammarella⁵⁰ Mammarella⁴⁸, Giovanni Manea⁵¹ Manca⁴⁹, Luca Beletti Marchesini⁵² Marchesini⁵,
21 Jaclyn Hatala Matthes⁵³ Matthes⁵¹, Trofim Maximon⁵⁴ Maximon⁵², Lutz Merbö⁵⁵ Merbö⁵³,
22 Bhaskar Mitra⁵⁶ Mitra⁵⁴, Timothy H. Morin⁵⁷ Morin⁵⁵, Eiko Nemitz³⁷ Nemitz³⁶, Mats B.
23 Nilsson⁵⁸ Nilsson⁵⁶, Shuli Niu¹⁹, Walter C. Oechel⁵⁹ Oechel⁵⁷, Patricia Y. Oikawa⁶⁰ Oikawa⁵⁸,
24 Keisuke Ono⁶¹ Ono⁵⁹, Matthias Peichl⁵⁸ Peichl⁵⁶, Olli Peltola⁹, Michele L. Reba⁶² Reba⁶, Andrew
25 D. Richardson^{63,64} Richardson^{61,62}, William Riley⁶, Benjamin R. K. Runkle⁶⁵ Runkle⁶³, Youngryel
26 Ryu⁶⁶ Ryu⁶⁴, Torsten Sachs³³ Sachs³², Ayaka Sakabe⁶⁷ Sakabe⁶⁵, Camilo Rey Sanchez¹⁰ Sanchez¹,
27 Edward A. Schuur⁶⁸ Schuur⁶⁶, Karina V.R. Schäfer⁶⁹ VR Schäfer⁶⁷, Oliver
28 Sonnentag⁷⁰ Sonnentag⁶⁸, Jed P. Sparks⁷¹ Sparks⁶⁹, Ellen Stuart-Haëntjens⁷² Haëntjens⁷, Cove
29 Sturtevant⁷³ Sturtevant⁷¹, Ryan C. Sullivan⁷⁴ Sullivan⁷², Daphne J. Szutu¹⁰ Szutu¹, Jonathan E.
30 Thom⁷⁵ Thom⁷³, Margaret S. Torn⁶, Eeva-Stiina Tuittila⁷⁶ Tuittila⁷⁴, Jessica Turner⁷⁷ Turner⁷⁵,
31 Masahito Ueyama⁷⁸ Ueyama⁷⁶, Alex C. Valach¹⁰ Valach¹, Rodrigo Vargas⁷⁹ Vargas⁷⁷, Andrej
32 Varlagin⁸⁰ Varlagin⁷⁸, Alma Vazquez-Lule⁷⁹ Lule⁷⁷, Joseph G. Verfaillie¹⁰ Verfaillie¹, Timo
33 Vesala⁵⁰ Vesala⁴⁸, George L. Vourlitis⁸¹ Vourlitis⁷⁹, Eric J. Ward¹⁴⁸ Ward⁴⁶, Christian
34 Wille³³ Wille³², Georg Wohlfahrt⁸² Wohlfahrt⁸, Guan Xhuan Wong⁸³ Wong⁸¹, Zhen
35 Zhang⁸⁴ Zhang⁸², Donatella Zona^{59,85} Zona^{57, 83}, Lisamarie Windham-Myers⁸⁶ Myers⁸⁴, Benjamin
36 Poulter⁸⁷ Poulter⁸⁵, Robert B. Jackson^{1,38,88 37, 86}

37

38

39

40

41

42

43

44

¹ Department of Earth System Science, Stanford University, Stanford, California

² Department of Geography, The University of British Columbia, Vancouver, British Columbia, Canada

³ Department of Physics, University of Santiago de Chile, Santiago, Chile

⁴ Dipartimento per la Innovazione nei Sistemi Biologici, Agroalimentari e Forestali, Università degli Studi della Toscana, Largo dell'Università, Viterbo, Italy e Forestali, Università

45 ⁵ euroMediterranean Center on Climate Change CMCC, Lecce, Italy
46 ⁶ Earth and Environmental Sciences Area, Lawrence Berkeley National Lab, Berkeley, California
47 ⁷ International Rice Research Institute, Los Banos, Laguna, Philippines
48 ⁸ Natural Resources Institute Finland (LUKE), Helsinki, Finland
49 ⁹ Finnish Meteorological Institute, PO Box 501, 00101 Helsinki, Finland
50 ¹⁰ Department of Environmental Science, Policy and Management, University of California, Berkeley, CA, USA
51 ¹¹ U.S. Geological Survey, Northern Prairie Wildlife Research Center, 8711 37th St Southeast, Jamestown, ND
52 58401 USA
53 ¹² University of Nebraska-Lincoln, Department of Biological Systems Engineering, Lincoln, NE 68583, USA
54 ¹³ Department of Civil, Environmental & Geodetic Engineering, Ohio State University
55 ¹⁴ School of Forest Resources and Conservation, University of Florida, Gainesville FL, 32611
56 ¹⁵ Department of Environmental Systems Science, Institute of Agricultural Sciences, ETH Zurich, 8092 Zurich,
57 Switzerland
58 ¹⁶ School of Science, University of Waikato, Hamilton, New Zealand
59 ¹⁷ Agronomy Department, University of Florida, Gainesville FL, 32601
60 ¹⁸ Department of Geography, Environment, and Spatial Sciences, Michigan State University, East Lansing, MI
61 48823, USA
62 ¹⁹ Institute of Geographic Sciences and Natural Resources Research, Chinese Academy of Sciences, Beijing 100101,
63 PR China.
64 ²⁰ Climate and Ecosystem Sciences Division, Lawrence Berkeley National Lab, Berkeley, CA 94702, USA
65 ²¹ Universidade de Cuiaba, Cuiaba, Mato Grosso, Brazil
66 ²² Dept of Atmospheric and Oceanic Sciences, University of Wisconsin-Madison, Madison, WI 53706 USA
67 ²³ Department of Ecology and Evolutionary Biology, Princeton University, Princeton NJ, USA
68 ²⁴ Department of Earth Sciences, Vrije Universiteit, Amsterdam, Netherlands
69 ²⁵ School of Biology and Environmental Science, University College Dublin, Ireland
70 ²⁶ University of Alaska Fairbanks, Institute of Arctic Biology, Fairbanks, AK, USA
71 ²⁷ C NR - institute for Mediterranean Agricultural and Forest Systems, Piazzale Enrico Fermi, 1 -Portici (Napoli)
72 Italy
73 ²⁸ University of Copenhagen, Department of Geosciences and Natural Resource Management
74 ²⁹²⁸ Institute of Meteorology and Climate Research - Atmos. Environ. at Atmospheric Environmental Research,
75 Karlsruhe Institute of Technology (KIT Campus Alpin), 82467 Garmisch-Partenkirchen, Germany
76 ³⁰²⁹ Max Planck Institute for Biogeochemistry, Jena, Germany
77 ³¹³⁰ ISTO, Université d'Orléans, CNRS, BRGM, UMR 7327, 45071, Orléans, France
78 ³²³¹ Okavango Research Institute, University of Botswana, Maun, Botswana.
79 ³³³² GFZ German Research Centre for Geosciences, Telegrafenberg, 14473 Potsdam, Germany
80 ³⁴³³ Manaaki Whenua - Landcare Research, Lincoln, NZ
81 ³⁵³⁴ Université de Montréal, Département de géographie, Université de Montréal, Montréal, QC H2V 0B3,
82 ³⁶³⁵ Canada & Dalhousie University, Department of Physics and Atmospheric Science, Halifax, NS B2Y 1P3,
83 Canada
84 ³⁷³⁶ UK Centre for Ecology and Hydrology, Edinburgh, UK
85 ³⁸³⁷ Woods Institute for the Environment, Stanford University, Stanford, California
86 ³⁹³⁸ Research Faculty of Agriculture, Hokkaido University, Sapporo, Japan
87 ⁴⁰³⁹ Northern Research Station, USDA Forest Service, Durham, NH 03824, USA
88 ⁴¹⁴⁰ Department of Environmental Science, Faculty of Science, Shinshu University
89 ⁴² Stockholm University, Department of Geological Sciences
90 ⁴³⁴¹ University of Rostock, Rostock, Germany
91 ⁴⁴⁴² National Center for Agro Meteorology, Seoul, South Korea
92 ⁴⁵⁴³ Department of Geography, University of Tartu, Vanemuise st 46, Tartu, 51410, Estonia
93 ⁴⁶⁴⁴ Department of Forestry and Environmental Resources, North Carolina State University, Raleigh, NC, USA
94 ⁴⁷⁴⁵ Vegetation Ecology, Institute of Ecology and Landscape, Department Landscape Architecture, Weißenstephan-
95 Triesdorf University of Applied Sciences, Am Hofgarten 1, 85354 Freising, Germany
96 ⁴⁸ USGS⁴⁶ U.S. Geological Survey, Wetland and Aquatic Research Center, Lafayette LA
97 ⁴⁹⁴⁷ Department of Geography and Resource Management, The Chinese University of Hong Kong, Shatin, New
98 Territories, Hong Kong SAR, China
99 ⁵⁰⁴⁸ Institute for Atmospheric and Earth System Research/Physics, Faculty of Science, University of Helsinki,
100 Helsinki, Finland

Formatted: Font: 14 pt

Formatted: Not Superscript/ Subscript

- 101 ⁵⁴⁴⁹ European Commission, Joint Research Centre (JRC), Ispra, Italy.
- 102 ⁵²⁵⁰ Dept. of Sustainable Agro-Ecosystems and Bioresources, Research and Innovation Centre, Fondazione Edmund
- 103 Mach, San Michele all'Adige, Italy
- 104 ⁵³⁵¹ Department of Biological Sciences, Wellesley College, Wellesley, MA 02481, USA
- 105 ⁵⁴⁵² Institute for Biological Problems of the Cryolithozone, RAS, Yakutsk, REp. Yakutia.
- 106 ⁵⁵⁵³ Mazingira Centre, International Livestock Research Institute (ILRI), Old Naivasha Road, PO Box 30709, 00100
- 107 Nairobi, Kenya
- 108 ⁵⁶⁵⁴ Northern Arizona University, School of Informatics, Computing and Cyber Systems
- 109 ⁵⁷⁵⁵ Environmental Resources Engineering, SUNY College of Environmental Science and Forestry
- 110 ⁵⁸⁵⁶ Dept. of Forest Ecology and Management, Swedish University of Agricultural Sciences, 901 83 Umeå, Sweden
- 111 ⁵⁹⁵⁷ Dept. Biology, San Diego State University, San Diego, CA 92182, USA
- 112 ⁶⁰⁵⁸ Department of Earth and Environmental Sciences, Cal State East Bay, Hayward CA 94542 USA
- 113 ⁶⁴⁵⁹ National Agriculture and Food Research Organization, Tsukuba, Japan
- 114 ⁶²⁶⁰ USDA-ARS Delta Water Management Research Unit, Jonesboro, Arkansas 72401, United States
- 115 ⁶³⁶¹ School of Informatics, Computing & Cyber Systems, Northern Arizona University, Flagstaff, AZ 86011, USA
- 116 ⁶⁴⁶² Center for Ecosystem Science and Society, Northern Arizona University, Flagstaff, AZ 86011, USA
- 117 ⁶⁵⁶³ Department of Biological & Agricultural Engineering, University of Arkansas, Fayetteville, Arkansas 72701,
- 118 United States
- 119 ⁶⁶⁶⁴ Department of Landscape Architecture and Rural Systems Engineering, Seoul National University, South Korea
- 120 ⁶⁷⁶⁵ Hakubi center, Kyoto University, Kyoto, Japan
- 121 ⁶⁸⁶⁶ Department of Biological Sciences, Northern Arizona University, Flagstaff, AZ, USA
- 122 ⁶⁹⁶⁷ Dept of Earth and Environmental Science, Rutgers University Newark, NJ
- 123 ⁷⁰⁶⁸ Université de Montréal, Département de géographie, Université de Montréal, Montréal, QC H2V 0B3, Canada
- 124 ⁷⁴⁶⁹ Department of Ecology and Evolution, Cornell
- 125 ⁷² ~~USGS~~⁷⁰ U.S. Geological Survey, California Water Science Center, 6000 J Street, Placer Hall, Sacramento, CA,
- 126 95819
- 127 ⁷³⁷¹ National Ecological Observatory Network, Battelle, 1685 38th St Ste 100, Boulder, Colorado, 80301, USA
- 128 ⁷⁴⁷² Environmental Science Division, Argonne National Laboratory, Lemont, IL, USA
- 129 ⁷⁵⁷³ Space Sciences and Engineering Center, University of Wisconsin-Madison, Madison, WI 53706 USA
- 130 ⁷⁶⁷⁴ School of Forest Sciences, University of Eastern Finland, Joesnuu, Finland
- 131 ⁷⁷⁷⁵ Freshwater and Marine Science, University of Wisconsin-Madison
- 132 ⁷⁸⁷⁶ Graduate School of Life and Environmental Sciences, Osaka Prefecture University
- 133 ⁷⁹⁷⁷ Department of Plant and Soil Sciences, University of Delaware, Newark, DE, USA
- 134 ⁸⁰⁷⁸ A.N. Severtsov Institute of Ecology and Evolution, Russian Academy of Sciences
- 135 ⁸⁴⁷⁹ California State University San Marcos, San Marcos, CA, USA
- 136 ⁸²⁸⁰ University of Innsbruck, Department of Ecology, Sternwartestr. 15, 6020 Innsbruck, AUSTRIA
- 137 ⁸³⁸¹ Sarawak Tropical Peat Research Institute, Sarawak, Malaysia
- 138 ⁸⁴⁸² Department of Geographical Sciences, University of Maryland, College Park, MD 20740, USA
- 139 ⁸⁵⁸³ Department of Animal and Plant Sciences, University of Sheffield, Western Bank, Sheffield, S10 2TN, United
- 140 Kingdom
- 141 ⁸⁶ ~~USGS~~⁸⁴ U.S. Geological Survey, Water Mission Area, 345 Middlefield Road, Menlo Park, CA, 94025
- 142 ⁸⁷⁸⁵ Biospheric Sciences Laboratory, NASA Goddard Space Flight Center, Greenbelt, Maryland
- 143 ⁸⁸⁸⁶ Precourt Institute for Energy, Stanford University, Stanford, California

Formatted: Not Superscript/ Subscript

- 144
- 145
- 146
- 147 *Correspondence to:* Kyle B. Delwiche (delwiche@stanford.edu)

Formatted: Superscript

148

149 **Abstract.** Methane (CH₄) emissions from natural landscapes constitute roughly half of global CH₄ contributions to

150 the atmosphere, yet large uncertainties remain in the absolute magnitude and the seasonality of emission quantities

151 and drivers. Eddy covariance (EC) measurements of CH₄ flux are ideal for constraining ecosystem-scale CH₄

152 emissions, ~~including their seasonality~~, due to quasi-continuous and high temporal resolution of CH₄ flux

153 measurements, coincident ~~measurements of carbon dioxide~~, water, and energy ~~fluxes~~flux measurements, lack of

ecosystem disturbance, and increased availability of datasets over the last decade. Here, we 1) describe the newly published dataset, FLUXNET-CH4 Version 1.0, the first, [open source](#) global dataset of CH₄ EC measurements (available at <https://fluxnet.org/data/fluxnet-ch4-community-product/>). FLUXNET-CH4 includes half-hourly and daily gap-filled and non gap-filled aggregated CH₄ fluxes and meteorological data from 79 sites globally: 42 freshwater wetlands, 6 brackish and saline wetlands, 7 formerly drained ecosystems, 7 rice paddy sites, 2 lakes, and 15 uplands. Then, we 2) evaluate FLUXNET-CH4 representativeness for freshwater wetland coverage globally, because the majority of sites in FLUXNET-CH4 Version 1.0 are freshwater wetlands ~~and because freshwater wetlands which~~ are a substantial source of total atmospheric CH₄ emissions; and 3) provide the first global estimates of the seasonal variability and seasonality predictors of freshwater wetland CH₄ fluxes. Our representativeness analysis suggests that the freshwater wetland sites in the dataset cover global wetland bioclimatic attributes (encompassing energy, moisture, and vegetation-related parameters) in arctic, boreal, and temperate regions, but only sparsely cover humid tropical regions. Seasonality metrics of wetland CH₄ emissions vary considerably across latitudinal bands. In freshwater wetlands (except those between 20° S to 20° N) the spring onset of elevated CH₄ emissions starts three days earlier, and the CH₄ emission season lasts 4 days longer, for each degree C increase in mean annual air temperature. On average, the [spring](#) onset of increasing CH₄ emissions lags soil warming by one month, with very few sites experiencing increased CH₄ emissions prior to the onset of soil warming. In contrast, roughly half of these sites experience the spring onset of rising CH₄ emissions prior to the spring increase in gross primary productivity (GPP). The timing of peak summer CH₄ emissions does not correlate with the timing for either peak summer temperature or peak GPP. Our results provide seasonality parameters for CH₄ modeling, and highlight seasonality metrics that cannot be predicted by temperature or GPP (i.e., seasonality of CH₄ peak). ~~The FLUXNET-CH4 dataset provides an open-access resource for CH₄ flux synthesis, has a range of applications, and is unique in that it includes coupled measurements of important CH₄ drivers such as GPP and temperature. Although FLUXNET-CH4 could certainly be improved by adding more sites in tropical ecosystems and by increasing the number of site-years at existing sites, it~~FLUXNET-CH4 is a powerful new resource for diagnosing and understanding the role of terrestrial ecosystems and climate drivers in the global CH₄ cycle, ~~and future additions of sites in tropical ecosystems and site-years of data collection will provide added value to this database.~~ All seasonality parameters are available at <https://doi.org/10.5281/zenodo.4408468>~~https://doi.org/10.5281/zenodo.4672601~~. Additionally, raw FLUXNET-CH4 data used to extract seasonality parameters can be downloaded from <https://fluxnet.org/data/fluxnet-ch4-community-product/>~~https://fluxnet.org/data/fluxnet-ch4-community-product/~~, and a complete list of the 79 individual site data DOIs is provided in Table 2 in the Data Availability section of this document. ▲

Formatted

184
185
186
187
188

189 1 Introduction

Methane (CH₄) has a global warming potential that is 28 times larger than carbon dioxide (CO₂) on a 100-year time scale (Myhre et al., 2013), and its atmospheric concentration has increased by >1000 ppb since 1800 (Etheridge et al., 1998). While atmospheric CH₄ concentrations are substantially lower than those of CO₂, ~~CH₄'s higher effectiveness at absorbing longwave radiation means that~~ CH₄ has contributed 20-25% as much radiative forcing as CO₂ since 1750 (Etminan et al., 2016). Despite its importance to global climate change, natural CH₄ sources and sinks remain poorly constrained, and with uncertain attribution to the various biogenic and anthropogenic sources (Saunio et al., 2016, 2020). Bottom-up and top-down estimates differ by 154 ~~TGTg/yr~~ (745 ~~vs~~versus 591 ~~TGTg/yr~~, respectively), ~~with~~; much of this difference ~~arising~~arises from natural sources (Saunio et al., 2020). Vegetated wetlands and inland water bodies account for most natural CH₄ emissions, as well as the majority of uncertainty in bottom-up emissions estimates (Saunio et al., 2016). Better diagnosis and prediction of terrestrial CH₄ sources to the

200 atmosphere requires high frequency and continuous measurements of CH₄ [exchanges](#) across a continuum of
201 [ecological](#)-time (hours to years) and space (meters to kilometers) scales.

202 Tower-based eddy covariance (EC) measurements provide ecosystem-scale CH₄ fluxes at high temporal
203 resolution across years, are coupled with measurements of key CH₄ drivers such as temperature, water and recent
204 substrate input (inferred from CO₂ flux), and thus help constrain bottom-up CH₄ budgets and improve CH₄ predictions.
205 Although EC towers began measuring CO₂ fluxes in the late 1970s (Desjardins 1974; Anderson et al., 1984), and
206 some towers began measuring CH₄ in the 1990s (Verma et al., 1992), most CH₄ flux EC measurements began within
207 the last decade. [\(2010s\)](#). Given that many EC CH₄ sites are relatively new, the flux community has only recently
208 compiled them for global synthesis efforts (e.g., Chang et al., in [review](#)) and is still working to standardize CH₄
209 flux measurements and establish gap-filling protocols (Nemitz et al., 2018; Knox et al., 2019). Furthermore, the growth
210 of EC networks for CH₄ fluxes has sometimes taken place in a relatively *ad hoc* fashion, often at sites that were already
211 measuring CO₂ fluxes or where higher CH₄ fluxes were expected, potentially introducing bias. The representativeness
212 and spatial distribution of CH₄ flux tower networks [has](#) been assessed to evaluate its ability to upscale fluxes
213 regionally (Hargrove et al., 2003; Hoffman et al., 2013; Papale et al., 2015; Villarreal et al., 2018, 2019) and globally
214 (Jung et al., 2009; 2020; [Kumar et al., 2016](#)). However, a relatively sparse coverage of CH₄ flux towers prompts the
215 question of how well the current observation network provides a sufficient sampling of global or ecosystem-specific
216 bioclimatic conditions.

217 Broad-scale wetland CH₄ seasonality estimates, such as when fluxes increase, peak, and decrease and the
218 predictors of seasonality, remain relatively unconstrained across wetlands globally. These key seasonality metrics
219 vary considerably across high-emitting systems such as wetlands and other aquatic systems (Desjardins, 1974; Dise,
220 1992; Melloh and Crill 1996; Wik et al., 2013; Zona et al., 2016; Treat et al., 2018). Few continuous CH₄ flux datasets
221 across representative site-years make it difficult to establish trends in seasonal dynamics, though monthly or annually
222 aggregated estimates of CH₄ fluxes from different seasons do exist for high latitudes (Zona et al., 2016; Treat et al.,
223 2018). Seasonal variability in [freshwater](#) wetland CH₄ fluxes is expected to be driven by changes in air and soil
224 temperature, soil moisture (including water table dynamics), and recent carbon substrate availability, which influence
225 the rates of CH₄ production and consumption (Lai, 2009; Bridgman et al., 2013; Dean et al., 2018). Temperature has
226 widely been found to strongly affect CH₄ flux (Chu et al., 2014; Yvon-Durocher et al., 2014; Sturtevant et al., 2016),
227 but the relationship is complex (Chang et al., 2020) and varies seasonally (Koebsch et al., 2015; Helbig et al., 2017).
228 [Methane](#)CH₄ flux is also driven by inundation depth since anoxic conditions are typically necessary for
229 methanogenesis (Lai, 2009; Bridgman et al., 2013), though CH₄ production under bulk-oxic conditions has been
230 observed (Angle et al., 2017). Substrate availability influences CH₄ production potential and is linked with gross
231 primary productivity (GPP) because recent photosynthate fuels methanogenesis though this relationship can vary by
232 ecosystem type, plant functional type and biome (Meron et al., 1999; [Chanton et al., 2008; Hatala et al., 2012; Lai](#)
233 [et al., 2014; Malhotra and Roulet, 2015; Sturtevant et al., 2016](#)); [Chanton et al., 2008; Hatala et al., 2012; Lai et al.,](#)
234 [2014; Malhotra and Roulet, 2015; Sturtevant et al., 2016](#)). In process models, the seasonality of CH₄ emissions from
235 wetlands globally is primarily constrained by inundation (Poulter et al., 2017), with secondary within-wetland
236 influences from temperature and availability of carbon (C) substrates (Melton et al., 2013; Castro-Morales et al.,
237 2018). Bottom-up and top-down global CH₄ estimates continue to disagree on total CH₄ flux magnitudes and
238 seasonality, including the timing of annual peak emissions (Spahni et al., 2011; Saunio et al., 2020). Thus, the
239 variability and predictors of wetland CH₄ seasonality globally remain a knowledge gap that high-frequency and long-
240 term EC data can help fill.

241 Here, we [first](#) describe Version 1.0 of the FLUXNET-CH₄ dataset (available at
242 <https://fluxnet.org/data/fluxnet-ch4-community-product/>). Version 1.0 of the dataset expands and formalizes the
243 publication of data scattered among regional flux networks as described previously in Knox et al., [\(2019\)](#).
244 FLUXNET-CH₄ includes half-hourly and daily gap-filled and non gap-filled aggregated CH₄ fluxes and
245 meteorological data from 79 sites globally: 42 freshwater wetlands, 6 brackish and saline wetlands, 7 formerly drained

Formatted: Subscript

246 ecosystems, 7 rice paddy sites, 2 lakes, and 15 upland ecosystems. [FLUXNET-CH4 includes an additional 2 wetland](#)
247 [sites \(RU-Vrk and SE-St1\), but they are not available under the CC BY 4.0 data policy and thus are excluded from](#)
248 [this analysis](#). Since the majority of sites in FLUXNET-CH4 Version 1.0 ([hereafter referred to solely as “FLUXNET-](#)
249 [CH4”](#)) are freshwater wetlands, [and freshwater wetlands which](#) are a substantial source of total atmospheric CH₄
250 emissions, we use the subset of data from freshwater wetlands to ~~then;~~ ²⁾ evaluate the representativeness of freshwater
251 wetland coverage in the [FLUXNET-CH4](#) dataset relative to wetlands globally, ³⁾ and ³⁾ provide the first assessment of
252 global variability and predictors of freshwater wetland CH₄ flux seasonality. We quantify a suite of CH₄ seasonality
253 metrics and evaluate temperature and GPP (a proxy for recent substrate input) as predictors of seasonality across four
254 latitudinal bands (northern, temperate, subtropical, and tropical). Due to a lack of high-temporal resolution water table
255 data at all sites, our analyses are unable to evaluate the critical role of water table on CH₄ seasonality. Here we provide
256 parameters for better understanding and modeling seasonal variability in freshwater wetland CH₄ fluxes and generate
257 new hypotheses and data resources for future syntheses.

258 2. Methods

259 2.1 FLUXNET-CH4 dataset

260 2.1.1 History and data description

261 The FLUXNET-CH4 dataset was initiated by the Global Carbon Project (GCP) in 2017 to better constrain
262 the global CH₄ budget (<https://www.globalcarbonproject.org/methanebudget/index.htm>). Beginning with a kick off
263 meeting in May 2018 in Washington DC, hosted by Stanford University, we coordinated with the AmeriFlux
264 Management Project, the European Ecosystem Fluxes Database, and the ICOS Ecosystem Thematic Centre (ICOS-
265 ETC) ~~in order~~ to avoid duplication of efforts, as most sites are part of different regional networks (albeit with different
266 data products). We ~~have~~ collected and standardized data for FLUXNET-CH4 with assistance from the regional flux
267 networks, AmeriFlux’s “Year of Methane”, FLUXNET, the EU’s Readiness of ICOS for Necessities of Integrated
268 Global Observations (RINGO) project, and a ~~USGS~~ [U.S. Geological Survey](#) Powell Center working group.
269 FLUXNET-CH4 is a community-led project, so while we developed it with assistance from FLUXNET, we do not
270 necessarily use standard FLUXNET data variables, formats, or methods.

271 FLUXNET-CH4 includes gap-filled half-hourly CH₄ fluxes and meteorological variables. ~~–~~ Gaps in
272 meteorological variables (TA - air temperature, SW_IN - incoming shortwave radiation, LW_IN - incoming longwave
273 radiation, VPD - vapor pressure deficient, PA - pressure, P - precipitation, WS - wind speed) were filled with the
274 ERA-Interim (ERA-I) reanalysis product (Vuichard and Papale, 2015). We used the REddyProc package (Wutzler et
275 al., 2018) to filter flux values with low friction velocity ($u_* > 0.2$) based on relating nighttime u_* , to fill gaps in CO₂, latent
276 heat, and sensible heat fluxes, and to partition net CO₂ fluxes into gross primary production (GPP) and ecosystem
277 respiration (RECO) using both the daytime (Lasslop et al., 2010) and nighttime (Reichstein et al., 2005) approaches
278 ~~in REddyProc~~. [Data gaps of CH₄ flux data gaps](#) were filled using artificial neural network (ANN) methods first
279 described in Knox et al. (2015) and in Knox et al. (2019), and summarized here in Sect. 2.1.2. Gap-filled data for
280 gaps exceeding two months are provided and flagged for quality. Please see Table B1 for variable description and
281 units, as well as quality flag information. For the seasonality analysis in this paper we excluded data from gaps
282 exceeding two months, and we encourage future users of FLUXNET-CH4 to critically evaluate gap-filled values from
283 long data gaps before including them in analyses (Dengel et al., 2013; Kim et al., 2020).

284 In addition to half-hourly data, the FLUXNET-CH4 Version 1.0 release also contains a full set of daily mean
285 values for all parameters except wind direction and precipitation. Daily precipitation is included as the daily sum of
286 the half-hourly data, and daily average wind direction is not included.

287 2.1.2 Gap-filling methods and uncertainty estimates

288 As described in Knox et al. (2015) and in Knox et al. (2019), the ANN routine used to gap-fill the CH₄ data
289 was optimized for generalizability and representativeness. To avoid biasing the ANN toward environmental conditions
290 with typically better data coverage (e.g., summer-time and daytime measurements), the explanatory data were divided
291 into a maximum of 15 clusters using a k-means clustering algorithm. Data used to train, test, and validate the ANN
292 were proportionally sampled from these clusters. For generalizability, the simplest ANN architecture with good
293 performance (<5% gain in model accuracy for additional increases in architecture complexity) was selected for 20
294 extractions of the training, test, and validation data. Within each extraction, each tested ANN architecture was
295 reinitialized 10 times, and the initialization with the lowest root-mean-square-error was selected to avoid local minima.
296 The median of the 20 predictions was used to fill each gap. A standard set of variables available across all sites
297 ~~were~~ used to gap-fill CH₄ fluxes (Dengel et al., 2013), which included the previously mentioned meteorological
298 variables TA, SW_IN, WS, PA, and sine and cosine functions to represent seasonality. These meteorological variables
299 were selected ~~since they are relevant~~ for their relevance to CH₄ exchange and were gap-filled using the ERA-I
300 reanalysis data. Other variables related to CH₄ flux (e.g., water table depth [WTD] and soil temperature [TS]) were
301 not included as explanatory variables as they were not available across all sites or had large gaps that could not be
302 filled using the ERA-I reanalysis data (Knox et al., 2019). The ANN gap-filling was performed using MATLAB
303 (MathWorks 2018, version 9.4.0).

304 While the median of the 20 predictions was used to fill each gap, the spread of the predictions was used to
305 provide a measure of uncertainty resulting from the ANN gap-filling procedure. Specifically, ~~for gap-filled values,~~
306 the combined annual gap-filling and random uncertainty was calculated from the variance of the cumulative sums of
307 the 20 ANN predictions (Knox et al., 2015; Anderson et al., 2016; Oikawa et al., 2017). The (non-cumulative) variance
308 of the 20 ANN predictions was also used to provide gap-filling uncertainty for each half-hourly gap-filled value
309 ~~included in the dataset.~~ While this ~~output~~ is useful for data-model comparisons, it cannot be used to estimate
310 cumulative annual gap-filling error because gap-filling error is not random, which is why the cumulative sums of the
311 20 ANN predictions are used to estimate annual gap-filling error.

312 Random errors in EC fluxes follow a double exponential (Laplace) distribution with the standard deviation
313 varying with flux magnitude (Richardson et al., 2006; Richardson et al., 2012). For half-hourly CH₄ flux
314 measurements, random error was estimated using the residuals of the median ANN predictions, providing a
315 conservative “upper limit” estimate of the random flux uncertainty (Moffat et al., 2007; Richardson et al., 2008). The
316 annual cumulative uncertainty at 95% confidence was estimated by adding the cumulative gap-filling and random
317 measurement uncertainties in quadrature (Richardson and Hollinger, 2007; Anderson et al., 2016). Annual
318 uncertainties in CH₄ flux for individual site-years are provided in Table B7B2. Throughout this paper, we include
319 uncertainties on individual site years when discussing single years of data. In sites with multiple years of data, we
320 report the standard deviation of the multiple years.

321 2.1.3 Dataset structure and site metadata

322 ~~To enable data use by the broader flux community, we have partnered with regional flux networks and~~
323 ~~FLUXNET to provide standardized and gap-filled EC-CH₄ data. FLUXNET-CH4 Version 1.0-CH4~~ contains two
324 comma-separated data files per site at half-hourly and daily resolutions. ~~Half-hourly and daily aggregations which~~
325 are available for download at <https://fluxnet.org/data/fluxnet-ch4-community-product/>, along with a file containing select
326 site metadata. Each site has a unique FLUXNET-CH4 DOI. All ~~site data from the 79 sites used in this analysis~~ are
327 available under CC BY 4.0 (<https://creativecommons.org/licenses/by/4.0/>) copyright license. ~~(FLUXNET-CH4 has an~~
328 ~~additional 2 sites available under the FLUXNET Tier 2 license~~ (<https://fluxnet.org/data/data-policy/>), though these
329 ~~sites are not included in our analysis).~~

330 Metadata (Table B2B3) include site coordinates, ecosystem classification based on site literature,
331 presence/absence and dominance for specific vegetation types, and DOI link, as well as calculated data such as annual
332 and quarterly CH₄ flux values. FLUXNET-CH4 Version 1.0 sites were classified based on site-specific literature as
333 fen, bog, swamp, marsh, salt marsh, lake, mangrove, rice paddy/field, wet tundra, upland, or drained ecosystems that
334 previously could have been wetlands, seasonally flooded pastures, or agricultural areas. To the extent possible, we
335 followed classification systems of previous wetland CH₄ syntheses (Olefeldt et al., 2013; Turetsky et al., 2014; Treat
336 et al., 2018). Drained systems are former wetlands that have subsequently been drained but may maintain a relatively
337 shallow water table, ~~which can contribute to occasional methane emissions, although we do not have specific water~~
338 ~~table depth information at all drained sites.~~ Upland ecosystems are further divided into alpine meadows, grasslands,
339 needleleaf forests, mixed forest, crops, tundra, and urban. Freshwater wetland classifications follow hydrological
340 definitions of bog (ombrotrophic), fen (minerotrophic), wet tundra, marshes and swamps, and were designated as per
341 primary literature on the site. For all sites, vegetation was classified for presence or absence of brown mosses,
342 ~~Sphagnum mosses, (all species from the division Bryophyta except those in the class Sphagnopsida), Sphagnum~~
343 ~~mosses (any species from class Sphagnopsida),~~ ericaceous shrubs, trees (of any height) and aerenchymatous species
344 (mostly Order Poales but includes exceptions). These categories closely follow Treat et al., (2018), except that
345 aerenchymatous species had to be expanded beyond Cyperaceae to incorporate wetlands globally. Presence/absence
346 of vegetation groups was designated based on species lists in primary literature from the site. Out of the vegetation
347 groups present, the dominant (most abundant) group is also reported and is based on ~~data from a survey of information~~
348 ~~provided by~~ lead site investigators.

349 In addition to the variable description table (Table B1) and the site metadata (Table B2B3), we provide
350 several more tables to complement our analysis. Table B3B4 includes the climatic data ~~focused in~~ the
351 representativeness analysis. ~~Seasonality~~ ~~Table 5 provides seasonality~~ parameters for CH₄ flux, air temperature, soil
352 temperature ~~(for sites with multiple probes, Table B4 includes parameters~~ from the probe closest to the ground
353 surface), and GPP ~~are provided in Table B4, with . For sites with multiple soil temperature probes,~~ the full set of soil
354 temperature parameters ~~from all probes are~~ in Table B5. ~~Table B6. Table B7~~ contains the soil temperature probe
355 depths. Table B7B2 contains the annual CH₄ flux and uncertainty. All Appendix B tables are also available at
356 <https://doi.org/10.5281/zenodo.44084684672601>.

357

358 2.1.4 Annual CH₄ fluxes

359 Annual CH₄ fluxes were calculated from gap-filled data for site-years with data gaps shorter than two
360 consecutive months, or for sites above 20° N where >2 month data gaps occurred outside of the highest CH₄-emission
361 months of May 1 through October 31. Since we did not sum gap-filled values for >2 month gaps during the winter,
362 annual sums from these years will be an underestimate since winter fluxes can be important (Zona et al., 2016; Treat
363 et al., 2018). Several sites had less than one year of data, and we report gap-filled CH₄ flux annual sums for sites with
364 between six months and one year of data (BW-Gum = 228 days, CH-Oe2 = 200 days, JP-Swl = 210 days, US-EDN =
365 182 days). While these sums will be an underestimate of annual CH₄ flux since they do not span a full year (and we
366 therefore do not use them in the seasonality analysis), their relative magnitude can still be informative. For example,
367 site JP-SWL is a lake site, and even with less than a year of data the summed CH₄ flux of 66 g C m⁻² is relatively high
368 (Taoka et al., 2020). In addition to sites with short time series, the annual CH₄ sum for site ID-Pag represents 365 days
369 spanning June 2016 to June 2017.

370 2.1.5 Subset analysis on freshwater wetland CH₄ flux

371 In addition to the FLUXNET-CH4-wide description of site class distributions and annual CH₄ fluxes, we
372 also include a subset analysis on freshwater wetlands, given that it is the dominant ecosystem type in our dataset and

Field Code Changed

Formatted: Default Paragraph Font, Underline, Font color: Custom Color(17,85,204)

Formatted: Default Paragraph Font, Underline, Font color: Custom Color(17,85,204)

373 an important global CH₄ source (Saunio et al., 2016). First, we analyze freshwater wetland representativeness, and
374 subsequently the seasonality of their CH₄ emissions. Freshwater wetlands included in the seasonality and
375 representativeness analysis are indicated in Table B2B3, column “IN_SEASONALITY_ANALYSIS”.

376

377 2.2 Wetland representativeness

378 2.2.1 Principal Component Analysis

379 To understand how compare the FLUXNET-CH₄ site distribution of FLUXNET-CH₄ Version 1.0 sites
380 compares withto the global wetland distribution, we evaluated thetheir representativeness of the FLUXNET-CH₄
381 Version 1.0 wetland sites in the entire global wetland cover along four bioclimatic gradients. Only freshwater wetland
382 sites were included in this analysis, with coastal. Coastal sites were excluded because, due to a lack of global gridded
383 datasets, salinity could not be included as an environmental variable despite being, an important control on CH₄
384 production, could not be evaluated across the tower network due to a lack of global gridded salinity data (Bartlett et
385 al., 1987; Poffenbarger et al., 2011)(Bartlett et al., 1987; Poffenbarger et al., 2011). The four bioclimatic variables
386 used were: mean annual air temperature (MAT), latent heat flux (LE), enhanced vegetation index (EVI), and simple
387 ratio water index (SRWI; data sources in Table B3-B4). We use EVI because it is a more direct measurement than
388 GPP from global gridded products and is considered a reasonable proxy for GPP (Sims et al., 2006). Thus, we used
389 EVI instead of GPP. Together, these environmental variables account for, or are, proxies for key controls of CH₄
390 production, oxidation at the surface, and transport (Bridgham et al., 2013). We use a principal components analysis
391 (PCA) to visualize the site distribution across the four environmental drivers at once. For this analysis, we consider
392 the annual average bioclimatic conditions over 2003-2015. In the PCA output, we evaluate the coverage of the 42
393 freshwater sites over 0.25° grid cells containing >5% wetland mean cover in Wetland Area and Dynamics for Methane
394 Modeling (WAD2M; Zhang et al., In-Review), 2020; Zhang et al., 2021) for the same time period.

395 2.2.2 Global Dissimilarity and Constituency Analysis

396 To further identify geographical gaps in the coverage of the FLUXNET-CH₄ Version 1.0 network, we
397 quantified the dissimilarity of global wetlands from the tower network, using a similar approach to that taken for CO₂
398 flux towers (Kumar et al., 2016; Meyer and Pebesma 2020). We calculated the 4-dimensional Euclidean distance from
399 the four bioclimatic variables between every point at the land surface to every tower location at the FLUXNET-CH₄
400 network. We then divided these distances by the average distance between towers to produce a dissimilarity index.
401 Dissimilarity scores <1 represent areas whose nearest tower is closer than the average distance among towers, while
402 areas with scores >1 are more distant. Lastly, we identified the importance of an individual tower in the network by
403 estimating the geographical area to which it is most analogous in bioclimate space. We divided the world's land
404 surface according to closest towers in bioclimatic space. The area to which each tower is nearest is defined as the
405 tower's constituency.

406 2.3 Wetland CH₄ seasonality

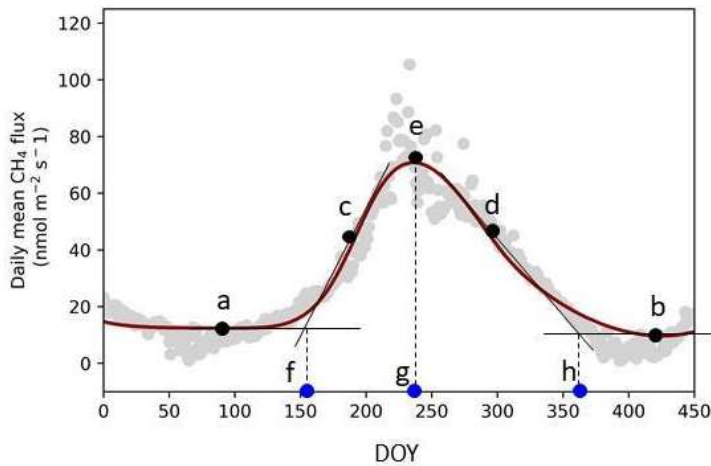
407 To examine freshwater wetland CH₄ seasonality across the global range of sites in FLUXNET-CH₄
408 Version 1.0, we extracted seasonality parameters for CH₄, temperature, and GPP using Timesat, a software package
409 designed to analyze seasonality of environmental systems (Jönsson and Eklundh, 2002; Jönsson and
410 Eklundh, 2004; Eklundh and Jönsson, 2015). Timesat calculates a range of several seasonality parameters, including
411 baseline flux, peak flux, and the slope of spring flux increase and fall decrease (Fig. 1). We also calculate
412 parameters such as amplitude ((“e” peak flux - baseline, which is the average of “a” spring and fall baselines; (“e” -
413 (“a” + “b”)/2) in Fig. 1), and relative peak timing ((“g” - “f”) / (“h” - “f”) in Fig. 1). Timesat uses a double-
414 logistic fitting function to create a series of localized fits centered on data minima and maxima. Localized fits are
415 minimized using a merit function and the Levenberg-Marquardt method (Madsen et al., 2004; Nielsen, 1999).

Formatted: Subscript

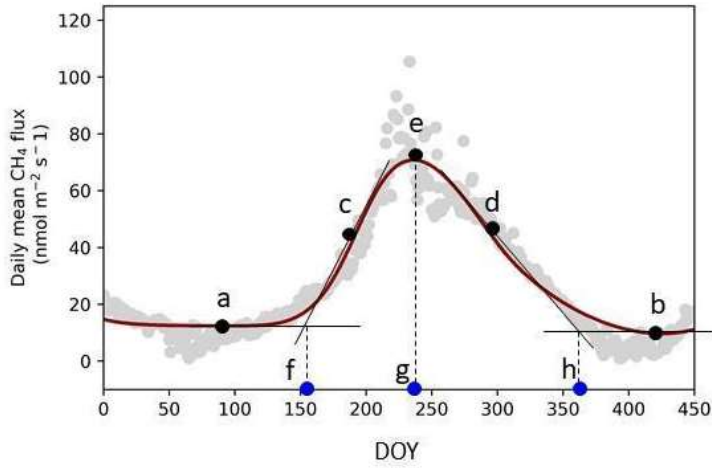
416 These localized fits are then merged using a global function to create a smooth fit over the full time interval. To fit
417 CH₄ time-series in Timesat, we used gap-filled data after removing gaps exceeding two months. We do not report
418 Timesat parameters when large gaps occur during CH₄ emissions spring increase, peak, or fall decrease.

419 We estimate 'start of elevated emissions season' when CH₄ emissions begin to increase in the spring ("f"
420 in Fig. 1), and 'end of elevated emissions season' when the period of elevated CH₄ flux ends in the fall ("h" in Fig.
421 1), as the intercept between the Timesat fitted baseline parameter and shoulder-season slope (similar to Gu et al.,
422 2009). To extract seasonality parameters with Timesat, sites need a sufficiently pronounced seasonality, a
423 sufficiently long time period, and minimal data gaps (we note that while Timesat is capable of fitting two peaks per
424 year, all the freshwater wetland sites have a single annual peak). We excluded site-years in restored wetlands when
425 wetlands were still under construction. We were able to fit 36 of the 42 freshwater wetland sites using Timesat,
426 within FLUXNET-CH₄ Version 1.0, 36 had sufficient data series to extract seasonality parameters. These 36
427 wetlands had 141 site-years of data, using total, which we fit with the double-logistic fitting method which followed
428 site data well (representative examples in Fig. 2). For extratropical sites in the Southern Hemisphere, we shifted all
429 data by 182 days so that maximum solar insolation seasonality would be congruent across the globe.

430 We also used Timesat to extract seasonality metrics for GPP, partitioned using the daytime-based approach
431 (Lasslop et al., 2010) (GPP_DT), air temperature (TA), and soil temperature (TS_1, TS_2, etc). For sites where
432 winter soil temperatures fall significantly below 0 °C, Timesat fits a soil temperature "start of elevated season" date
433 to periods when the soil is still frozen. In order for Timesat to define the soil temperature seasonality within the
434 thawed season, we converted all negative soil temperatures to zero (simply removing these values results in too
435 many missing values for Timesat to fit). Many sites have more than one soil temperature probe, so we extracted
436 separate seasonality metrics from each individual probe (although we used the metrics from the shallowest
437 temperature probe in our analysis). Tables B4 contain the Timesat seasonality parameters used in the seasonality
438 analysis. We did not include water table depth in the seasonality analysis because many sites either lack water table
439 depth measurements or have sparse data.

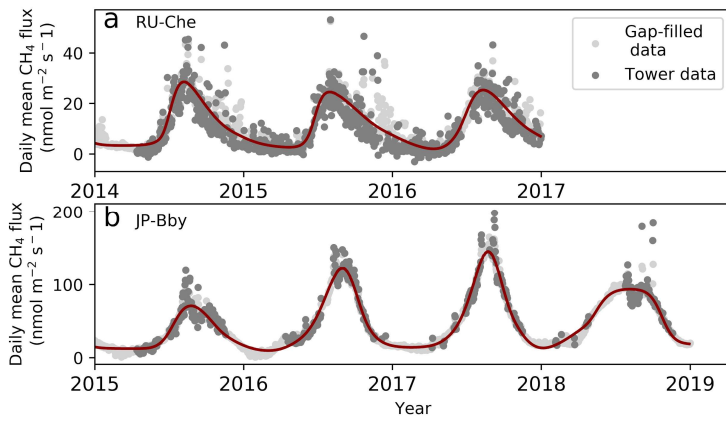


440



441
 442 Figure 1: TIMESAT parameter description. (a) and (b) base values (Timesat reports the average of these two values), (c)
 443 and (d) slopes of seasonal curves (lines drawn between 20% and 80% of the amplitude), (e) peak value, and day of year
 444 (DOY) for the -start (f), peak (g), and end (h) of the elevated methane (CH₄) emissions season. Data points are the mean
 445 daily gap-filled CH₄ fluxes from site JP-Bby in 2015.

446
 447



448

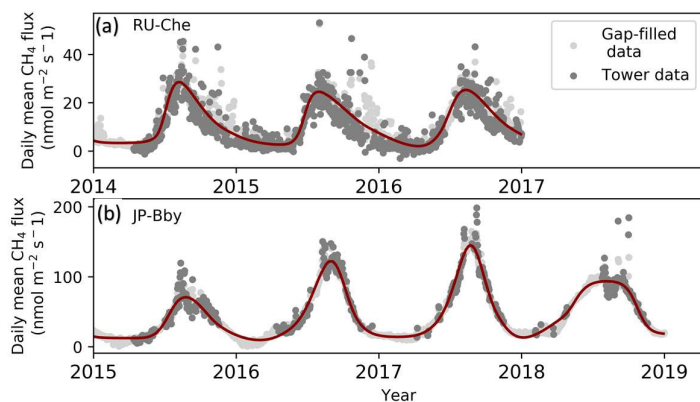


Figure 2: Examples of Timesat fits for two FLUXNET-CH₄ sites, (a) RU-Che and (b) JP-BBY. FluxBby, Methane (CH₄) flux data showing daily average flux tower data, with several high outliers excluded to improve the plot (dark gray), gap-filled values (light gray), and Timesat-fitted curve (dark red line) for sites JP-BBY and RU-Che. Timesat captures the size and shape as well as size of peaks (note different scale on y-axes). CH₄ = methane.

We regressed the CH₄ seasonality parameters from Timesat against a range of annual temperature, moisture, annual water table depth, and Timesat seasonality parameters for air temperature, soil temperature, and GPP (proxy for recent carbon input available as substrate) metrics using linear mixed-effect modeling with the *lmer* command (with site as a random effect) from the R (R Core Team 2018, version 3.6.2) package *lmerTest* (Kuznetsova et al., 2017). For these regressions we present the marginal R² outputs from *lmer*, which represent the variance explained only by the fixed effects. Mixed-effect modeling was necessary to account for the non-independence between measurements taken at the same site during different years (Zona et al., 2016; Treat et al., 2018). We also compared how seasonality metrics varied across latitudinal bands by dividing sites into northern (>= 60° N), temperate (between 40° N and 60° N), subtropical (absolute value between 20° and 40° latitude, with site NZ-KOP being the only Southern hemisphere site), and tropical (absolute value below 20°). Site-year totals for the northern, temperate, subtropical, and tropical bands were *n* = 57, 36, 39, and 9, respectively. We used the Kruskal-Wallis test to establish whether groups (either across quarters or across latitudes) were from similar distributions, and the post hoc multiple comparison “Dwass, Steel, Critchlow, and Fligner” procedure for inter-group comparisons. Kruskal-Wallis and post-hoc tests were implemented in Python Version 3.7.4, using stats from *scipy* for Kruskal-Wallis and *posthoc_dscf* from *scikit_posthocs*.

In addition to comparing CH₄ flux seasonality across latitudinal bands and to the seasonality of potential drivers, we also compared quarterly CH₄ flux sums by dividing data into quarterly periods: January/February/March (JFM), April/May/June (AMJ), July/August/September (JAS), and October/November/December (OND). For the sake of simplicity, we chose to compare quarterly periods rather than site-specific growing/non-growing season periods so that all time periods would be the same length. Quarterly sums were computed from the gap-filled CH₄ fluxes when the longest continuous data gap within the quarter did not exceed 30 days, leading to site-year counts of 67, 92, 95, 72 for JFM, AMJ, JAS, and OND, respectively. We compared quarterly CH₄ fluxes across latitudinal bands both for the total CH₄ flux, and for the quarterly percentage of the annual CH₄ flux. Quarterly statistics were also conducted with the Kruskal-Wallis test and the post hoc

Formatted: Subscript

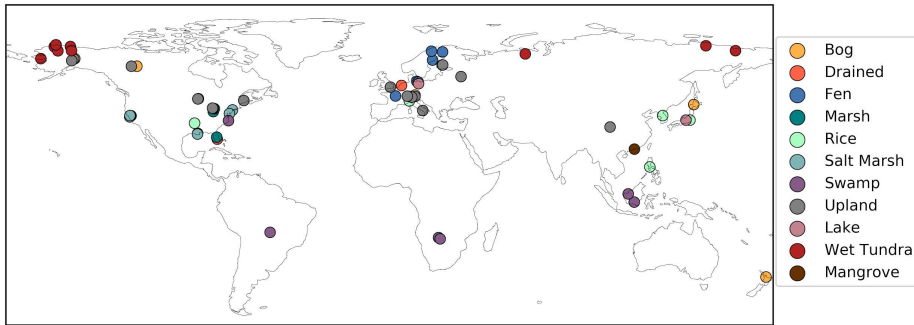
479 multiple comparison “Dwass, Steel, Critchlow, and Fligner” procedure implemented in Python. Quarterly values
480 are provided in Table B2B3, and the sum of mean quarterly CH₄ flux does not always equal mean annual CH₄ flux
481 because some quarters either do not have data, or have data gaps that exceed 30 days.
482

483 3. Results and Discussion

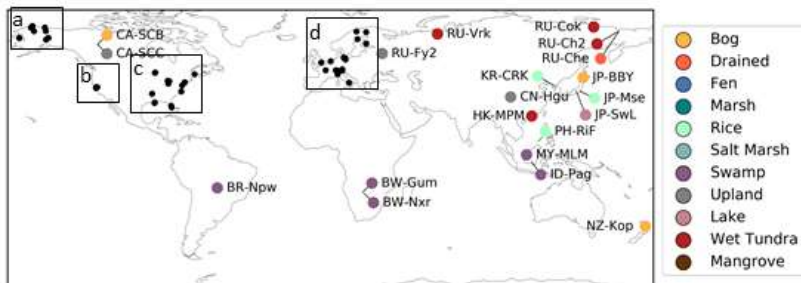
484 3.1 FLUXNET-CH₄ dataset

485 3.1.1 Dataset description

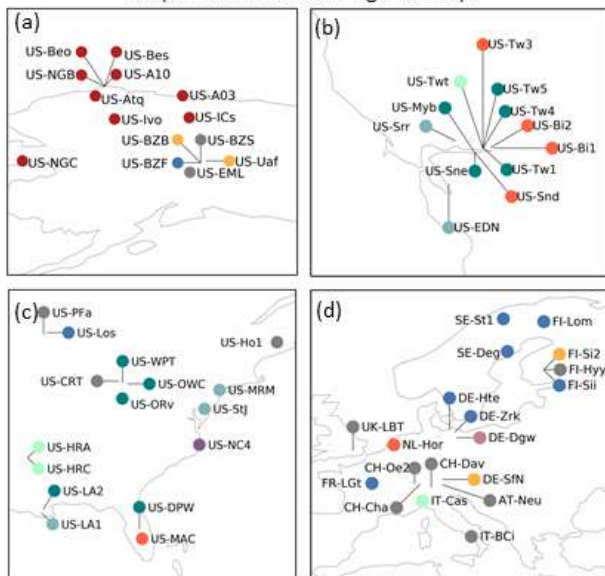
486 Version 1.0 of the FLUXNET-CH₄ dataset contains 79 unique sites, 293 total site-years of data, and 201
487 site-years with sufficient data to estimate annual CH₄ emissions. A ~~previous~~ synthesis paper, published prior to the
488 public data release of FLUXNET-CH₄ Version 1.0, had 60 unique sites and 139 site-years with annual CH₄ emissions
489 estimates (Knox et al., 2019). Freshwater wetlands make up the majority of sites (n = 42), and the dataset also includes
490 five salt marshes and one mangrove wetland. Notable additions to FLUXNET-CH₄ ~~Version 1.0~~ from the previous
491 unpublished dataset used in Knox et al., (2019) include six tropical sites (between 20° S and 20° N), including one
492 site in South America, two sites in southern Africa, and three sites in Southeast Asia. The 15 upland sites include six
493 needleleaf forests, three crop sites (excluding rice), two alpine meadows, one grassland, one mixed forest, one tundra,
494 and one urban site. The drained sites represent former wetlands that have been artificially drained for use as grasslands
495 (n = 3) or croplands (n = 3). FLUXNET-CH₄ ~~Version 1.0~~ sites span the globe, though are concentrated in North
496 America and Europe (Fig. 3). Table B2B3 includes characteristics of all sites in the dataset.



497



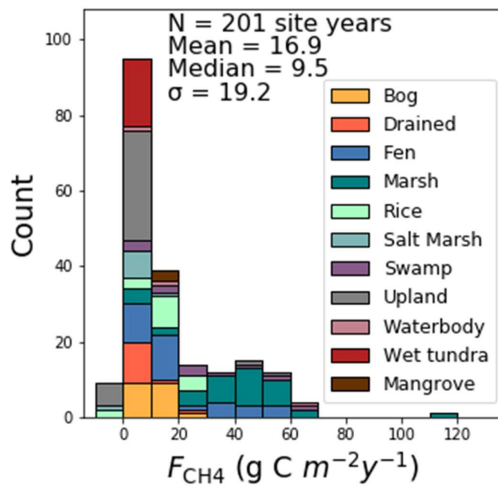
Subpanels as defined on global map:



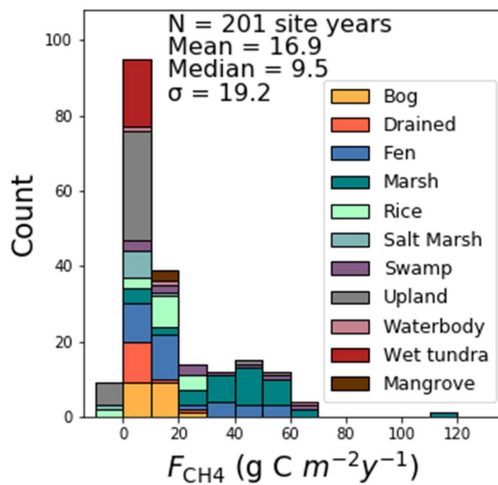
498

499 Figure 3. Global map of FLUXNET-CH4 Version 1.0 site locations colored by site type. The bog and upland site
 500 insets (a)-
 501 (d) show sites that were too closely located to distinguish in the Northwest Territories of Canada have been slightly offset
 502 from each other so that both are visible on the global map.

Formatted: Font color: Auto
 Formatted: Font: 11 pt, Not Bold, Not Highlight



503



504

505 **Figure 4. Histogram of annual CH_4 methane fluxes (F_{CH_4} , $g\ C\ m^{-2}\ yr^{-1}$) grouped by site type.**

506 Sites represent a range of ecosystem types, latitudes, median fluxes, and seasonality patterns (Table 1).
 507 Across all FLUXNET-CH4 Version 1.0 sites, mean average annual CH_4 flux is positively skewed with a median
 508 flux of $9.5\ g\ C\ m^{-2}\ yr^{-1}$, a mean flux of $16.9\ g\ C\ m^{-2}\ yr^{-1}$, and numerous annual CH_4 fluxes exceeding $60\ g\ C\ m^{-2}\ yr^{-1}$.
 509 The addition of 19 sites from the 60 sites aggregated in Knox et al., (2019) therefore do not significantly change the
 510 distribution of annual CH_4 fluxes. Marshes and swamps have the highest median flux, and upland, salt marsh, and
 511 tundra sites have the lowest (Fig. 4). Lake emissions are highly variable due to one high-flux lake site (JP-SWL).
 512 Flux data at many sites show strong seasonality in CH_4 emissions, but data coverage is also lower outside the

513 growing season. (Table 1). Data coverage is lowest during the JFM quarter (on average 20% of half-hourly time
 514 periods contain flux data) reflecting the predominance of Northern hemisphere sites and the practical difficulties in
 515 maintaining EC tower sites during colder winter months (Table 1). Bogs, fens, and marshes have pronounced
 516 seasonality, with fluxes being highest in the AMJ and JAS quarters. In contrast, CH₄ fluxes from uplands, drained
 517 sites, and salt marshes are more uniform and low year-round.

518 **Table 1: Summary table of sites grouped by ecosystem class reporting annual mean flux (Ann_Flux) and standard**
 519 **deviation from inter-annual variability (Ann_Flux_SD), site-years of data, % data cover per quarter, and median (med.)**
 520 **flux across site class. JFM= January, February, March; AMJ = April, May, June; JAS = July, August, September; OND**
 521 **= October, November, December.**

	# of Sites	# of Site-Years	Ann_Flux g C m ⁻² year ⁻¹	Ann_Flux_SD g C m ⁻² year ⁻¹	JFM cover-age (%)	AMJ cover-age (%)	JAS cover-age (%)	OND cover-age (%)	JFM flux (med.)	AMJ flux (med.)	JAS flux (med.)	OND flux (med.)
Salt marsh	5	10	2.9	4.7	7	42	50	37	1.5	1.7	2.1	1.6
Wet tundra	11	39	3.8	1.8	8	28	40	18	0.4	2.6	8.1	3.2
Upland	15	47	4.0	10.5	23	35	39	28	1.2	0.5	1.4	0.8
Drained	7	20	6.3	7.1	22	39	39	29	4.6	3.6	5.1	3.6
Bog	7	32	10.5	6.4	8	27	37	18	7.2	11.0	24.8	9.5
Mangrove	1	3	11.1	0.5	46	28	30	41	3.2	7.2	22.5	14.1
Rice	7	20	14.4	8.8	16	37	45	27	3.2	11.9	43.1	4.2
Fen	8	40	20.5	16.0	29	43	40	30	2.8	14.2	26.0	6.4
Swamp	6	15	26.4	19.9	24	34	29	19	14.7	24.9	31.0	24.4
Lake	2	4	28.2	33.4	15	13	27	36	0.2	47.6	90.2	40.3
Marsh	10	42	40.8	20.7	22	43	53	30	13.5	55.0	85.8	36.1

Formatted Table

522

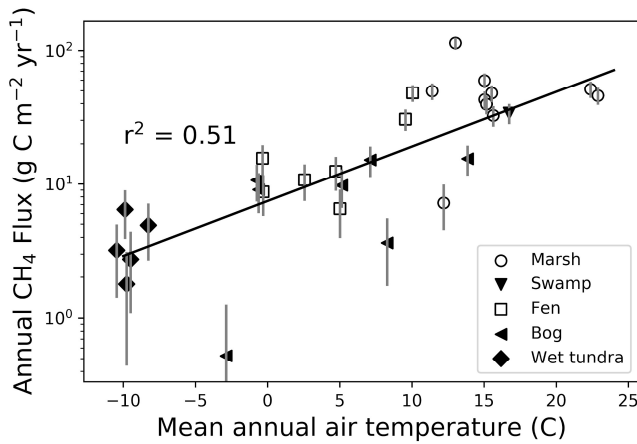
523

524 3.1.2 Freshwater wetland CH₄ characteristics

525 The FLUXNET-CH4 Version 1.0 dataset contains 42 freshwater wetlands that span 37°S to 69°N, including
526 bogs, fens, wet tundra, marshes, and swamps, and a range of annual CH₄ emission rates (Fig. 4). The majority of
527 freshwater wetlands in our dataset emit 0-20 g C m⁻² yr⁻¹, with 10 emitting 20-60 g C m⁻² yr⁻¹, and one more than 60 g
528 C m⁻² yr⁻¹. Differences in annual CH₄ flux among wetland types is partially driven by temperature (which is often
529 linked to site type), with mean annual air temperature explaining 51% of the variance between sites (Fig. 5, exponential
530 relationship). The global relationship between annual methane emissions and temperature can be described using a
531 Q₁₀ relationship where $Q_{10} = R_2/R_1^{(T_2-T_1)/10}$, with R₂ and R₁ being the methane CH₄ emission rates at temperatures
532 T₂ and T₁, respectively (temperature in degrees C). The Q₁₀ based on Fig. 5 data is 2.57. We also note that annual
533 CH₄ flux from individual biomes may have different relationships with temperature, as previous work has shown
534 biome-specific trends in CH₄ flux with environmental drivers (Abdalla et al., 2016). However, there currently are not
535 enough data points in each biome category to compare relationships between mean annual CH₄ flux and temperature.
536 Annual CH₄ flux is not correlated with mean annual water table depth in FLUXNET-CH4 Version 1.0, unlike in Knox
537 [set et al., \(2019\)](#), which used a subset of the FLUXNET-CH4 Version 1.0 sites) where CH₄ flux was correlated with
538 water table depth only for sites with water table below ground for 90% of measured days ($r^2 = 0.31$, $p < 0.05$, $n = 27$
539 site years, [Knox et al., 2019](#)). Freshwater wetland seasonality is further described in Sect. 3.3.

Formatted: Subscript

Formatted: Superscript



542

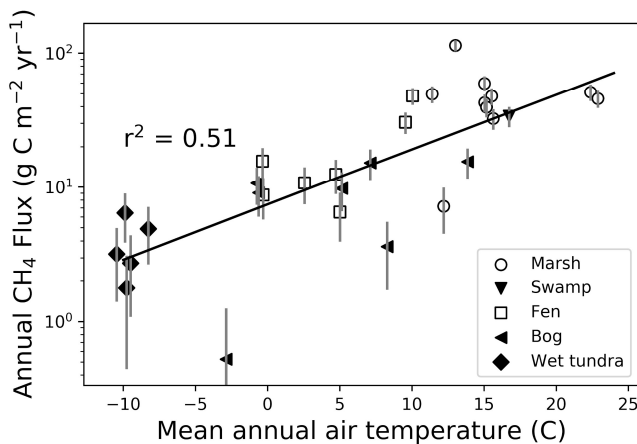


Figure 5: Relationship between mean annual wetland methane (CH_4) flux ($\text{g C m}^{-2} \text{yr}^{-1}$, logarithmic scale) and mean annual air temperature ($^{\circ}\text{C}$, logarithmic scale) for each freshwater wetland site, with wetland type indicated by symbol. The difference in emissions across site types is partially driven by difference in mean annual temperature. Markers represent individual site means, with vertical error bars representing the standard deviation of interannual variability.

- Formatted: Font: 11 pt, Not Bold, Not Highlight
- Formatted: Font: Bold, Underline
- Formatted: Indent: Left: 1", Space Before: 12 pt, After: 12 pt
- Formatted: Font: Not Bold, Italic, No underline
- Formatted: Indent: Left: 0"

3.1.3 Non-wetland Upland, rice and urban CH_4 characteristics

Upland agricultural sites are characterized by a lack of seasonal pattern in CH_4 emissions, relatively low flux, and *sometimes* negative daily flux (i.e., CH_4 uptake) averages. All of the upland non-agricultural sites in FLUXNET- CH_4 Version 1.0 are net (albeit weak) CH_4 sources except for the needleleaf forest site US-Ho1, which has mean annual CH_4 flux of $-0.1 \pm 0.1 \text{ g C m}^{-2} \text{yr}^{-1}$ (see Table B2B3 for site acronyms and metadata). The average agricultural site emissions are $1.3 \pm 0.8 \text{ g C m}^{-2} \text{yr}^{-1}$ and non-agricultural site emissions are $1.6 \pm 1.2 \text{ g C m}^{-2} \text{yr}^{-1}$ across sites.

Rice sites ($n = 7$) have average annual emissions across all sites of $16.7 \pm 7.7 \text{ g C m}^{-2} \text{yr}^{-1}$ and are characterized by strong seasonal patterns, with either one or more CH_4 emission peaks per year depending on the number of rice seasons and field water management. One peak is typically observed during the reproductive period for the continuously flooded sites with one rice season (i.e., US-HRC, JP-MSE) (Iwata et al., 2018; Runkle et al., 2019; Hwang et al., 2020). For sites with only one rice season but with single or multiple drainage and re-flooding periods, a secondary peak may appear before the reproductive peak (i.e., KR-CRK, IT-Cas, and US-HRA; Mejjide et al., 2011; Runkle et al., 2019; Hwang et al., 2020); Hwang et al., 2020). Two reproductive peaks appear for sites with two rice seasons (i.e., PH-RiF), and each reproductive peak may be accompanied by a secondary peak due to drainage events (Alberto et al., 2015). Even sites with one, continuously flooded rice season may experience a second peak if the field is flooded during the fallow season to provide habitat for migrating birds (e.g., US-Twt; Knox et al., 2016).

568 The dataset has one year of urban data from site UK-LBT in London, England. UK-LBT observes CH₄ fluxes
569 from a 190 m tall communications tower in the center of London, and ~~had~~ has a mean annual CH₄ flux of 46.5 ± 5.6 g
570 C m⁻² yr⁻¹. This flux is more than twice as high as the mean annual CH₄ flux across all FLUXNET-CH4 ~~Version 1.0~~
571 sites, 16.9 g C m⁻² yr⁻¹. The London site has higher CH₄ emissions in the winter compared to summer, which is
572 attributed to a seasonal increase in natural gas usage (Helffer et al., 2016.)

Formatted: Superscript

573 3.1.4 ~~Non-freshwater~~ Saltwater and mangrove wetland CH₄ characteristics

574 Three of the five saltwater wetlands in FLUXNET-CH4 ~~Version 1.0~~ (US-Edn, US-MRM, and US-Srr) have
575 a very low mean annual CH₄ flux (see Table B7B2 for individual site-year CH₄ flux sums and associated uncertainty)
576 and minimal seasonality. Two other FLUXNET-CH4 ~~Version 1.0~~ saltwater sites (US-La1, and US-StJ) have
577 significantly higher fluxes, with annual sums of 12.6 ± 0.6 and 9.6 ± 1.0 g C m⁻² yr⁻¹, respectively, while the mangrove
578 site HK-MPM has annual mean fluxes of 11.1 ± 0.5 g C m⁻² yr⁻¹. This range of CH₄ fluxes across different saltwater
579 ecosystems could be valuable for exploring the effect of salinity and different biogeochemical pathways of CH₄
580 production, oxidation, and transport of CH₄ (Bartlett et al., 1987; Poffenbarger et al., 2011). Saltwater wetlands along
581 the coast have unique CH₄ dynamics attributable to the presence of abundant electron acceptors, most importantly
582 sulphates, which inhibit methanogenesis (Pattnaik et al., 2000; Mishra et al., 2003; Weston et al., 2006), but at low
583 concentrations can have no effect (Chambers et al., 2011) or even increase methanogenesis (Weston et al., 2011). In
584 fact, estuarine wetlands with moderate salinity can still be significant sources of CH₄ (Liu et al., 2020). Even under
585 sulfate-rich conditions, high CH₄ production can be found via methylotrophic methanogenesis (Seyfferth et al.,
586 2020)(Dalcin Martins et al. 2017; Seyfferth et al., 2020.) or because the processes of sulfate reduction and
587 methanogenesis are spatially separated (Koebsch et al., 2019). Consequently, representing the biophysical drivers of
588 ecosystem-scale CH₄ fluxes in non-freshwater wetlands is challenging and may represent a combination of competing
589 or confounding effects (Vazquez-Lule and Vargas 2021).
590

Formatted: Superscript

591 3.2 Wetland Representativeness

592 We evaluated the representativeness of freshwater wetland sites in the FLUXNET-CH4 Version 1.0 dataset
593 against wetlands globally. ~~Specifically, we asked how representative the bioclimatic conditions of our sites are,~~
594 ~~relative to bioclimatic conditions in all wetlands globally. Parameters defining bioclimatic conditions are selected~~
595 ~~from those known to affect CH₄ production, consumption, and transport processes (e.g., energy, moisture, substrate~~
596 ~~availability, and vegetation): based on bioclimatic conditions of our sites.~~ When evaluating bioclimatic variables
597 individually, the distribution across the network was significantly different from the global distribution (alpha > 0.05;
598 two-tailed Kolmogorov-Smirnov tests; see Table B3B4).

599 When considering the four bioclimatic variables, MAT, LE, EVI and SRWI in a PCA, we found that our
600 tower network generally samples the bioclimatic conditions of global wetland cover, but some noticeable gaps remain
601 (Fig. 6). Three clusters of the world's wetland-dense regions are identified, but are not equally sampled by the network.
602 A cluster of low temperature wetlands is sampled by a large number of high-latitude sites. The other two wetland
603 clusters are not as well sampled: a high temperature and LE cluster is represented only by two towers (ID-Pag and
604 MY-MLM), while drier and temperate and subtropical wetlands including large swathes of the Sahel in Africa only
605 have a site in Botswana (BW-Npw) as their closest analog tower.
606

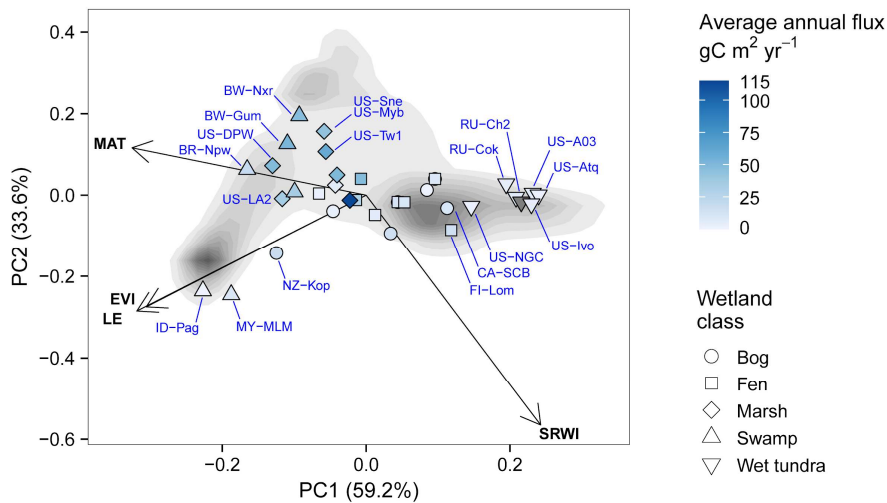
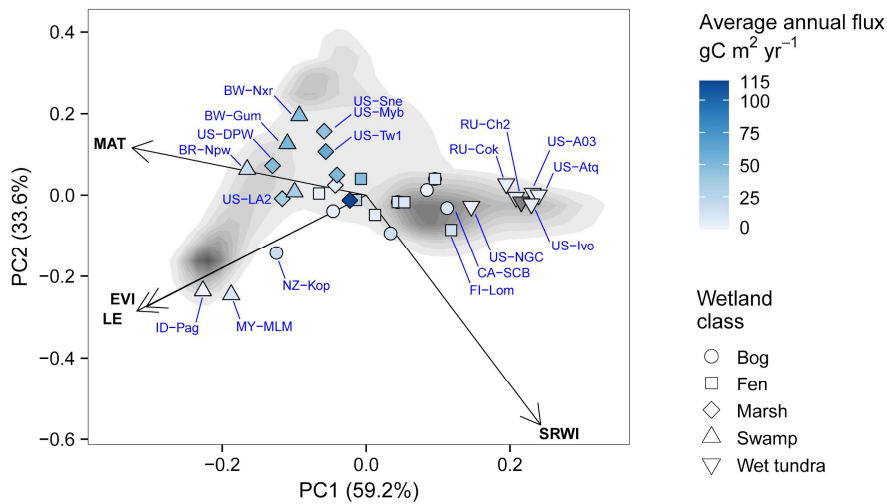
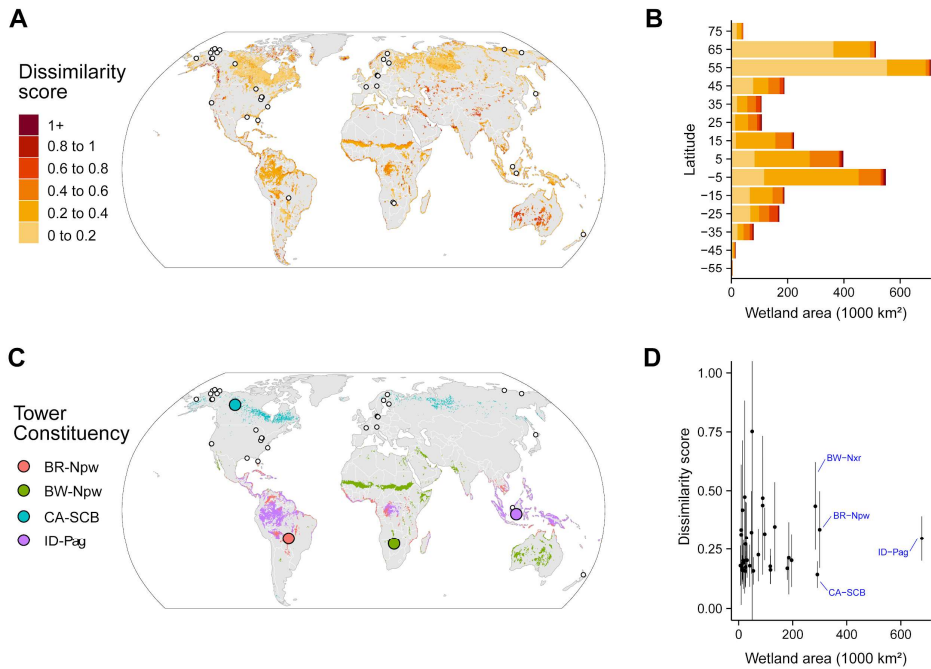


Figure 6: Principal Component Analysis displaying the distribution of freshwater wetland sites (blue-points) along the two main principal components together accounting for 91.9% of variance. Tower sites are represented as the larger points with shapes representing their wetland type and color shade representing the annual methane (CH_4) flux (greyed gray points represent sites for which <6 months of flux data was available to estimate annual budget). The size of wetland points are made larger for visual clarity and site codes are labeled in blue. The background shades of grey represent the density of land pixels (excluding Greenland and Antarctica) that have a >5% wetland fraction according to the WAD2M map (Zhang et al., In Review); text for selected sites deviating from average conditions. Loading variables are represented by the arrows: mean annual temperature (MAT), simple ratio water index (SRWI), latent heat flux (LE)

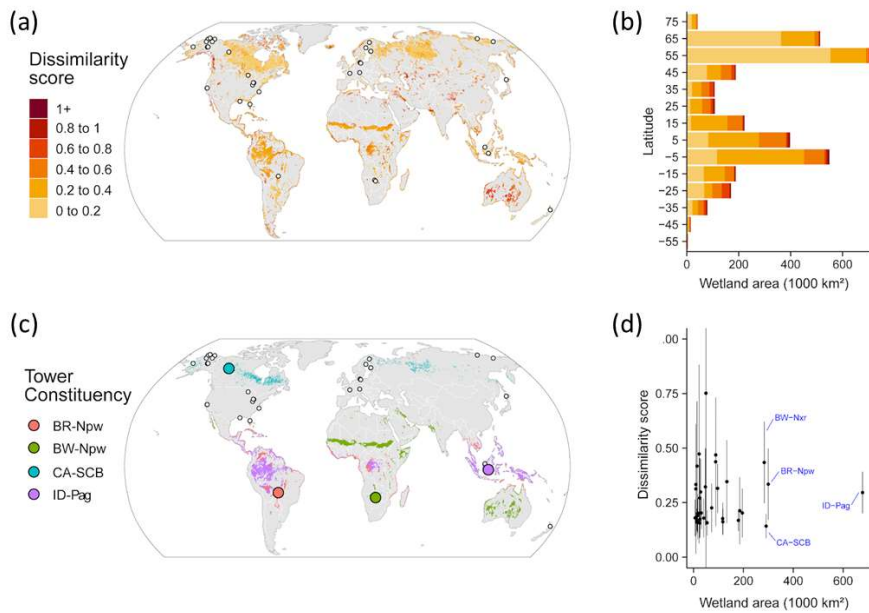
617 and enhanced vegetation index (EVI). The background shades of gray are a qualitative representation of the density of
 618 global wetland pixels and their distribution in the PCA climate-space, with darker color representing higher densities
 619 (excluding Greenland and Antarctica). Only grid cells with >5% average wetland fraction according to the WAD2M over
 620 2000-2018 are included (Zhang et al., 2020). The loading variables are represented by the arrows: mean annual temperature
 621 (MAT), simple ratio water index (SRWI), latent heat flux (LE) and enhanced vegetation index (EVI).

622
 623 Evaluating the bioclimatic dissimilarity of global wetlands to the FLUXNET-CH4 Version 1.0 network
 624 shows the least captured regions are in the tropics and mountainous regions (Fig. 7A). Sparse coverage in the tropics
 625 also means that the few existing towers occupy a critical place in the network, particularly as tropical wetlands are the
 626 largest CH₄ emitters (Bloom et al., 2017; Poulter et al., 2017). Highly dissimilar wetlands are limited in extent and
 627 distributed across all latitudes, but the average dissimilarity is higher in north temperate (55° to 65°) and tropical (-5°
 628 to 5°) latitudes (Fig. 7B). To evaluate the importance of individual towers in the network, we estimated the
 629 geographical area to which it is most analogous in bioclimate-space (Fig. 7C). We found that some towers have
 630 disproportionately large constituencies (i.e., wetland areas that share the same closest bioclimatic analog tower).
 631 Towers in Indonesia (ID-Pag), Brazilian Pantanal (BR-Npw), and Botswana floodplains (BW-Nxr) represent the
 632 closest climate analog for much of the tropics (678, 300 and 284 thousand km², respectively) while CA-SCB
 633 represents a vast swath (291 thousand km²) of boreal/arctic regions (Fig. 7D).

634



635



636

637 Figure 7: **(Aa)** Distance in bioclimatic space between global land surface and the FLUXNET-CH4 Version 1.0 tower
 638 network. **(gray areas indicate no mapped wetlands)**. The Euclidean distance was computed on the **fivefour** bioclimatic
 639 variables and was then standardized by the average distance within-network. Most of the land surface has a dissimilarity
 640 score lower than 1, meaning these areas are closer than the average tower distance (lower dissimilarity score means a similar
 641 bioclimate to that represented by towers in the network). However, this pattern reflects more the sparsity of the tower
 642 network than a similarity of the land surface to the network. Areas with <5% coverage by wetlands were excluded to focus
 643 on wetland-dense regions. **(Bb)** Latitudinal distribution of dissimilarity score, **(Cc)** Map of the four largest tower
 644 constituencies, **(Dd)** Scatterplot of wetland area in each tower constituency plotted against the average dissimilarity score
 645 (point) and +/- standard deviation (error bar).

646 Our assessment of wetland CH₄ tower coverage determines the ability of our dataset to represent global
 647 wetland distributions and highlights some clear representation gaps in the network—, **particularly in** tropical, **and**
 648 humid, **and mountainous** regions. Other geographic regions such India, China and Australia, where towers exist but
 649 are not included in the current network should be prioritized when expanding the network, even though they are not
 650 among the most distant areas to the current network. Similar representativeness assessments have been developed for
 651 CO₂ tower networks to identify gaps and priorities for expansion (Jung et al., 2009; **Kumar et al., 2016**). To improve
 652 the geographic coverage of the network for representing global-scale fluxes, locations for new tower sites can be
 653 targeted to cover bio-climatically distant areas from the current network (Villarreal et al., 2019). Candidate regions
 654 for expansion that are both high CH₄ emitting **and** **(Saunois et al., 2020)** as well as located in under-sampled **climates**
 655 are: African Sahel, Amazon basin, Congo basin, South-East Asia. **Climatic conditions over boreal and arctic biomes**
 656 **are generally better represented (primarily at lower elevations), but there is scope to expand the network in wetland-**
 657 **dense regions like the Hudson Bay Lowlands and Northern Siberian Lowlands.** Moreover, **establishing sites should**
 658 **be established** in other ecosystem types, especially lakes and reservoirs **(Bastviken et al., 2011; Deemer et al., 2016;**
 659 **Matthews et al., 2020)** **(see Deemer et al. 2016, Bastviken et al. 2011, Matthews et al. 2020)** in most climatic zones **in**
 660 **order to would help** capture CH₄ fluxes from these ecosystems.

661 Understanding the representativeness of the network is essential when inferring general patterns of flux
662 magnitude, seasonality, and drivers from the tower data (Villarreal et al., 2018). We produced a first-order
663 representativeness of average bioclimatic conditions, but temporal representativeness (across seasons, climate
664 anomalies and extreme events) is particularly needed given the episodic nature of CH₄ fluxes (Chu et al., 2017;
665 Mahecha et al., 2017; Chu et al., 2017; Mahecha et al., 2017; Göckede et al., 2019).

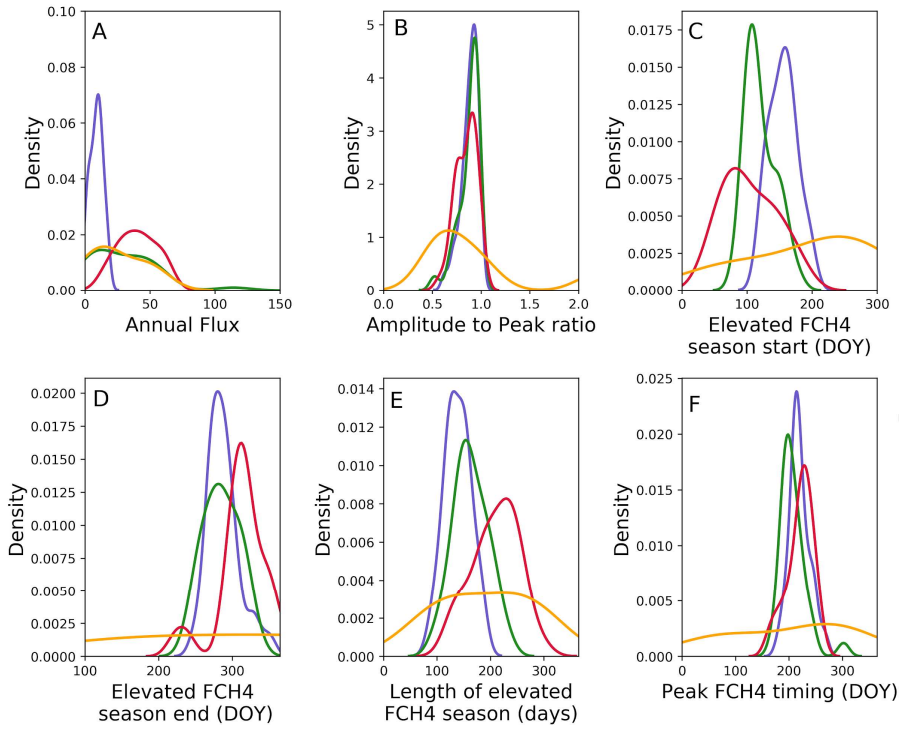
666 Assessing representation of wetland CH₄ sites is complicated by the fact that wetlands occupy only a fraction
667 of most landscapes (except wetland dense regions such as Northern Siberian Lowlands, Hudson Bay Lowlands, Congo
668 basin, etc.) and that not all relevant factors affecting CH₄ production and consumption could be considered in our
669 analysis. For instance, our assessment of representation did not consider wetland types as such maps are limited by
670 the inherent difficulties in remotely sensing wetland features (Gallant, 2015). The attribution of representativeness is
671 further complicated by the fact that many EC tower locations are subject to small-scale variability within the field of
672 view, or footprint, of the sensor. Consequently, the individual time steps within EC flux time series may represent a
673 mixture of different wetland types, or different fractions of wetland contribution to the total CH₄ flux, varying with
674 wind direction, atmospheric stability, or season (Chu et al 2021). This further complicates upscaling efforts.
675 Additionally, this representativeness analysis did not apply weights to the drivers to reflect their varying influence on
676 CH₄ flux. Such weights can be included in future versions as they are generated by a cross-validated machine learning
677 approach (Jung et al., 2020). Future efforts will include the dissimilarity index from this analysis as a metric of
678 extrapolation in a CH₄ flux upscaling effort.

680 3.3 Freshwater wetland flux seasonality

681 We used seasonality parameters extracted by Timesat to describe typical seasonal patterns in freshwater wetland
682 CH₄ fluxes, and to compare them with seasonality in soil temperature and GPP. Of the 42 freshwater wetland sites
683 in FLUXNET-CH4 Version 1.0, 36 had sufficient data series to extract seasonality parameters.

684 3.3.1 Seasonal flux comparisons by latitudinal bands

685 CH₄ flux and seasonality varied substantially across latitudinal bands (northern, temperate, subtropical, and
686 tropical) (Fig. 8). Annual CH₄ fluxes for temperate, and subtropical sites were significantly higher than for northern
687 sites (8.7 ± 5.0 , 29.7 ± 25.2 , 40.1 ± 14.6 , and 24.5 ± 20.7 g C m⁻² yr⁻¹ for northern, temperate, subtropical, and tropical,
688 respectively, $p < 0.0001$ using Kruskal Wallis and post hoc comparisons; Fig. 8a), and tropical sites were similar to all
689 other latitudinal bands likely because of their small sample size. The ratio of seasonal amplitude to peak flux provides
690 a measure of the relative seasonal increase in emissions compared with baseline, where a ratio of zero indicates no
691 seasonal change in amplitude, a ratio of one indicates the off-season flux is zero, and values over one means the off-
692 season baseline CH₄ fluxes were negative (i.e., uptake). Average amplitude to peak flux ratios were similar across all
693 latitudinal bands (0.9 ± 0.1 , 0.9 ± 0.1 , 0.9 ± 0.1 , 1.0 ± 0.7 , for northern, temperate, subtropical, and tropical,
694 respectively; Fig. 8b). The spring increase in CH₄ emissions begins later in northern sites compared with
695 temperate and subtropical sites (end of May versus April, respectively, $p = 0.001$; Fig. 8c), while tropical sites vary
696 widely in elevated emission season start date. Northern sites also have had shorter elevated CH₄ flux season lengths
697 (138 ± 24 days) compared to temperate sites (162 ± 32 days), and both were shorter than subtropical sites ($209 \pm$
698 43 days; $p < 0.0001$; Fig. 8d,e). On average, CH₄ flux peaks earlier for temperate sites compared to northern
699 ($p = 0.008$) and subtropical sites ($p = 0.02$; mid to late July compared with early August; Fig. 8e,f), while tropical
700 sites again vary widely. Given their unique seasonality, and low number of site-years ($n = 9$), tropical systems are
701 discussed separately in Sect. 3.3.3, and not included in the comparisons in the remainder of this section. While our
702 results on CH₄ seasonality corroborate expected trends for these latitudinal bands, they provide some of the first
703 estimates of CH₄ seasonality parameters and ranges across a global distribution of sites.



706
707

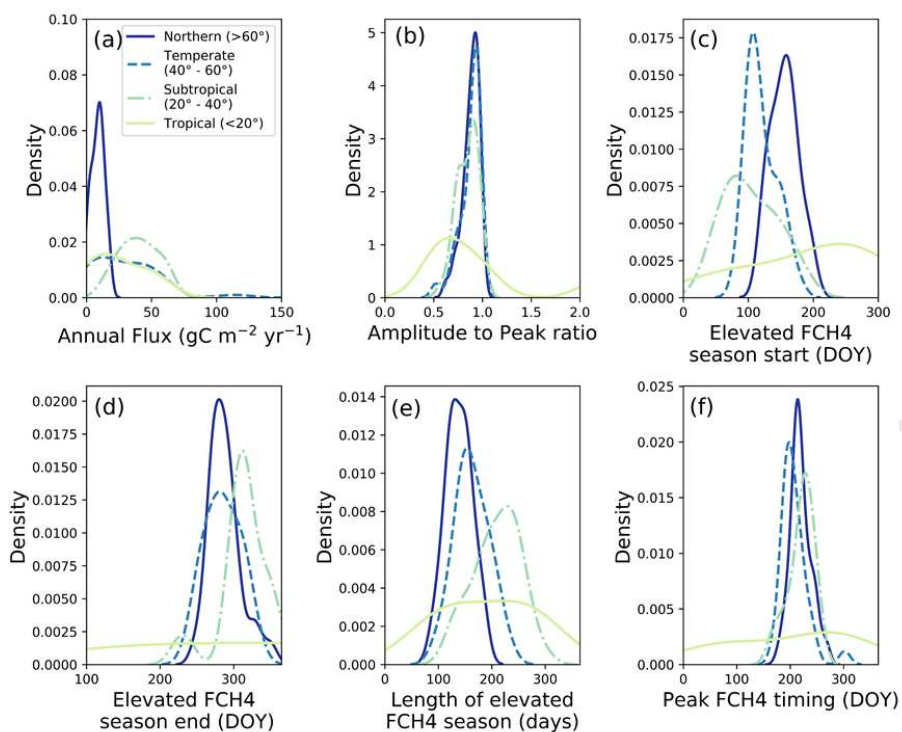


Figure 8: (a) Annual methane (CH_4) flux ($\text{g C m}^{-2} \text{yr}^{-1}$), (b) Ratio of seasonal amplitude to seasonal peak, where values of 0 indicate uniform annual CH_4 flux, values of one indicate zero off-season fluxes, and values exceeding one indicate negative off-season fluxes, (c) CH_4 flux (FCH₄) elevated emissions season start, by day of year (DOY), (d) FCH₄ elevated emissions season end by DOY, (e) Length of elevated CH_4 flux season, (days), and (f) DOY of peak timing metrics for high, mid, FCH₄. Northern (dark blue, solid line), Temperate (blue, dashed line), Sub-tropical (green, dot-dash line) and lower latitude Tropical (light green, solid line) wetlands (purple, green, red, respectively) plotted using the kernel density function. Each panel has lines that represent latitudinal bands as follows: northern ($>60^\circ$), temperate (between 40° and 60°), subtropical (between 20° and 40°), and tropical ($<20^\circ$), though the site-year totals vary between these groups ($n = 57$, $n = 36$, $n = 39$, and $n = 9$ respectively). All total CH_4 flux values and elevated season start values are positive, and the apparent continuation of the data distribution into negative values is an artifact of the kernel density function. Southern Hemisphere sites below 20°S were shifted by 182 days to make summer the middle of the year for comparability with Northern Hemisphere sites.

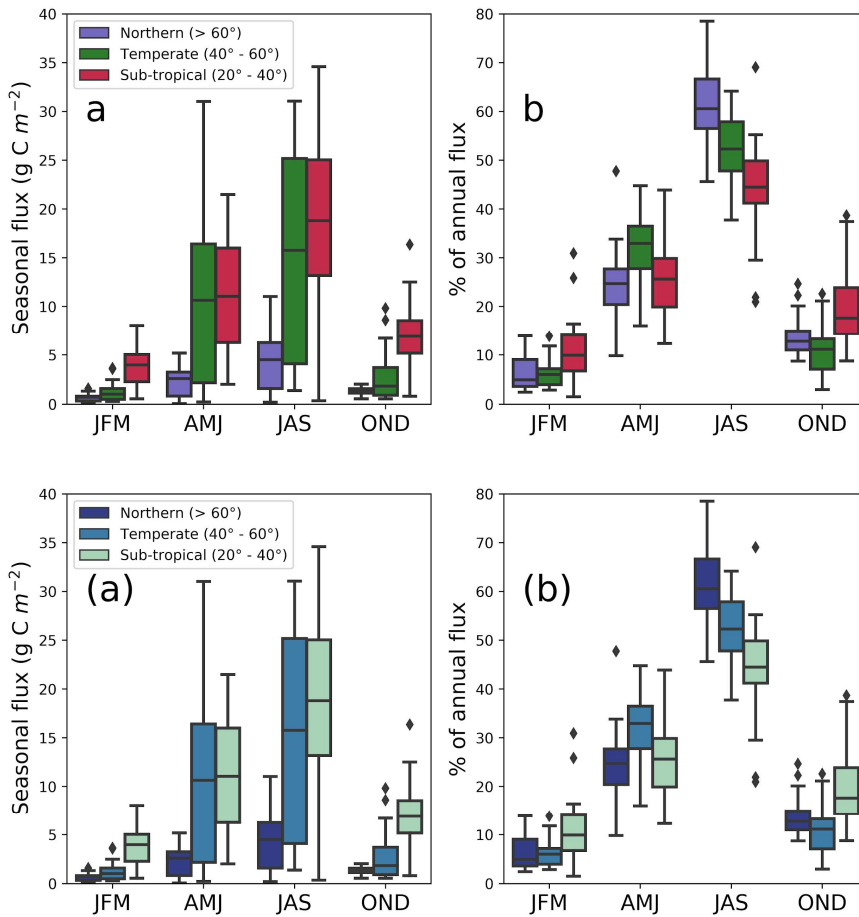
We found that latitudinal groups showed strong differences in absolute CH_4 flux across quarters, and narrower differences in percentage of annual CH_4 flux (Fig. 9a versus 9b). Thus, the AMJ quarter had a similar relative contribution to the annual CH_4 flux across latitudes, regardless of the absolute annual CH_4 flux. Methane CH_4 fluxes (Fig. 9a) were highest during JAS for northern, temperate, and subtropical sites and highest in AMJ and JAS for temperate sites ($p < 0.01$). Though CH_4 fluxes in northern sites are most commonly measured during warm summer months (Sachs et al., 2010; Parmentier et al., 2011), fluxes in JFM and OND (50% of the yearly duration) on average make up $18.1 \pm 3.6\%$, $15.3 \pm 0.1\%$, and $31.2 \pm 0.1\%$ (northern, temperate, subtropical, respectively) of annual

Formatted: Font: 10 pt, Not Bold

Formatted: Subscript

Formatted: Not Superscript/ Subscript

730 emissions. This pattern indicates that a substantial fraction of annual CH₄ fluxes occurs during cooler months. The
 731 fraction would be even higher if we added April, May, and September emissions to the northern (> 60°N) sites, as
 732 done in (Zona et al., 2016), where > 50% of emissions were found to come from non-growing season months. The
 733 contribution of non-growing season CH₄ emissions to annual CH₄ fluxes has previously been described for arctic and
 734 boreal regions (Zona et al., 2016; Treat et al., 2018; Treat et al., 2018) and our analysis suggests comparable
 735 contributions in temperate and subtropical systems for the same quarterly periods.
 736
 737
 738



739
 740
 741
 742
 743 **Figure 9: (Aa) Quarterly contribution to total annual CH₄ flux in g C m⁻², and (Ab) percentage of annual CH₄ flux. Sites**
 744 **were divided into northern (> 60° N), temperate (40° N - 60° N), and subtropical (20° N - 40° N). Quarters with**
 745 **continuous data gaps exceeding 30 days were excluded. We used the following quarterly periods:**

Formatted: Font: 10 pt, Not Bold

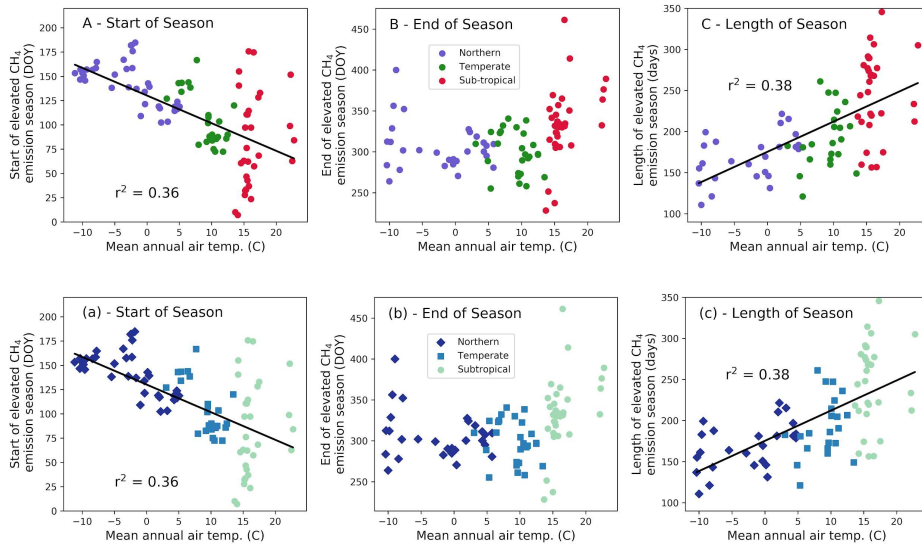
746 January/February/March (JFM), April/May/June (AMJ), July/August/September (JAS), and
 747 October/November/December (OND). Tropical sites are discussed separately in Sect. 3.3.3 because of their unique
 748 seasonality and low number of sites.
 749

750 **3.3.2 Predictors of CH₄ flux phenology**

751 The start of the elevated CH₄ flux season, and how long the elevated flux season lasts, ~~correlates~~correlated
 752 strongly with mean annual air temperature (Fig. 10; $p < 0.0001$ for each). Methane flux ~~begins~~began to increase
 753 roughly two months earlier in the warmest systems (mean annual temperature > 20 °C) compared to the coldest
 754 (mean annual temperature near -10 °C), though several of the warmer sites ~~have~~had high variability. Our data
 755 suggest that the CH₄ season ~~starts~~started 2.8 ± 0.5 days earlier for every degree Celsius increase in mean annual
 756 temperature (Fig. 10a). In contrast, the end of the CH₄ emission season ~~is~~was not correlated with mean annual
 757 temperature, but a positive trend ~~exists~~existed despite high variability in warmest and coldest sites (Fig. 10b). The
 758 high variability seen in the end of CH₄ season at northern sites is important to note and would likely be better
 759 resolved by incorporating other seasonality or phenological characteristics, such as moisture, active layer depth, and
 760 plant community composition. (e.g., Kittler et al., 2017). Plants with aerenchymatous tissue, for example, influence
 761 the timing of plant-mediated CH₄ flux and are a key source of uncertainty while predicting CH₄ seasonality for
 762 northern wetlands (Xu et al., 2016, Kwon et al., 2017). Despite the relative lack of trend with season end date, the
 763 season length ~~is~~was still positively correlated with mean annual temperature, with the warmest sites having roughly
 764 three more months of seasonally elevated CH₄ emissions than the coldest sites (Fig. 10c). ~~Methane~~CH₄ season
 765 length ~~increases~~increased 3.6 ± 0.6 days for every °Cdegree Celsius increase in mean annual temperature (note that
 766 these relationships are correlations, and we cannot disentangle causality with this analysis). Temperature is highly
 767 correlated with other parameters (i.e., radiation, days of snow cover, etc.), so CH₄ flux is also likely to correlate with
 768 other environmental parameters.

769

770

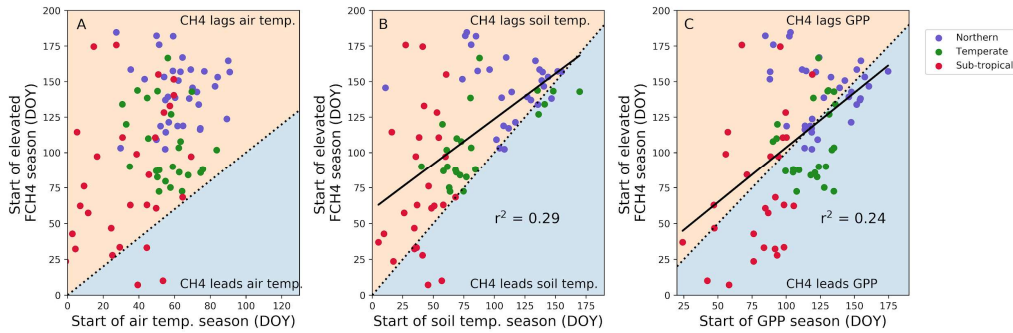


771 Figure 10. The (a) start of the elevated methane (CH₄) emission season ($y = -2.8x + 130$, with 'x' in °C and 'y' in day of
 772 year), (DOY), (b) the end of the elevated emission season in DOY, and (c) the length of the emission season with mean
 773 annual site air temperature ($y = 3.6x + 176.6$, with 'x' in °C and 'y' in days). Each point represents a site-year of data and
 774 all reported r^2 are significant to $p < 0.0001$). Tropical sites are discussed separately in Sect. 3.3.3.

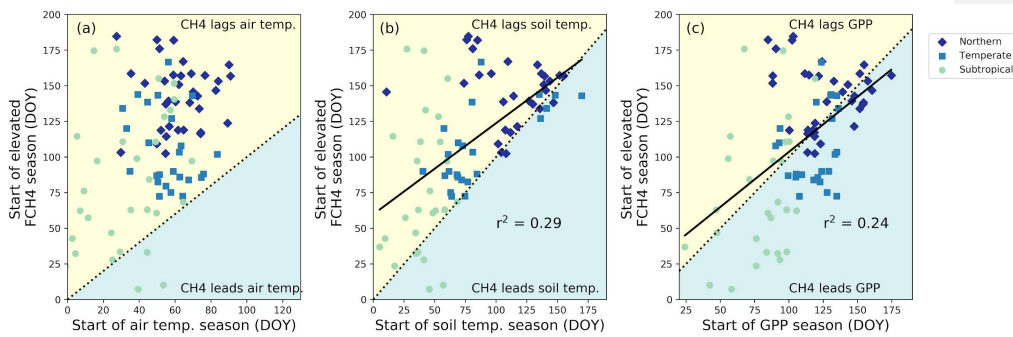
775 Although the spring onset of increasing CH₄ emissions ~~correlates~~ correlated with mean annual air
 776 temperature, on average it ~~lags~~ lagged the spring increase in the shallowest soil temperatures by 31 ± 40 days (Fig.
 777 11, lag is significantly different than zero, $p < 0.001$), with very few instances of CH₄ emissions beginning before
 778 seasonal soil temperatures increase (and by 20 ± 50 days for the deepest temperature probes). In contrast, for
 779 roughly half of the sites, CH₄ emission ~~increases~~ increased prior to seasonal GPP (a proxy for fresh substrate
 780 availability) increases. This suggests that the initiation of increased CH₄ fluxes at the beginning of the season ~~is was~~
 781 not limited by availability of substrate derived from recent photosynthate, especially in cooler climates.
 782 Additionally, the onset of CH₄ fluxes ~~tended~~ tended to occur closer to the onset of soil temperature increase for cooler
 783 temperature sites (sites with later start dates tend to be cooler; Fig. 11a). This result is likely attributable to the direct
 784 influence of increased temperature on microbial processes (Chadburn et al., 2020), as well as the indirect influences
 785 of snow melt, both via release of CH₄ from the snowpack as well as a higher water table leading to more CH₄
 786 production (Hargreaves et al., 2001; Tagesson et al., 2012; Mastepanov et al., 2013; Helbig et al., 2017). These
 787 observed trends hold for the entire temperature or GPP range of freshwater wetland sites, but are not necessarily
 788 applicable within individual latitudinal bands.

Formatted: Subscript

789



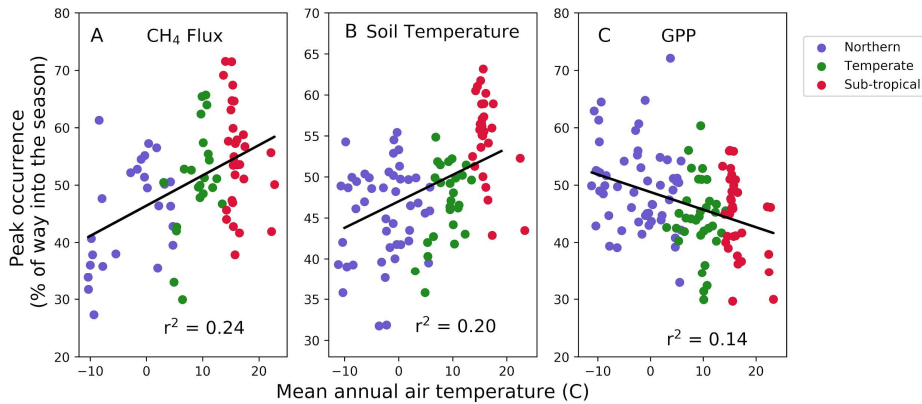
790



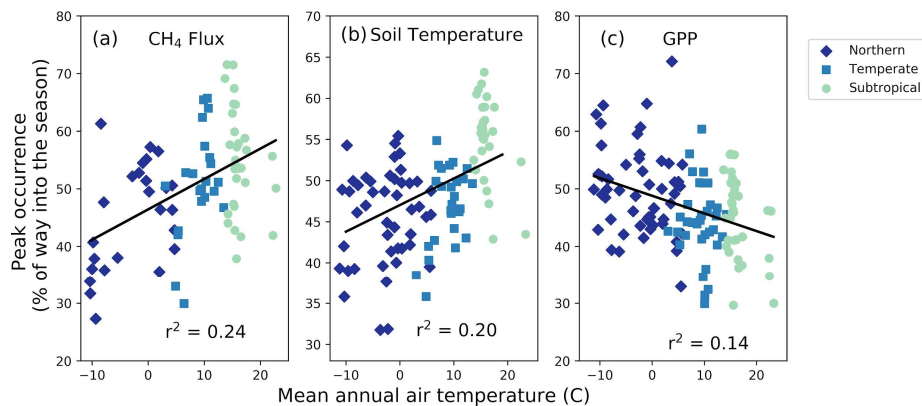
791

792 Figure 11. Relationship between the onset of the methane (CH₄) emission season to (a) the beginning of the air
 793 warming, by day of year (DOY), (b) soil warming at the shallowest probe depth per site by DOY, and (c) gross primary
 794 productivity (GPP) increase for the subset of sites with soil temperature data by DOY. Each point represents a site-year
 795 of data. Dashed lines represent a 1:1 relationship, solid lines are significant (p < 0.05) regression fits. On average, the
 796 CH₄ emission season lags the soil temperature increase by 31 ± 40 days, and is more synchronous with GPP.

797 In contrast with the CH₄ season-start timing, the timing of the CH₄ peak does not correlate with either
 798 the timing of the soil temperature peak or the GPP peak (Fig. A1). For 63% of the sites, the average timing of peak
 799 CH₄ emissions lags the soil temperature peak, and at 83% of the sites average peak CH₄ lags peak GPP
 800 (Fig. A1). Although there is no simple relationship between absolute CH₄ peak timing and the environmental
 801 drivers we investigated, there is a correlation (p = 0.0005) between the relative timing of peak CH₄ compared to
 802 season onset (calculated as described in Section 2.3) and mean annual air temperature (Fig. 12a). For cooler sites,
 803 the peak of seasonal CH₄ emissions occurs closer to the onset of the CH₄ emission season than the end of
 804 the season, resulting in an asymmetrical seasonal CH₄ flux shape that is illustrated in Fig. 2a. Soil temperature also
 805 peaks earlier in the season for cooler wetlands, though the relationship is not as pronounced (p = 0.009, Fig.
 806 12b). In contrast, GPP peaks later in the season for cooler wetlands (p = 0.009, Fig. 12c). Previous work on
 807 Arctic sites (sites US-Ivo, US-Beo, US-Atq, US-Bes, and RU-CH2) has highlighted the asymmetrical annual CH₄
 808 peak, with higher fall emissions being attributed to the “zero curtain” period when soil below the surface remains
 809 thawed for an extended period of time due to snow insulation (Zona et al., 2016; Kittler et al., 2017). Furthermore,
 810 soils can stay above the “zero curtain” range for an extended time into the fall and winter (Helbig et al., 2017),
 811 which may also be caused by snow insulation. The rapid onset of emissions in the spring following snowmelt could
 812 be attributed to the release of accumulated CH₄ (Friborg et al., 1997), and other high latitude sites have seen
 813 similarly sharp increases in CH₄ emissions at snowmelt (Dise, 1992; Windsor, 1992). However, not all studies in
 814 high latitudes have observed asymmetrical CH₄ emission peaks, pointing to the inherent complexity of these
 815 ecosystems (Rinne et al., 2007; Tagesson et al., 2012).



816



817

818 Figure 12. Site-year peak methane (CH₄) emission (a) and peak soil temperature (b) occur earlier in the season for sites
 819 with lower mean annual temperatures. (c) Gross primary productivity (GPP) tends to peak earlier in the season for
 820 warmer sites, though the trend is weak. All r² values are significant at p < 0.001. Each point represents a site-year of
 821 data.

822 3.3.3 Uniqueness of tropical wetlands

823 Tropical wetlands typically do not experience the large swings in temperature and GPP that contribute to
 824 CH₄ flux seasonality in temperate and northern sites. Indeed, the relatively constant high temperatures and high
 825 GPP in tropical ecosystems may lead to the lower ratio between seasonal amplitude and peak CH₄ flux compared
 826 with temperate and northern sites (Fig. 8b). Tropical flux sites have historically been under-studied, leading to a
 827 lack of synthesized information about these ecosystems. FLUXNET-CH4-Version-1.0 has five tropical wetland sites
 828 (latitude between 20° S and 20° N), and one tropical rice site, representing 13 site-years of data. ~~The-tropical~~These
 829 sites are especially insightful as they provide the first estimates of CH₄ fluxes from tropical, large seasonal
 830 floodplain systems ~~found in the tropics~~.

831
 832 We ~~find~~found a broad range of annual CH₄ fluxes across tropical sites in FLUXNET-CH4 Version 1.0.
 833 Annual CH₄ flux emissions from two Southeast Asian flooded peat forests were relatively low, 0.01 ± 0.1 and 9.5 ±
 834 0.6 g C m⁻² yr⁻¹ for ID-PAG and MY-MLM, respectively, which is consistent with annual CH₄ fluxes measured at
 835 another peat forest in Indonesia (Deshmukh et al., 2020). In contrast, mean annual CH₄ flux for a seasonally flooded
 836 swamp in the Brazilian Pantanal region (BR-NPW) was over twice as high as MY-MLM, at 19.2 ± 2.5 g C m⁻² yr⁻¹.
 837 Similarly high annual CH₄ fluxes were observed at the two Botswana swamp sites in the Okavango Delta (51.7 ±
 838 10.6 and 47.3 ± 3.7 g C m⁻² yr⁻¹ for BW-GUM and BW-NXR, respectively), one of which is seasonally inundated
 839 and surrounded by grassland (BW-NXR) and the other is a permanently flooded lagoon covered in a floating
 840 papyrus mat (BW-GUM). The relatively low fluxes found at the two Southeast Asian peat forest sites indicate that
 841 these ecosystems may be smaller CH₄ sources than expected, given their location in the humid tropics. Even the
 842 higher-emitting tropical sites in Brazil and Botswana are still well within the range of annual CH₄ flux typical in
 843 cooler latitudes (Fig. 1).

844 In addition to having highly variable CH₄ flux magnitudes, the tropical sites differ from each other in their
 845 seasonality. Methane-CH₄ flux ~~hit~~hit a minimum around July for two sites (BW-GUM, latitude 18.965 °S and MY-
 846 MLM, latitude 1.46 °N), while CH₄ flux ~~increases~~increased through July and the subsequent months for the other
 847 Botswana site, BW-NXR (latitude 19.548 °S). Site ID-Pag (latitude 2.32 °S) ~~has~~had minimal seasonality, whereas

848 the flooded forest site in Brazil (BR-NPW, latitude 16.49 °S) **has had** near-zero fluxes from approximately July to
 849 January, and consistently high fluxes for the remainder of the year. The rice site PH-RiF (latitude 14.14 °N) **has had**
 850 two annual CH₄ flux peaks, which is consistent with some other rice sites and likely reflects management practices.
 851 Baseline CH₄ flux values also **differed**, with the two Botswana sites having the highest off-season fluxes (29 and
 852 133 nmol m⁻² s⁻¹ for BW-NXR and BW-GUM, respectively, estimated by Timesat), MY-MLM having an intermediate
 853 baseline CH₄ flux (16 nmol m⁻² s⁻¹, estimated by Timesat), and the remainder of the sites having essentially zero flux
 854 at baseline. While more tropical wetland data will be needed to extract broad scale conclusions about these ecosystems,
 855 the six tropical sites in FLUXNET-CH4 provide an important starting point for synthesis studies and highlight tropical
 856 wetland CH₄ variability.

857

858 4.0 Data Availability

859 Half-hourly and daily aggregations are available for download at [https://fluxnet.org/data/fluxnet-ch4-](https://fluxnet.org/data/fluxnet-ch4-community-product/)
 860 [community-product/](https://fluxnet.org/data/fluxnet-ch4-community-product/), along with a table containing site metadata compiled from Table B2B3. Variable descriptions
 861 and units are provided in Table B1, and at [https://fluxnet.org/data/fluxnet-ch4-community-](https://fluxnet.org/data/fluxnet-ch4-community-product/)
 862 [product/-https://fluxnet.org/data/fluxnet-ch4-community-product/](https://fluxnet.org/data/fluxnet-ch4-community-product/). Each site has a unique FLUXNET-CH4 DOI as
 863 listed in Table B2B3. All site data used in this analysis are available under the CC BY 4.0
 864 (<https://creativecommons.org/licenses/by/4.0/>) copyright policy. (2
 865 additional sites in FLUXNET-CH4 are available under the more restrictive Tier 2 data policy,
 866 <https://fluxnet.org/data/data-policy/>; these sites are not used in our analysis). The individual site DOIs are provided
 867 below in Table 2. All seasonality parameters used in these analyses are available at
 868 <https://doi.org/10.5281/zenodo.44084684672601>.

869

870 **Table 2: Site identification (SITE_ID), data DOI, and DOI reference for each FLUXNET-CH4 site.**

SITE_ID	DOI	DOI_REFERENCE
AT-Neu	10.18140/FLX/1669365	Wohlfahrt et al., 2020.
BR-Npw	10.18140/FLX/1669368	Vourlitis et al., 2020.
BW-Gum	10.18140/FLX/1669370	Helfter, 2020a.
BW-Nxr	10.18140/FLX/1669518	Helfter, 2020b.
CA-SCB	10.18140/FLX/1669613	Sonnentag and Helbig, 2020a.
CA-SCC	10.18140/FLX/1669628	Sonnentag and Helbig, 2020b.
CH-Cha	10.18140/FLX/1669629	Hörtnagl et al., 2020a.
CH-Dav	10.18140/FLX/1669630	Hörtnagl et al., 2020b.
CH-Oe2	10.18140/FLX/1669631	Hörtnagl, et al., 2020c.

Field Code Changed

Formatted: Default Paragraph Font, Underline, Font color: Custom Color(17,85,204)

Formatted: Default Paragraph Font, Underline, Font color: Custom Color(17,85,204)

Formatted Table

CN-Hgu	10.18140/FLX/1669632	Niu and Chen, 2020.
DE-Dgw	10.18140/FLX/1669633	Sachs et al, 2020a.
DE-Hte	10.18140/FLX/1669634	Koebisch and Jurasinski, 2020.
DE-SfN	10.18140/FLX/1669635	Klatt et al., 2020.
DE-Zrk	10.18140/FLX/1669636	Sachs et al., 2020b.
FI-Hyy	10.18140/FLX/1669637	Mammarella et al. 2020.
FI-Lom	10.18140/FLX/1669638	Aurela et al., 2020.
FI-Si2	10.18140/FLX/1669639	Vesala et al., 2020a.
FI-Sii	10.18140/FLX/1669640	Vesala et al., 2020b
FR-LGt	10.18140/FLX/1669641	Jacotot et al., 2020.
HK-MPM	10.18140/FLX/1669642	Lai and Liu, 2020.
ID-Pag	10.18140/FLX/1669643	Sakabe et al., 2020.
IT-BCi	10.18140/FLX/1669644	Magliulo et al., 2020.
IT-Cas	10.18140/FLX/1669645	Manca and Goded, 2020.
JP-BBY	10.18140/FLX/1669646	Ueyama et al., 2020.
JP-Mse	10.18140/FLX/1669647	Iwata, 2020a.
JP-SwL	10.18140/FLX/1669648	Iwata, 2020b.
KR-CRK	10.18140/FLX/1669649	Ryu et al., 2020.
MY-MLM	10.18140/FLX/1669650	Tang et al., 2020.
NL-Hor	10.18140/FLX/1669651	Dolman et al., 2020a.
NZ-Kop	10.18140/FLX/1669652	Campbell and Goodrich, 2020.
PH-RiF	10.18140/FLX/1669653	AlbertAlberto and Wassmann, 2020.
RU-Ch2	10.18140/FLX/1669654	Goeckede, 2020.
RU-Che	10.18140/FLX/1669655	Merbold et al., 2020.
RU-Cok	10.18140/FLX/1669656	Dolman et al., 2020b.

RU-Fy2	10.18140/FLX/1669657	Varlagin, 2020.
SE-Deg	10.18140/FLX/1669659	Nilsson and Peichl, 2020.
UK-LBT	10.18140/FLX/1670207	Helfter, 2020c.
US-A03	10.18140/FLX/1669661	Billesbach and Sullivan, 2020a.
US-A10	10.18140/FLX/1669662	Billesbach and Sullivan, 2020b.
US-Atq	10.18140/FLX/1669663	Zona and Oechel, 2020a.
US-Beo	10.18140/FLX/1669664	Zona and Oechel, 2020b.
US-Bes	10.18140/FLX/1669665	Zona and Oechel, 2020c.
US-Bi1	10.18140/FLX/1669666	Rey-Sanchez et al., 2020a.
US-Bi2	10.18140/FLX/1669667	Rey-Sanchez et al., 2020b.
US-BZB	10.18140/FLX/1669668	Euskirchen and Edgar, 2020a.
US-BZF	10.18140/FLX/1669669	Euskirchen and Edgar, 2020b.
US-BZS	10.18140/FLX/1669670	Euskirchen and Edgar, 2020c.
US-CRT	10.18140/FLX/1669671	Chen and Chu, 2020a.
US-DPW	10.18140/FLX/1669672	Hinkle and Bracho, 2020.
US-EDN	10.18140/FLX/1669673	Oikawa, 2020.
US-EML	10.18140/FLX/1669674	Schuur, 2020.
US-Ho1	10.18140/FLX/1669675	Richardson and Hollinger, 2020.
US-HRA	10.18140/FLX/1669676	Runkle et al., 2020.
US-HRC	10.18140/FLX/1669677	Reba et al., 2020.
US-ICs	10.18140/FLX/1669678	Euskirchen et al., 2020d.
US-Ivo	10.18140/FLX/1669679	Zona and Oechel, 2020d.
US-LA1	10.18140/FLX/1669680	Holm et al., 2020a.
US-LA2	10.18140/FLX/1669681	Holm et al., 2020b.
US-Los	10.18140/FLX/1669682	Desai and Thom, 2020a.

US-MAC	10.18140/FLX/1669683	Sparks, 2020.
US-MRM	10.18140/FLX/1669684	Schafer, 2020.
US-Myb	10.18140/FLX/1669685	Matthes et al., 2020.
US-NC4	10.18140/FLX/1669686	Noormets et al., 2020.
US-NGB	10.18140/FLX/1669687	Torn and Dengel, 2020a.
US-NGC	10.18140/FLX/1669688	Torn and Dengel, 2020b.
US-ORv	10.18140/FLX/1669689	Bohrer and Morin, 2020a.
US-OWC	10.18140/FLX/1669690	Bohrer et al., 2020b.
US-PFa	10.18140/FLX/1669691	Desai and Thom, 2020b.
US-Snd	10.18140/FLX/1669692	Detto et al., 2020.
US-Sne	10.18140/FLX/1669693	Short et al., 2020.
US-Srr	10.18140/FLX/1669694	Windham-Myers et al., 2020.
US-StJ	10.18140/FLX/1669695	Vazquez-Lule and Vargas, 2020.
US-Tw1	10.18140/FLX/1669696	Valach et al., 2020a.
US-Tw3	10.18140/FLX/1669697	Chamberlain et al., 2020.
US-Tw4	10.18140/FLX/1669698	Eichelmann et al., 2020.
US-Tw5	10.18140/FLX/1669699	Valach et al., 2020b.
US-Twt	10.18140/FLX/1669700	Knox et al., 2020.
US-Uaf	10.18140/FLX/1669701	Iwata et al., 2020c.
US-WPT	10.18140/FLX/1669702	Chen and Chu, 2020b.

871

872

873

874 5.0 Conclusions

875 The breadth and scope of CH₄ flux data in the FLUXNET-CH₄ [Version 1.0](#) dataset make it possible to
876 study the global patterns of CH₄ fluxes, particularly for global freshwater wetlands which release a substantial

877 fraction of atmospheric CH₄. ~~We~~To help data users understand seasonal patterns within the dataset, we provide the
878 first global estimates of CH₄ flux patterns and predictors in CH₄ seasonality using freshwater wetland data. In the
879 seasonality analysis, we find that, on average, the seasonal increase in CH₄ emissions begins about three months
880 earlier and lasts about four months longer at the warmest sites compared with the coolest sites. We also find that the
881 beginning of the CH₄ emission season lags the beginning of seasonal soil warming by approximately one month,
882 with almost no instances of CH₄ emissions increasing before temperature increases. Additionally, roughly half the
883 sites have CH₄ emissions increasing prior to GPP increase; highlighting the importance of substrate ~~vs~~versus
884 temperature limitations on wetland CH₄ emissions. Furthermore, relative to warmer climates, wetland CH₄
885 emissions in cooler climates increase faster in the warming season and decrease slower in the cooling season. This
886 phenomenon has previously been noted on a regional scale and we show that it persists at the global scale.
887 Constraining the seasonality of CH₄ fluxes on a global scale can help improve the accuracy of global wetland
888 models.

Formatted: Subscript

889 FLUXNET-CH₄ is an important new resource for the research community, but critical data gaps and
890 opportunities remain. The current FLUXNET-CH₄ ~~Version 1.0~~dataset is biased towards sites in boreal and
891 temperate regions, which influence the relationships presented in our analyses. Tropical ecosystems are estimated to
892 account for 64% of potential natural CH₄ emissions (<30° N, Saunio et al., 2020) but only account for 13% of the
893 FLUXNET-CH₄ ~~Version 1.0~~ sites in the dataset. Unsurprisingly, tropical sites in our network do not represent the
894 range of bioclimatic wetland conditions present in the tropics. Therefore, while maintaining flux towers in tropical
895 ecosystems is challenging, it is necessary to further constrain the global CH₄ cycle. Coastal wetlands are also poorly
896 represented in FLUXNET-CH₄ even though there is evidence of substantial CH₄ emissions from these ecosystems,
897 so better representation across salinity gradients is warranted. Lastly, the average time series for FLUXNET-CH₄
898 Version 1.0 is relatively short, only 3.7 site-years on average compared with 7.2 for CO₂ sites in FLUXNET
899 (Pastorello et al., 2020). Adding additional site-years of data from existing sites, as a complement to adding new
900 sites, will increase the community's ability to explain interannual variability in CH₄ emission and seasonality.
901 Nevertheless, FLUXNET-CH₄ is an important and unprecedented resource with which to diagnose and understand
902 drivers of the global CH₄ cycle.

903

904 Author contribution

905 Kyle B. Delwiche oversaw the data release, performed the seasonality analysis, gathered metadata, and
906 prepared the manuscript with contributions from all co-authors. Sara Helen Knox gathered and standardized the
907 data, and gap-filled the CH₄ flux data. Avni Malhotra prepared the manuscript and gathered metadata. Etienne
908 Fluet-Chouinard did the representativeness analysis and prepared the manuscript. Gavin McNicol gathered data and
909 prepared the manuscript. Robert B. Jackson oversaw the data collection, processing, analysis, and release. Danielle
910 Christianson and You-Wei Cheah oversaw the FLUXNET-CH₄ dataset release on fluxnet.org. Dario Papale,
911 Eleonora Canfora, and Carlo Trotta did the data collection, curation, and ~~pre~~-processing for ~~a majority~~all of the ~~non-~~
912 ~~American~~ sites: outside North and South America. Remaining co-authors contributed eddy-covariance data to
913 FLUXNET-CH₄ ~~Version 1.0~~ dataset and/or participated in editing the manuscript.

914 Competing interests

915 The authors declare that they have no conflict of interest.

916

917

918 **Acknowledgements**

919 We acknowledge primary support from the Gordon and Betty Moore Foundation (Grant GBMF5439, “Advancing
920 Understanding of the Global Methane Cycle”; Stanford University) and from the John Wesley Powell Center for
921 Analysis and Synthesis of the U.S. Geological Survey (“Wetland FLUXNET Synthesis for Methane” working
922 group). Benjamin R. K. Runkle was supported by the U.S. National Science Foundation CBET CAREER Award
923 1752083. Ankur R. Desai acknowledges support of the DOE AmeriFlux Network Management Project. Masahito
924 Ueyama was supported by ArCS II (JPMXD1420318865) and JSPS KAKENHI (20K21849). Dario Papale and Nina
925 Buchmann acknowledge the support of the RINGO (GA 730944) H2020 EU project. Nina Buchmann and Kathrin
926 Fuchs acknowledge the SNF project M4P (40FA40_154245/1) and InnoFarm (407340_172433). Nina Buchmann
927 acknowledges support from the SNF for ICOS-CH Phases 1 and 2 (20FI21_148992, 20FI20_173691). Carlo Trotta
928 acknowledges the support of the E-SHAPE (GA 820852) H2020 EU project. William J. Riley was supported by the
929 US Department of Energy, BER, RGCN, RUBISCO project under contract no. DEAC02-05CH11231. Jessica
930 Turner acknowledges support from NSF GRFP (DGE-1747503) and NTL LTER (DEB-1440297). Minseok Kang
931 was supported by the National Research Foundation of Korea (NRF-2018 R1C1B6002917). Carole Helfter
932 acknowledges the support of the UK Natural Environment Research Council (the Global Methane Budget project,
933 grant number NE/N015746/1). Rodrigo Vargas acknowledges support from the National Science Foundation
934 (1652594). Dennis Baldocchi acknowledges the California Department of Water Resources for a funding contract
935 from the California Department of Fish and Wildlife and the United States Department of Agriculture (NIFA grant
936 #2011-67003-30371), as well as the U.S. Department of Energy’s Office of Science (AmeriFlux contract #7079856)
937 for funding the AmeriFlux core sites. US-A03 and US-A10 are operated by the Atmospheric Radiation
938 Measurement (ARM) user facility, a U.S. Department of Energy Office of Science user facility managed by the
939 Biological and Environmental Research Program (doi:10.5439/1025039, doi:10.5439/1025274,
940 doi:10.5439/1095578). Work at ANL was supported by the U.S. Department of Energy, Office of Science, Office of
941 Biological and Environmental Research, under contract DE-AC02-06CH11357. Any use of trade, firm, or product
942 names is for descriptive purposes only and does not imply endorsement by the U.S. Government. The CH-Dav, DE-
943 StN, FI-Hyy, FI-Lom, FI-Sii, FR-LGt, IT-BCi, SE-Deg and SE-Sto sites are part of the ICOS European Research
944 Infrastructure. Oliver Sonnentag acknowledges funding by the Canada Research Chairs, Canada Foundation for
945 Innovation Leaders Opportunity Fund, and Natural Sciences and Engineering Research Council Discovery Grant
946 Programs for work at CA-SCC and CA-SCB. Benjamin Poulter acknowledges support from the NASA Carbon
947 Cycle and Ecosystems Program. Derrick Lai acknowledges the support of the Research Grants Council of the Hong
948 Kong Special Administrative Region, China (Project No. CUHK 458913). We thank Nathaniel Goenawan for his
949 help with the representativeness analysis.

Formatted: Font: Times New Roman, 10 pt

Formatted: Normal, Space Before: 12 pt, After: 12 pt

Formatted: Font: Times New Roman, 10 pt

Formatted: Font: Times New Roman, 10 pt

Formatted: Font: Times New Roman, 10 pt

950

References

951
952
953

Abdalla, M., Hastings, A., Truu, J., Espenberg, M., Mander, Ü, Smith, P. Emissions of methane from northern peatlands: a review of management impacts and implications for future management options. *Ecol. Evol.*, 6, 7080-7102. <https://doi.org/10.1002/ece3.2469>.

954
955
956
957

Alberto, M. C. R., Wassmann, R., Gummert, M., Buresh, R. J., Quilty, J. R., Correa, T. Q., Centeno, C. A. R., & Oca, G. M. Straw incorporated after mechanized harvesting of irrigated rice affects net emissions of CH4 and CO2 based on eddy covariance measurements. *Field Crop. Res.*, 184, 162–175. <https://doi.org/10.1016/j.fcr.2015.10.004>, 2015.

958
959

Alberto, M., & Wassmann, R. FLUXNET-CH4 PH-RiF Philippines Rice Institute flooded. Philippines. <https://doi:10.18140/FLX/1669653>. 2020.

960
961
962

Anderson, D. E., Verma, S. B., & Rosenberg, N. J. Eddy correlation measurements of CO2, latent heat, and sensible heat fluxes over a crop surface. *Bound. Lay. Meteorol.*, 29(3), 263–272. <https://doi.org/10.1007/bf00119792>, 1984.

963
964
965
966
967

Anderson, F. E., Bergamaschi, B., Sturtevant, C., Knox, S., Hastings, L., Windham-Myers, L., Detto, M., Hestir, E. L., Drexler, J., Miller, R. L., Matthes, J. H., Verfaillie, J., Baldocchi, D., Snyder, R. L., & Fujii R. Variation of energy and carbon fluxes from a restored temperate freshwater wetland and implications for carbon market verification protocols. *J. of Geophys. Res. – Biogeo.*, 121(3), 777–795. <https://doi.org/10.1002/2015JG003083>. 2016.

968
969
970
971

Angle, J. C., Morin, T. H., Solden, L. M., Narrowe, A. B., Smith, G. J., Borton, M. A., Rey-Sanchez, C., Daly, R. A., Mirfenderesgi, G., Hoyt, D. W., Riley, W. J., Miller, C. S., Bohrer, G., & Wrighton, K. C. Methanogenesis in oxygenated soils is a substantial fraction of wetland methane emissions. *Nat. Comm.*, 8(1), 1567. <https://doi.org/10.1038/s41467-017-01753-4>, 2017.

972
973

Aurela, M., Lohila, A., J.-P., Hatakka, J., Rainne, J., Mäkelä, T., & Lauria, T. FLUXNET-CH4 FI-Lom Lompolojankka. Finland. <https://doi:10.18140/FLX/1669638>. 2020.

974
975
976
977
978

Bartlett, K. B., Bartlett, D. S., Harriss, R. C., & Sebacher, D. I. Methane emissions along a salt marsh salinity gradient. *Biogeochemistry*, 4(3), 183–202. <https://doi.org/10.1007/bf02187365>, 1987.
Bastviken, D., Tranvik, L. J., Downing, J. A., Crill, P. M., & Enrich-Prast, A. Freshwater methane emissions offset the continental carbon sink. *Science*, 331(6013), 50. <https://doi.org/10.1126/science.1196808>, 2011.

979
980

Billesbach, D., & Sullivan, R. FLUXNET-CH4 US-A03 ARM-AMF3-Olitok. United States. <https://doi:10.18140/FLX/1669661>. 2020a.

981
982

Billesbach, D., & Sullivan, R. FLUXNET-CH4 US-A10 ARM-NSA-Barrow. United States. <https://doi:10.18140/FLX/1669662>. 2020b.

983
984
985
986

Bloom, A. A., Bowman, K. W., Lee, M., Turner, A. J., Schroeder, R., Worden, J. R., Weidner, R., McDonald, K. C., & Jacob, D. J. A global wetland methane emissions and uncertainty dataset for atmospheric chemical transport models (WetCHARTs version 1.0). *Geosci. Model Dev.*, 10, 2141–2156. <https://doi.org/10.5194/gmd-10-2141-2017>, 2017.

987
988
989

Bridgman, S. D., Cadillo-Quiroz, H., Keller, J. K., & Zhuang, Q. Methane emissions from wetlands: biogeochemical, microbial, and modeling perspectives from local to global scales. *Glob. Change Biol.*, 19(5), 1325–1346. <https://doi.org/10.1111/gcb.12131>, 2013.

990
991

Bohrer, G., & Morin, T. H. FLUXNET-CH4 US-ORv Olentangy River Wetland Research Park. United States. <https://doi:10.18140/FLX/1669689>. 2020a.

992
993

Bohrer, G., Kerns, J., Morin, T. H., Rey-Sanchez, A. C., Villa, J., & Ju, Y. FLUXNET-CH4 US-OWC Old Woman Creek. United States. <https://doi:10.18140/FLX/1669690>. 2020b.

994
995

Campbell, D., & Goodrich, J. FLUXNET-CH4 NZ-Kop Kopuatai. New Zealand. <https://doi:10.18140/FLX/1669652>. 2020.

996
997

Castro-Morales, K., Kleinen, T., Kaiser, S., Zaehle, S., Kittler, F., Kwon, M. J., Beer, C., & Göckede, M. Year-round simulated methane emissions from a permafrost ecosystem in Northeast Siberia. *Biogeosciences*, 15(9), 2691–2722. <https://doi.org/10.5194/bg-15-2691-2018>, 2018.

998
999

Chadburn, S. E., Aalto, T., Aurela, M., Baldocchi, D., Biasi, C., Boike, J., Burke, E. J., Comyn-Platt, E., Dolman, A. J., Duran-Rojas, & Others. Modeled microbial dynamics explain the apparent temperature sensitivity of wetland methane emissions. *Global Biogeochemical Cycles*, 34(11). <https://doi.org/10.1029/2020gb006678>. 2020.

1000
1001
1002

Formatted: Underline

Formatted: Font: Times New Roman

Formatted: Normal, Space Before: 0 pt, After: 10 pt. Add space between paragraphs of the same style, Keep with next, Keep lines together

Formatted: Font: Times New Roman

Formatted: Keep with next, Keep lines together

Formatted: Font: Times New Roman, Font color: Black

Formatted: Normal, Add space between paragraphs of the same style, Keep with next, Keep lines together, Border: Top: (No border), Bottom: (No border), Left: (No border), Right: (No border), Between : (No border)

Formatted: Font: Times New Roman, Font color: Black

Formatted: Font: Times New Roman, Font color: Black

Formatted: Font: Times New Roman, Font color: Black

Formatted: Normal, Add space between paragraphs of the same style, Border: Top: (No border), Bottom: (No border), Left: (No border), Right: (No border), Between : (No border)

Formatted: Font: Times New Roman, Font color: Black

Formatted: Font: Times New Roman, Font color: Black

Formatted: Font: Times New Roman, Font color: Black

Formatted: Normal, Add space between paragraphs of the same style, Border: Top: (No border), Bottom: (No border), Left: (No border), Right: (No border), Between : (No border)

Formatted: Font: Times New Roman, Font color: Black

Formatted: Font: Times New Roman, Font color: Black

Formatted: Font: Times New Roman, Font color: Black

Formatted: Normal, Add space between paragraphs of the same style, Border: Top: (No border), Bottom: (No border), Left: (No border), Right: (No border), Between : (No border)

Formatted: Font: Times New Roman, Font color: Black

1003 Chamberlain, S. D., Oikawa, P., Sturtevant, C., Szutu, D., Verfaillie, J., & Baldocchi, D. FLUXNET-CH4 US-Tw3
1004 Twitchell Alfalfa. United States. <https://doi.org/10.18140/FLX/1669697>. 2020.

1005 Chambers, L. G., Ramesh Reddy, K., & Osborne, T. Z. Short-Term Response of Carbon Cycling to Salinity Pulses
1006 in a Freshwater Wetland. Soil Sci. Soc. Am. J., 75(5), 2000–2007.
1007 <https://doi.org/10.2136/sssaj2011.0026-10.2136/sssaj2011.0026>, 2011.

1008 Chang, K. Y., W. J. Riley, S. H. Knox, R. B. Jackson, G. McNicol, B. Poulter, M. Aurela, D. Baldocchi, S.
1009 Bansal, G. Bohrer, D. I. Campbell, A. Cescatti, H. Chu, K. B. Delwiche, A. Desai, E. Euskirchen, T.
1010 Friborg, M. Goeckede, G. Holm, M. Kang, T. Keenan, K. W. Krauss, A. Lohila, I. Mammarella, A.
1011 Miyata, M. B. Nilsson, A. Noormets, D. Papale, B. R. K. Runkle, Y. Ryu, T. Sachs, K. V. R. Schäfer,
1012 H. P. Schmid, N. Shurpali, O. Sonnentag, A. C. I. Tang, M. S. Torn, C. Trotta, M. Ueyama, R.
1013 Vargas, T. Vesala, L. Windham-Myers, Z. Zhang, & D. Zona. Global wetland methane emissions
1014 have hysteretic responses to seasonal temperature. In Review: Nature Communications. Chang, K.
1015 Y., W. J. Riley, S. H. Knox, R. B. Jackson, G. McNicol, B. Poulter, M. Aurela, D. Baldocchi, S. Bansal, G.
1016 Bohrer, D. I. Campbell, A. Cescatti, H. Chu, K. B. Delwiche, A. Desai, E. Euskirchen, T. Friborg, M.
1017 Goeckede, G. Holm, M. Kang, T. Keenan, K. W. Krauss, A. Lohila, I. Mammarella, A. Miyata, M. B. Nilsson,
1018 A. Noormets, D. Papale, B. R. K. Runkle, Y. Ryu, T. Sachs, K. V. R. Schäfer, H. P. Schmid, N. Shurpali, O.
1019 Sonnentag, A. C. I. Tang, M. S. Torn, C. Trotta, M. Ueyama, R. Vargas, T. Vesala, L. Windham-Myers, Z.
1020 Zhang, & D. Zona. Global wetland methane emissions have hysteretic responses to seasonal temperature.
1021 Nature Communications [In press]. 2021.

1022 Chanton, J. P., Glaser, P. H., Chasar, L. S., Burdige, D. J., Hines, M. E., Siegel, D. I., Tremblay, L. B., & Cooper,
1023 W. T. Radiocarbon evidence for the importance of surface vegetation on fermentation and methanogenesis in
1024 contrasting types of boreal peatlands. *Global Biogeochem. Cy.*, 22(4).
1025 <https://doi.org/10.1029/2008gb003274>. 2008.

1026 Chen, J., & Chu, H. FLUXNET-CH4 US-CRT Curtrice Walter-Berger cropland. United States.
1027 <https://doi.org/10.18140/FLX/1669671>. 2020a.

1028 Chen, J., & Chu, H. FLUXNET-CH4 US-WPT Winous Point North Marsh. United States.
1029 <https://doi.org/10.18140/FLX/1669702>. 2020b.

1030 Chu, H., Chen, J., Gottgens, J. F., Ouyang, Z., John, R., Czajkowski, K., & Becker, R. Net ecosystem methane and
1031 carbon dioxide exchanges in a Lake Erie coastal marsh and a nearby cropland. J. Geophys. Res.: Biogeo.,
1032 119(5), 722–740. <https://doi.org/10.1002/2013JG002520>. <https://doi.org/10.1002/2013JG002520>, 2014.

1033 Chu, H., Baldocchi, D. D., John, R., Wolf, S., & Reichstein, M. Fluxes all of the time? A primer on the temporal
1034 representativeness of FLUXNET. Journal of Geophysical Research: Biogeosciences, 122(2), 289–307.
1035 <https://doi.org/10.1002/2016JG003576>. 2017.

1036 Chu, H., Luo, X., Ouyang, Z., Chan, W. S., Dengel, S., Biraud, S. C., Torn, M. S., Metzger, S., Kumar, J., Arain, M.
1037 A., & Others. Representativeness of Eddy-Covariance flux footprints for areas surrounding AmeriFlux sites.
1038 Agricultural and Forest Meteorology, 301-302, 108350. <https://doi.org/10.1016/j.agrformet.2021.108350>.
1039 2021.

1040 Dalcin Martins, P., Hoyt, D. W., [10.1002/2016JG003576](https://doi.org/10.1002/2016JG003576), Bansal, S., Mills, C. T., Tffaily, M., Tangen, B. A.,
1041 Finocchiaro, R. G., Johnston, M. D., McAdams, B. C., Solensky, M. J., Smith, G. J., Chin, Y.-P., & Wilkins,
1042 M. J. Abundant carbon substrates drive extremely high sulfate reduction rates and methane fluxes in Prairie
1043 Pothole Wetlands. Global Change Biology, 23(8), 3107–3120. <https://doi.org/10.1111/gcb.13633>, 2017.

1044 Dean, J. F., Middelburg, J. J., Röckmann, T., Aerts, R., Blauw, L. G., Egger, M., Jetten, M. S. M., de Jong, A. E. E.,
1045 Meisel, O. H., Rasigraf, O., Slomp, C. P., in't Zandt, M. H., & Dolman, A. J. Methane Feedbacks to the Global
1046 Climate System in a Warmer World. Rev. Geophys., 56(1), 207–250.
1047 <https://doi.org/10.1002/2017rg000559>, 2018.

1048 Deemer, B. R., Harrison, J. A., Li, S., Beaulieu, J. J., DelSontro, T., Barros, N., Bezerra-Neto, J. F., Powers, S. M.,
1049 Dos Santos, M. A., & Vonk, J. A. Greenhouse Gas Emissions from Reservoir Water Surfaces: A New Global
1050 Synthesis. Bioscience, 66(11), 949–964. <https://doi.org/10.1093/biosci/biw117>, 2016.

1051 Dengel, S., Zona, D., Sachs, T., Aurela, M., Jammot, M., Parmentier, F.-J. W., Oechel, W., & Vesala, T. Testing the
1052 applicability of neural networks as a gap-filling method using CH4 flux data from high latitude wetlands.
1053 Biogeosciences, 10, 8185–8200. <https://doi.org/10.5194/bg-10-8185-2013>.

1054 Deshmukh, C. S., Julius, D., Evans, C. D., Nardi, Susanto, A. P., Page, S. E., Gauci, V., Laurén, A., Sabiham, S.,
1055 Agus, F., Asyhari, A., Kurnianto, S., Suardiwerianto, Y., & Desai, A. R. Impact of forest plantation on
1056 methane emissions from tropical peatland. Glob. Change Biol., 26, 2477-2495.
1057 <https://doi.org/10.4141/gcb.15019>, 2020.

Formatted: Font: Times New Roman, Font color: Black

Formatted: Normal, Add space between paragraphs of the same style, Border: Top: (No border), Bottom: (No border), Left: (No border), Right: (No border), Between : (No border)

Formatted: Font: Times New Roman, Font color: Black

Formatted: Font: Times New Roman, Font color: Black

Formatted: Font: Times New Roman, Font color: Black

Formatted: Font: Times New Roman, Font color: Black

Formatted: Normal, Add space between paragraphs of the same style, Border: Top: (No border), Bottom: (No border), Left: (No border), Right: (No border), Between : (No border)

Formatted: Font: Times New Roman, Font color: Black

Formatted: Normal, Add space between paragraphs of the same style, Border: Top: (No border), Bottom: (No border), Left: (No border), Right: (No border), Between : (No border)

Formatted: Font: Times New Roman

Formatted: Font: Times New Roman

Formatted: Font: Times New Roman, Font color: Black

Formatted: Font: Times New Roman, Font color: Black

Formatted: Font: Times New Roman, Font color: Black

Formatted: Font: Times New Roman, Font color: Black, Pattern: Clear, Highlight

Formatted: Font: Times New Roman, Font color: Black

Formatted: Font: Times New Roman, Font color: Black

1058 Desai, A. R., & Thom, J. FLUXNET-CH4 US-Los Lost Creek. United States. <https://doi.org/10.18140/FLX/1669682>.
1059 2020a.
1060 Desai, A. R., & Thom, J. FLUXNET-CH4 US-PFa Park Falls/WLEF. United States.
1061 <https://doi.org/10.18140/FLX/1669691>. 2020b.
1062 Desjardins, R. L. A technique to measure CO2 exchange under field conditions. *Int. J. Biometeorol.*, 18(1), 76–83.
1063 <https://doi.org/10.1007/bf01450667>. 1974.
1064 Detto, M., Sturtevant, C., Oikawa, P., Verfaillie, J., & Baldocchi, D. FLUXNET-CH4 US-Snd Sherman Island.
1065 United States. <https://doi.org/10.18140/FLX/1669692>. 2020.
1066 Dise, N. Winter fluxes of methane from Minnesota peatlands. *Biogeochemistry*, 17(2).
1067 <https://doi.org/10.1007/bf00002641>. 1992.
1068 Dolman, H., Hendriks, D., Parmentier, F.-J., Marchesini, L. B., Dean, J., & van Huissteden, K. FLUXNET-CH4
1069 NL-Hor Horstermeer. Netherlands. <https://doi.org/10.18140/FLX/1669651>. 2020a.
1070 Dolman, H., van der Molen, H., Parmentier, F.-J., Marchesini, L. B., Dean, J., van Huissteden, K., & Maximov, T.
1071 FLUXNET-CH4 RU-Cok Chokurdakh. Russian Federation. <https://doi.org/10.18140/FLX/1669656>. 2020b.
1072 Eichelmann, E., Knox, S., Rey Sanchez, C., Valach, A., Sturtevant, C., Szutu, D., Verfaillie, J., & Baldocchi, D.
1073 FLUXNET-CH4 US-Tw4 Twitchell East End Wetland. United States. <https://doi.org/10.18140/FLX/1669698>.
1074 2020.
1075 Eklundh, L., & Jönsson, P. TIMESAT: A Software Package for Time-Series Processing and Assessment of
1076 Vegetation Dynamics. *Remote Sensing Time Series* (pp. 141–158). https://doi.org/10.1007/978-3-319-15967-6_7. 2015.
1077
1078 Etheridge, D. M., Steele, L. P., Francey, R. J., & Langenfelds, R. L. Atmospheric methane between 1000 A.D. and
1079 present: Evidence of anthropogenic emissions and climatic variability. *J. Geophys. Res. – Atmos.*, 103(D13),
1080 15979–15993. <https://doi.org/10.1029/98jd00923>. 1998.
1081 Etminan, M., Myhre, G., Highwood, E. J., & Shine, K. P. Radiative forcing of carbon dioxide, methane, and nitrous
1082 oxide: A significant revision of the methane radiative forcing. *Geophys. Res. Lett.*, 43(24), 12,614–12,623.
1083 <https://doi.org/10.1002/2016gl071930>. 2016.
1084 Euskirchen, E., & Edgar, C. FLUXNET-CH4 US-BZB Bonanza Creek Thermokarst Bog. United States.
1085 <https://doi.org/10.18140/FLX/1669668>. 2020a.
1086 Euskirchen, E., & Edgar, C. FLUXNET-CH4 US-BZF Bonanza Creek Rich Fen. United States.
1087 <https://doi.org/10.18140/FLX/1669669>. 2020b.
1088 Euskirchen, E., & Edgar, C. FLUXNET-CH4 US-BZS Bonanza Creek Black Spruce. United States.
1089 <https://doi.org/10.18140/FLX/1669670>. 2020c.
1090 Euskirchen, E., Bret-Harte, M., & Edgar, C. Marion Bret-Harte. FLUXNET-CH4 US-ICs Imnavait Creek
1091 Watershed Wet Sedge Tundra. United States. <https://doi.org/10.18140/FLX/1669678>. 2020d.
1092 Gallant, A. The Challenges of Remote Monitoring of Wetlands. *Remote Sensing*, 7(8), 10938–10950.
1093 <https://doi.org/10.3390/rs70810938>. 2015.
1094 Göeckede, M., Kittler, F., & Schaller, C. Quantifying the impact of emission outbursts and non-stationary
1095 flow on eddy covariance CH4 flux measurements using wavelet techniques. *Biogeosciences*, 16(16),
1096 3443–3434. Gallant, A. The Challenges of Remote Monitoring of Wetlands. *Remote Sensing*, 7(8), 10938–
1097 10950. <https://doi.org/10.3390/rs70810938>. 2015.
1098 Göeckede, M., Kittler, F., & Schaller, C. Quantifying the impact of emission outbursts and non-stationary flow on
1099 eddy covariance CH4 flux measurements using wavelet techniques. *Biogeosciences*, 16(16), 3113–3131.
1100 <https://doi.org/10.5194/bg-16-3113-2019>. 2019.
1101 Goeckede, M. FLUXNET-CH4 RU-Ch2 Chersky reference. Russian Federation.
1102 <https://doi.org/10.18140/FLX/1669654>. 2020.
1103 Gu, L., Post, W. M., Baldocchi, D. D., Andrew Black, T., Suyker, A. E., Verma, S. B., Vesala, T., & Wofsy, S. C.
1104 Characterizing the Seasonal Dynamics of Plant Community Photosynthesis Across a Range of Vegetation
1105 Types. In: Noormets A. (eds) Phenology of Ecosystem Processes. Springer, New York, NY, pp. 35–58.
1106 https://doi.org/10.1007/978-1-4419-0026-5_2. 2009.
1107 Hargreaves, K. J., Fowler, D., Pitcairn, C. E. R., & Aurela, M. Annual methane emission from Finnish mires
1108 estimated from eddy covariance campaign measurements. *Theor. Appl. Climatol.*, 70, 203–213.
1109 <https://doi.org/10.1007/s007040170015>. 2001.
1110 Hargrove, W. W., Hoffman, F. M., & Law, B. E. New analysis reveals representativeness of the AmeriFlux
1111 network. *Eos, Transactions American Geophysical Union*, 84(48), 529.
1112 <https://doi.org/10.1029/2003EO480004>. 2003.

- Formatted:** Font: Times New Roman, Font color: Black
- Formatted:** Normal, Add space between paragraphs of the same style, Border: Top: (No border), Bottom: (No border), Left: (No border), Right: (No border), Between : (No border)
- Formatted:** Font: Times New Roman, Font color: Black
- Formatted:** Font: Times New Roman, Font color: Black
- Formatted:** Normal, Add space between paragraphs of the same style, Border: Top: (No border), Bottom: (No border), Left: (No border), Right: (No border), Between : (No border)
- Formatted:** Font: Times New Roman, Font color: Black
- Formatted:** Font: Times New Roman, Font color: Black
- Formatted:** Normal, Add space between paragraphs of the same style, Border: Top: (No border), Bottom: (No border), Left: (No border), Right: (No border), Between : (No border)
- Formatted:** Font: Times New Roman, Font color: Black
- Formatted:** Font: Times New Roman, Font color: Black
- Formatted:** Font: Times New Roman, Font color: Black
- Formatted:** Normal, Add space between paragraphs of the same style, Border: Top: (No border), Bottom: (No border), Left: (No border), Right: (No border), Between : (No border)
- Formatted:** Font: Times New Roman, Font color: Black, Pattern: Clear, Highlight
- Formatted:** Font: Times New Roman, Font color: Black
- Formatted:** Font: Times New Roman, Font color: Black
- Formatted:** Normal, Add space between paragraphs of the same style, Border: Top: (No border), Bottom: (No border), Left: (No border), Right: (No border), Between : (No border)
- Formatted:** Font: Times New Roman, Font color: Black, Not Expanded by / Condensed by
- Formatted:** Font: Times New Roman, Font color: Black
- Formatted:** Font: Times New Roman, Font color: Black
- Formatted:** Font: Times New Roman, Font color: Black
- Formatted:** Font: Times New Roman, Font color: Black

1113 Hatala, J. A., Detto, M., & Baldocchi, D. D. Gross ecosystem photosynthesis causes a diurnal pattern in methane
1114 emission from rice. *Geophys. Res. Lett.*, 39(6).
1115 <https://doi.org/10.1029/2012gl051303>, 2012.

1116 Helbig, M., Quinton, W. L., & Sonnentag, O. Warmer spring conditions increase annual methane emissions from a
1117 boreal peat landscape with sporadic permafrost. *Environ. Res. Lett.*, 12(11), 115009.
1118 <https://doi.org/10.1088/1748-9326/aa8c85>, 2017.

1119 Helfter, C., Tremper, A. H., Halios, C. H., Kotthaus, S., Björkegren, A., Grimmond, C. S. B., Barlow, J. F., &
1120 Nemitz, E. Spatial and temporal variability of urban fluxes of methane, carbon monoxide and carbon dioxide
1121 above London, UK. *Atmos. Chem. Phys.* 16, 10543-10557. <https://doi.org/10.5194/acp-2016-216-ae4-10.5194/acp-2016-216-ac1>, 2016.

1122 Helfter, C. FLUXNET-CH4 BW-Gum Guma. Botswana. <https://doi:10.18140/FLX/1669370>. 2020a.

1123 Helfter, C. FLUXNET-CH4 BW-Nxr Nxaraga. Botswana. <https://doi:10.18140/FLX/1669518>. 2020b.

1124 Helfter, C. FLUXNET-CH4 UK-LBT London_BT. United Kingdom. <https://doi:10.18140/FLX/1670207>. 2020c.

1125 Hinkle, C. R., & Bracho, R. FLUXNET-CH4 US-DPW Disney Wilderness Preserve Wetland. United States.
1126 <https://doi:10.18140/FLX/1669672>. 2020.

1127 Hoffman, F. M., Kumar, J., Mills, R. T., & Hargrove, W. W. Representativeness-based sampling network design for
1128 the State of Alaska. *Landscape Ecol.*, 28(8), 1567–1586. <https://doi.org/10.1007/s10980-013-9902-0>, 2013.

1129 Hollinger, D. Y., and A. D. Richardson. *Uncertainty in Eddy Covariance Measurements and Its Application to*
1130 *Physiological Models. Tree Physiology* 25 (7): 873–85. <https://doi.org/10.1093/treephys/25.7.873>. 2005.

1131 Holm, G. O., Perez, B. C., McWhorter, D. E., Krauss, K. W., Raynie, R. C., & Killebrew, C. J. FLUXNET-CH4
1132 US-LA1 Pointe-aux-Chenes Brackish Marsh. United States. <https://doi:10.18140/FLX/1669680>. 2020a.

1133 Holm, G. O., Perez, B. C., McWhorter, D. E., Krauss, K. W., Raynie, R. C., & Killebrew, C. J. FLUXNET-CH4
1134 US-LA2 Salvador WMA Freshwater Marsh. United States. <https://doi:10.18140/FLX/1669681>. 2020b.

1135 Hörtnagl, L., Feigenwinter, I., Fuchs, K., Merbold, L., Buchmann, N., Eugster, W., Zeeman, M., Pluess, P., Käslin,
1136 F., Meier, P., Koller, P., & Baur, T. FLUXNET-CH4 CH-Cha Chamau. Switzerland.
1137 <https://doi:10.18140/FLX/1669629>. 2020a.

1138 Hörtnagl, Lukas, Werner Eugster, Lutz Merbold, Nina Buchmann, Mana Gharun, Sophia Etzold, Rudolf Haesler,
1139 Matthias Haeni, Philip Meier, Florian Käslin, Thomas Baur, & Peter Pluess. FLUXNET-CH4 CH-Dav Davos.
1140 Switzerland. <https://doi:10.18140/FLX/1669630>. 2020b.

1141 Hörtnagl, Lukas, Regine Maier, Werner Eugster, Nina Buchmann, Carmen Emmel, Patrick Koller, Thomas Baur,
1142 Peter Pluess, Florian Käslin, & Philip Meier. FLUXNET-CH4 CH-Oe2 Oensingen crop. Switzerland.
1143 <https://doi:10.18140/FLX/1669631>. 2020c.

1144 Hwang, Y., Ryu, Y., Huang, Y., Kim, J., Iwata, H., & Kang, M. Comprehensive assessments of carbon dynamics in
1145 an intermittently-irrigated rice paddy. *Agr. Forest Met.*, 285–286, 107933.
1146 <https://doi.org/10.1016/j.agrformet.2020.107933>, 2020.

1147 Iwata, H., Mano, M., Ono, K., Tokida, T., Kawazoe, T., Kosugi, Y., Sakabe, A., Takahashi, K., & Miyata, A.
1148 Exploring sub-daily to seasonal variations in methane exchange in a single-crop rice paddy in central Japan.
1149 *Atmos. Environ.*, 179, 156–165.
1150 <https://doi.org/10.1016/j.atmosenv.2018.02.045>, 2018.

1151 Iwata, Hiroki. FLUXNET-CH4 JP-Mse Mase rice paddy field. Japan. <https://doi:10.18140/FLX/1669647>. 2020a.

1152 Iwata, Hiroki. FLUXNET-CH4 JP-SwL Suwa Lake. Japan. <https://doi:10.18140/FLX/1669648>. 2020b.

1153 Iwata, Hiroki, Masahito Ueyama, & Yoshinobu Harazono. FLUXNET-CH4 US-Uaf University of Alaska,
1154 Fairbanks. United States. <https://doi:10.18140/FLX/1669701>. 2020c.

1155 Jacotot, Adrien, Sébastien Gogo, & Fatima Laggoun-Défarge. FLUXNET-CH4 FR-LGt La Gnette. France.
1156 <https://doi:10.18140/FLX/1669641>. 2020.

1157 Jung, M., Reichstein, M., & Bondeau, A. Towards global empirical upscaling of FLUXNET eddy covariance
1158 observations: validation of a model tree ensemble approach using a biosphere model. *Biogeosciences*, 6(10),
1159 2001–2013. <https://doi.org/10.5194/bg-6-2001-2009>, 2009.

1160 Jung, M., Schwalm, C., Migliavacca, M., Walther, S., Camps-Valls, G., Koirala, S., Anthoni, P., Besnard, S.,
1161 Bodesheim, P., Carvalhais, N., Chevallier, F., Gans, F., Goll, D. S., Haverd, V., Kohler, P., Ichii, K., Jain, A.
1162 K., Liu, J., Lombardozi, D., Nabel, J. E. M. S., Nelson, J. A., O’Sullivan, M., Pallandt, M., Papale, D., Peters,
1163 W., Pongrats, J., Rodenbeck, C., Sitch, S., Tramonatana, G., Walker, A., Weber, U., & Reichstein, M. Scaling
1164 carbon fluxes from eddy covariance sites to globe: synthesis and evaluation of the FLUXCOM approach.
1165 *Biogeosciences*, 17(5), 1343–1365. <https://doi.org/10.5194/bg-17-1343-2020>,
1166 2020.

Formatted: Font: Times New Roman, Font color: Black

Formatted: Font: Times New Roman, Font color: Black

Formatted: Font: Times New Roman, Font color: Black

Formatted: Font: Times New Roman, Font color: Black

Formatted: Normal, Add space between paragraphs of the same style, Border: Top: (No border), Bottom: (No border), Left: (No border), Right: (No border), Between : (No border)

Formatted: Font: Times New Roman, Font color: Black

Formatted: Font: Times New Roman, Font color: Black

Formatted: Normal, Add space between paragraphs of the same style, Border: Top: (No border), Bottom: (No border), Left: (No border), Right: (No border), Between : (No border)

Formatted: Font: Times New Roman, Font color: Black

Formatted: Font: Times New Roman, Font color: Black

Formatted: Font: Times New Roman, Font color: Black

Formatted: Normal, Add space between paragraphs of the same style, Border: Top: (No border), Bottom: (No border), Left: (No border), Right: (No border), Between : (No border)

Formatted: Font: Times New Roman, Font color: Black

Formatted: Font: Times New Roman, Font color: Black

1169 Kim, Y., Johnson, M. S., Knox, S. H., Andrew Black, T., Dalmagro, H. J., Kang, M., Kim, J., & Baldocchi, D. Gap-
 1170 filling approaches for eddy covariance methane fluxes: A comparison of three machine learning algorithms and
 1171 a traditional method with principal component analysis. *Glob. Change Biol.*, 26(3), 1499–1518.
 1172 <https://doi.org/10.1111/gcb.14845>, 2020.

1173 Kittler, F., Heimann, M., Kolle, O., Zimov, N., Zimov, S., & Göckede, M. Long-Term Drainage Reduces CO₂
 1174 Uptake and CH₄ Emissions in a Siberian Permafrost Ecosystem: Drainage impact on Arctic carbon cycle.
 1175 *Global Biogeochem. Cy.*, 31(12), 1704–1717.
 1176 <https://doi.org/10.1002/2017GB005774>, 2017.

1177 Klatt, Janina, Hans Peter Schmid, Matthias Mauder, & Rainer Steinbrecher. FLUXNET-CH₄ DE-SfN Schechenfilz
 1178 Nord. Germany. <https://doi.org/10.18140/FLX/1669635>. 2020.

1179 Knox, S. H., Sturtevant, C., Matthes, J. H., Koteen, L., Verfaillie, J., & Baldocchi, D. Agricultural peatland
 1180 restoration: effects of land-use change on greenhouse gas (CO₂ and CH₄) fluxes in the Sacramento-San
 1181 Joaquin Delta. *Glob. Change Biol.*, 21(2), 750–765. <https://doi.org/10.1111/gcb.12745>. 2015.

1182 Knox, S. H., Matthes, J. H., Sturtevant, C., Oikawa, P. Y., Verfaillie, J., & Baldocchi, D. Biophysical controls on
 1183 interannual variability in ecosystem-scale CO₂ and CH₄ exchange in a California rice paddy. *J. Geophys. Res.-
 1184 Biogeophys.*, 121(3), 978–1001. <https://doi.org/10.1002/2015jg003247>, 2016.

1185 Knox, S. H., Jackson, R. B., Poulter, B., McNicol, G., Fluet-Chouinard, E., Zhang, Z., Hugelius, G., Bousquet, P.,
 1186 Canadell, J. G., Saunio, M., Papale, D., Chu, H., Keenan, T. F., Baldocchi, D., Torn, M. S., Mammarella, I.,
 1187 Trotta, C., Aurela, M., Bohrer, G., Campbell, D. L., Cescatti, A., Chamberlain, S., Chen, J., Chen, W., Dengel,
 1188 S., Desai, A. R., Euskirchen, E., Friborg, T., Gasbarra, D., Godeed, I., Goeckede, M., Heimann, M., Helbig, M.,
 1189 Hirano, T., Hollinger, D. Y., Iwata, H., & Others. FLUXNET-CH₄ Synthesis Activity: Objectives,
 1190 Observations, and Future Directions. *B. Am. Meteorol. Soc.*, 100(12), 2607–2632.
 1191 <https://doi.org/10.1175/bams-d-18-0268.1>, 2019.

1192 Knox, Sara, Jaclyn Hatala Matthes, Joseph Verfaillie, & Dennis Baldocchi. FLUXNET-CH₄ US-Twt Twitchell
 1193 Island. United States. <https://doi.org/10.18140/FLX/1669700>. 2020.

1194 Koebisch, F., Jurasinski, G., Koch, M., Hofmann, J., & Glatzel, S. Controls for multi-scale temporal variation in
 1195 ecosystem methane exchange during the growing season of a permanently inundated fen. *Agr. Forest
 1196 Meteorol.*, 204, 94–105. <https://doi.org/10.1016/j.agrformet.2015.02.002>,
 1197 2015.

1198 Koebisch, F., Winkel, M., Liebner, S., Liu, B., Westphal, J., Schmiedinger, I., Spitz, A., Gehre, M., Jurasinski, G.,
 1199 Köhler, S., & Others. Sulfate deprivation triggers high methane production in a disturbed and rewetted coastal
 1200 peatland. *Biogeosciences*, 16, 1937–1953. <https://doi.org/10.5194/bg-16-1937-2019>, 2019.

1201 Koebisch, Franziska, & Gerald Jurasinski. FLUXNET-CH₄ DE-Hte Huettelmoor. Germany.
 1202 <https://doi.org/10.18140/FLX/1669634>. 2020.

1203 Kumar, J., Hoffman, F. M., Hargrove, W., Kuznetsova A., Brockhoff P. B., & Christensen R. H. B. “ImerTest
 1204 Package: Tests in Linear Mixed
 1205 Effects Models.” *Journal of Statistical Software*, 82(13), 1–26.
 1206 <https://doi.org/10.18637/jss.v082.i13>. 2017.

1207 Kwon, M. J., Beulig, F., Ilie, I., Wildner, M., Küsel, K., Merbold, L., Mahecha, M. D., Zimov, N., Zimov, S. A.,
 1208 Heimann, M., Schuur, E. A. G., Kostka, J. E., Kolle, O., Hilke, I., & Göckede, M. Plants, microorganisms, and
 1209 soil temperatures contribute to a decrease in methane fluxes on a drained Arctic floodplain. *Global Change
 1210 Biology*, 23(6), 2396–2412. <https://doi.org/10.1111/gcb.13558>. 2017.

1211 W., & Collier, N. Understanding the representativeness of FLUXNET for upscaling carbon flux from eddy
 1212 covariance measurements. *Earth Syst. Sci. Data* [preprint]. <https://doi.org/10.5194/essd-2016-36>. 2016.

1213 Lai, D. Y. F. Methane Dynamics in Northern Peatlands: A Review. *Pedosphere*, 19(4), 409–421.
 1214 [https://doi.org/10.1016/s1002-0160\(09\)00003-4](https://doi.org/10.1016/s1002-0160(09)00003-4), 2009.

1215 Lai, D. Y. F., Roulet, N. T., & Moore, T. R. The spatial and temporal relationships between CO₂ and CH₄
 1216 exchange in a temperate ombrotrophic bog. *Atmos. Environ.*, 89, 249–259.
 1217 <https://doi.org/10.1016/j.atmosenv.2014.02.034>, 2014.

1218 Lai, Derrick Y. F., & Jianguo Liu. FLUXNET-CH₄ HK-MPM Mai Po Mangrove. Hong Kong.
 1219 <https://doi.org/10.18140/FLX/1669642>. 2020.

1220 Lasslop, G., Reichstein, M., Papale, D., Richardson, A. D., Arneith, A., Barr, A., Stoy, P., & Wohlfahrt, G.
 1221 Separation of net ecosystem exchange into assimilation and respiration using a light response curve approach:
 1222 critical issues and global evaluation. *Glob. Change Biol.*, 16(1), 187–208. <https://doi.org/10.1111/j.1365-2486.2009.02041.x>,
 1223 2010.

Formatted: Font: Times New Roman, Font color: Black

Formatted: Font: Times New Roman, Font color: Black

Formatted: Font: Times New Roman, Font color: Black

Formatted: Normal, Add space between paragraphs of the same style, Border: Top: (No border), Bottom: (No border), Left: (No border), Right: (No border), Between : (No border)

Formatted: Font: Times New Roman, Font color: Black

Formatted: Font: Times New Roman, Font color: Black

Formatted: Font: Times New Roman, Font color: Black

Formatted: Normal, Add space between paragraphs of the same style, Border: Top: (No border), Bottom: (No border), Left: (No border), Right: (No border), Between : (No border)

Formatted: Font: Times New Roman, Font color: Black

Formatted: Font: Times New Roman, Font color: Black, Pattern: Clear, Highlight

Formatted: Font: Times New Roman, Font color: Black

Formatted: Font: Times New Roman, Font color: Black

Formatted: Normal, Add space between paragraphs of the same style, Border: Top: (No border), Bottom: (No border), Left: (No border), Right: (No border), Between : (No border)

Formatted: Font: Times New Roman, Font color: Black

Formatted: Font: Times New Roman, Font color: Black

Formatted: Font: Times New Roman, Font color: Black

Formatted: Normal, Add space between paragraphs of the same style, Border: Top: (No border), Bottom: (No border), Left: (No border), Right: (No border), Between : (No border)

Formatted: Font: Times New Roman, Font color: Black

1224 Liu, J., Zhou, Y., Valach, A., Shortt, R., Kasak, K., Rey-Sanchez, C., Hemes, K. S., Baldocchi, D., & Lai, D. Y. F.
1225 Methane emissions reduce the radiative cooling effect of a subtropical estuarine mangrove wetland by half.
1226 *Glob. Change Biol.*, 26(9), 4998–5016. <https://doi.org/10.1111/gcb.15247>, 2020.

1227 Madsen, K., Nielsen, H. B., & Tingleff, O. Methods for non-linear least squares problems. Informatics and
1228 Mathematical Modelling, Technical University of Denmark. 2nd Edition. 2004.

1229 Magliulo, Vincenzo, Paul Di Tommasi, Daniela Famulari, Daniele Gasbarra, Luca Vitale, Antonio Manco,
1230 Ferdinando di Matteo, Andrea Esposito, & Maurizio Tosca. FLUXNET-CH4 IT-BCi Borgo Cioffi. Italy.
1231 <https://doi:10.18140/FLX/1669644>. 2020.

1232 Mahecha, M. D., Gans, F., Sippel, S., Donges, J. F., Kaminski, T., Metzger, S., Migliavacca, M., Papale, D.,
1233 Rammig, A., & Zscheischler, J. Detecting impacts of extreme events with ecological in situ monitoring
1234 networks. *Biogeosciences*, 14(18), 4255–4277. <https://doi.org/10.5194/bg-14-4255-2017>, 2017.

1235 Malhotra, A., & Roulet, N. T. Environmental correlates of peatland carbon fluxes in a thawing landscape: do
1236 transitional thaw stages matter? *Biogeosciences*, 12(10), 3119–3130. <https://doi.org/10.5194/bg-12-3119-2015>, 2015.

1237 Mammarella, Ivan, Timo Vesala, Petri Keronen, Pasi Kolari, Samuli Launiainen, Jukka Pumpanen, Üllar Rannik,
1238 Erkki Siivola, Janne Levula, & Toivo Pohja. FLUXNET-CH4 FI-Hyy Hyttiala. Finland.
1239 <https://doi:10.18140/FLX/1669637>. 2020.

1240 Manca, Giovanni, & Ignacio Goded. FLUXNET-CH4 IT-Cas Castellaro. Italy. <https://doi:10.18140/FLX/1669645>.
1241 2020.

1242 Mastepanov, M., Sigsgaard, C., Tagesson, T., Ström, L., Tamstorf, M. P., Lund, M., & Christensen, T. R.
1243 Revisiting factors controlling methane emissions from high-Arctic tundra. *Biogeosciences*, 10(7), 5139–5158.
1244 <https://doi.org/10.5194/bg-10-5139-2013>, 2013.

1245 Matthes, Jaclyn Hatala, Cove Sturtevant, Patty Oikawa, Samuel D Chamberlain, Daphne Szutu, Ariane Arias Ortiz,
1246 Joseph Verfaillie, & Dennis Baldocchi. FLUXNET-CH4 US-Myb Mayberry Wetland. United States.
1247 <https://doi:10.18140/FLX/1669685>. 2020.

1248 Matthews, E., Johnson, M. S., Genovese, V., Du, J., & Bastviken, D. Methane emission from high latitude lakes:
1249 methane-centric lake classification and satellite-driven annual cycle of emissions. *Sci. Rep.* - UK, 10(1), 12465.
1250 <https://doi.org/10.1038/s41598-020-68246-1>, 2020.

1251 Megonigal, J. P., Whalen, S. C., Tissue, D. T., Bovard, B. D., Allen, A. S., & Albert, D. B. A Plant-Soil-
1252 Atmosphere Microcosm for Tracing Radiocarbon from Photosynthesis through Methanogenesis. *Soil Sci. Soc.
1253 Am. J.* 63(3), 665–671.
1254 <https://doi.org/10.2136/sssaj1999.03615995006300030033x>, 1999.

1255 Meijide, A., Manca, G., Goded, I., Magliulo, V., Di Tommasi, P., Seufert, G., & Cescatti, A. Seasonal trends and
1256 environmental controls of methane emissions in a rice paddy field in Northern Italy. *Biogeosciences*, 8(12),
1257 3809. <https://doi.org/10.5194/bg-8-3809-2011>, 2011.

1258 Melloh, R. A., & Crill, P. M. Winter methane dynamics in a temperate peatland. *Global Biogeochem. Cy.*, 10(2),
1259 247–254. <https://doi.org/10.1029/96gb00365>, 1996.

1260 Melton, J. R., Wania, R., Hodson, E. L., Poulter, B., Ringeval, B., Spahni, R., Bohn, T., Avis, C. A., Beerling, D. J.,
1261 Chen, G., Eliseev, A. V., Denisov, S. N., Hopcroft, P. O., Lettenmaier, D. P., Riley, W. J., Singarayer, J. S.,
1262 Subin, Z. M., Tian, H., Zürcher, S., & Others. Present state of global wetland extent and wetland methane
1263 modelling: conclusions from a model inter-comparison project (WETCHIMP). *Biogeosciences*, 10(2), 753–
1264 788. <https://doi.org/10.5194/bg-10-753-2013>, 2013.

1265 Merbold, Lutz, Corinna Rebmann, & Chiara Corradi. FLUXNET-CH4 RU-Che Cherski. Russian Federation.
1266 <https://doi:10.18140/FLX/1669655>. 2020.

1267 Meyer, H., & Pebesma, E. Predicting into unknown space? Estimating the area of applicability of spatial prediction
1268 models. *arXiv [stat.ML]*. <http://arxiv.org/abs/2005.07939>, 2020.

1269 Mishra, S. R., Pattnaik, P., Sethunathan, N., & Adhya, T. K. Anion-Mediated Salinity Affecting Methane
1270 Production in a Flooded Alluvial Soil. *Geomicrobiol. J.*, 20(6), 579–586.
1271 <https://doi.org/10.1080/713851467>, 2003.

1272 Moffat, A. M., Papale, D., Reichstein, M., Hollinger, D. Y., Richardson, A. D., Barr, A. G., Beckstein, C., Braswell,
1273 B. H., Churkina, G., Desai, A. R., Falge, E., Gove, J. H., Heimann, M., Hui, D., Jarvis, A. J., Kattge, J.,
1274 Noormets, A., & Stauch, V. J. Comprehensive comparison of gap-filling techniques for eddy covariance net
1275 carbon fluxes. *Agr. Forest Meteorol.*, 147(3), 209–232.
1276 <https://doi.org/10.1016/j.agrformet.2007.08.011>, 2007.

- Formatted: Font: Times New Roman, Font color: Black
- Formatted: Font: Times New Roman, Font color: Black
- Formatted: Normal, Add space between paragraphs of the same style, Border: Top: (No border), Bottom: (No border), Left: (No border), Right: (No border), Between : (No border)
- Formatted: Font: Times New Roman, Font color: Black, Pattern: Clear, Highlight
- Formatted: Font: Times New Roman, Font color: Black
- Formatted: Font: Times New Roman, Font color: Black
- Formatted: Normal, Add space between paragraphs of the same style, Border: Top: (No border), Bottom: (No border), Left: (No border), Right: (No border), Between : (No border)
- Formatted: Font: Times New Roman, Font color: Black
- Formatted: Font: Times New Roman, Font color: Black
- Formatted: Normal, Add space between paragraphs of the same style, Border: Top: (No border), Bottom: (No border), Left: (No border), Right: (No border), Between : (No border)
- Formatted: Font: Times New Roman, Font color: Black
- Formatted: Font: Times New Roman, Font color: Black
- Formatted: Font: Times New Roman, Font color: Black, Pattern: Clear, Highlight
- Formatted: Font: Times New Roman, Font color: Black
- Formatted: Default Paragraph Font, Font: Times New Roman
- Formatted: Font: Times New Roman, Font color: Black
- Formatted: Default Paragraph Font, Font: Times New Roman
- Formatted: Font: Times New Roman, Font color: Black
- Formatted: Normal, Add space between paragraphs of the same style, Border: Top: (No border), Bottom: (No border), Left: (No border), Right: (No border), Between : (No border)
- Formatted ... [1]
- Formatted: Font: Times New Roman, Font color: Black
- Formatted ... [2]
- Formatted: Font: Times New Roman, Font color: Black
- Formatted ... [3]
- Formatted: Font: Times New Roman, Font color: Black

1279 [Myhre, G., D. Shindell, F.-M. Bréon, W. Collins, J. Fuglestedt, J. Huang, D. Koch, J.-F. Lamarque, D.](#)
1280 [Lee, B. Mendoza, T. Nakajima, A. Robock, G. Stephens, T. Takemura and H. Zhang. Anthropogenic](#)
1281 [and Natural Radiative Forcing Supplementary Material. In Stocker, T.F., D. Qin, G.-K. Plattner, M.](#)
1282 [Tignor, S.K. Allen, J. Boschung, A. Nauels, Y. Xia, V. Bex and P.M. Midgley \(Ed.\), *Climate Change*](#)
1283 [2013: The Physical Science Basis. Contribution of Working Group I to the Fifth Assessment Report](#)
1284 [of the Intergovernmental Panel on Climate Change.](#) Myhre, G., D. Shindell, F.-M. Bréon, W. Collins, J.
1285 [Fuglestedt, J. Huang, D. Koch, J.-F. Lamarque, D. Lee, B. Mendoza, T. Nakajima, A. Robock, G. Stephens,](#)
1286 [T. Takemura and H. Zhang. Anthropogenic and Natural Radiative Forcing Supplementary Material. In Stocker,](#)
1287 [T.F., D. Qin, G.-K. Plattner, M. Tignor, S.K. Allen, J. Boschung, A. Nauels, Y. Xia, V. Bex and P.M. Midgley](#)
1288 [\(Ed.\), *Climate Change 2013: The Physical Science Basis. Contribution of Working Group I to the Fifth*](#)
1289 [Assessment Report of the Intergovernmental Panel on Climate Change, 2013.](#)

1290 Nemitz, E., Mammarella, I., Ibrom, A., Aurela, M., Burba, G. G., Dengel, S., Gielen, B., Grelle, A., Heinesch, B.,
1291 Herbst, M., Hörtnagl, L., Klemmedtsson, L., Lindroth, A., Lohila, A., McDermitt, D. K., Meier, P., Merbold, L.,
1292 Nelson, D., Nicolini, G., & Others. Standardisation of eddy-covariance flux measurements of methane and
1293 nitrous oxide. *Int. Agrophys.*, 32(4), 517–549. [https://doi.org/10.1515/intag-2017-](https://doi.org/10.1515/intag-2017-0042)
1294 [0042](https://doi.org/10.1515/intag-2017-0042), 2018.

1295 Nielsen, H. B. Damping parameter in Marquardt's method. Department of Mathematical Modeling, IMM, Technical
1296 University of Denmark. Technical Report, IMM-REP-1999-05. 1999.

1297 Nilsson, Mats B., & Matthias Peichl. FLUXNET-CH4 SE-Deg Degero. Sweden.
1298 <https://doi.org/10.18140/FLX/1669659>. 2020.

1299 Niu, Shuli, & Weinan Chen. FLUXNET-CH4 CN-Hgu Hongyuan. China. <https://doi.org/10.18140/FLX/1669632>. 2020.

1300 Noormets, Asko, John King, Bhaskar Mitra, Guofang Miao, Maricar Aguilos, Kevan Minick, Prajaya Prajapati,
1301 Jean-Christophe Domec, Jonathan Furst, & Maxwell Wightman. FLUXNET-CH4 US-NC4
1302 NC AlligatorRiver. United States. <https://doi.org/10.18140/FLX/1669686>. 2020.

1303 Oikawa, P. Y., Jenerette, G. D., Knox, S. H., Sturtevant, C., Verfaillie, J., Dronova, I., Poindexter, C. M.,
1304 Eichelmann, E., & Baldocchi, D. D. Evaluation of a hierarchy of models reveals importance of substrate
1305 limitation for predicting carbon dioxide and methane exchange in restored wetlands. *J. Geophys. Res.-Biogeo.*,
1306 122(1), 145–167. <https://doi.org/10.1002/2016JG003438>. 2017.

1307 Oikawa, Patty. FLUXNET-CH4 US-EDN Eden Landing Ecological Reserve. United States.
1308 <https://doi.org/10.18140/FLX/1669673>. 2020.

1309 Olefeldt, D., Turetsky, M. R., Crill, P. M., & McGuire, A. D. Environmental and physical controls on northern
1310 terrestrial methane emissions across permafrost zones. *Glob. Change Biol.*, 19(2), 589–603.
1311 <https://doi.org/10.1111/gcb.12071>, 2013.

1312 Papale, D., Andrew Black, T., Carvalhais, N., Cescatti, A., Chen, J., Jung, M., Kiely, G., Lasslop, G., Mahecha, M.
1313 D., Margolis, H., Merbold, L., Montagnani, L., Moors, E., Olesen, J. E., Reichstein, M., Tramontana, G., van
1314 Gorsel, E., Wohlfahrt, G., & Ráduly, B. Effect of spatial sampling from European flux towers for estimating
1315 carbon and water fluxes with artificial neural networks. *J. Geophys. Res.-Biogeo.*, 120(10), 1941–1957.
1316 <https://doi.org/10.1002/2015jg002997>; [10.1002/2015jg002997](https://doi.org/10.1002/2015jg002997), 2015.

1317 Parmentier, F. J. W., van Huissteden, J., van der Molen, M. K., Schaepman-Strub, G., Karsanaev, S. A., Maximov,
1318 T. C., & Dolman, A. J. Spatial and temporal dynamics in eddy covariance observations of methane fluxes at a
1319 tundra site in northeastern Siberia. *J. Geophys. Res.*, 116(G3), 1368.
1320 <https://doi.org/10.1029/2010JG001637>, 2011.

1321 Pastorello, G., Trotta, C., Canfora, E., Chu, H., Christianson, D., Cheah, Y.-W., Poindexter, C., Chen, J.,
1322 Elbashaandy, A., Humphrey, M., Isaac, P., Polidori, D., Ribeca, A., van Ingen, C., Zhang, L., Amiro, B.,
1323 Ammann, C., Arain, M. A., Ardo, J., & Others. The FLUXNET2015 dataset and the ONEFlux processing
1324 pipeline for eddy covariance data. *Scientific Data*, 7(1), 225. [https://doi.org/10.1038/s41597-020-0534-](https://doi.org/10.1038/s41597-020-0534-3)
1325 [3](https://doi.org/10.1038/s41597-020-0534-3), 2020.

1326 Pattnaik, P., Mishra, S. R., Bharati, K., Mohanty, S. R., Sethunathan, N., & Adhya, T. K. Influence of salinity on
1327 methanogenesis and associated microflora in tropical rice soils. *Microbiol. Res.*, 155(3), 215–220.
1328 [https://doi.org/10.1016/S0944-5013\(00\)80035-X](https://doi.org/10.1016/S0944-5013(00)80035-X), 2000.

1329 Poffenbarger, H. J., Needelman, B. A., & Patrick Megonigal, J. Salinity Influence on Methane Emissions from
1330 Tidal Marshes. *Wetlands*, 31(5), 831–842. [https://doi.org/10.1007/s13157-011-](https://doi.org/10.1007/s13157-011-0197-0)
1331 [0197-0](https://doi.org/10.1007/s13157-011-0197-0), 2011.

1332 Poulter, B., Bousquet, P., Canadell, J. G., Ciais, P., Peregón, A., Saunio, M., Arora, V. K., Beerling, D. J., Brovkin,
1333 V., Jones, C. D., Joos, F., Gedney, N., Ito, A., Kleinen, T., Koven, C. D., McDonald, K., Melton, J. R., Peng,
1334 C., Peng, S., & Others. Global wetland contribution to 2000–2012 atmospheric methane growth rate dynamics.

Formatted: Default Paragraph Font, Font: Times New Roman

Formatted: Font: Times New Roman, Font color: Black

Formatted: Default Paragraph Font, Font: Times New Roman

Formatted: Font: Times New Roman, Font color: Black

Formatted: Font: Times New Roman, Font color: Black

Formatted: Normal, Add space between paragraphs of the same style, Border: Top: (No border), Bottom: (No border), Left: (No border), Right: (No border), Between : (No border)

Formatted: Font: Times New Roman, Font color: Black

Formatted: Normal, Add space between paragraphs of the same style, Border: Top: (No border), Bottom: (No border), Left: (No border), Right: (No border), Between : (No border)

Formatted: Default Paragraph Font, Font: Times New Roman

Formatted: Font: Times New Roman, Font color: Black

Formatted: Default Paragraph Font, Font: Times New Roman

Formatted: Font: Times New Roman, Font color: Black

Formatted: Default Paragraph Font, Font: Times New Roman

Formatted: Font: Times New Roman, Font color: Black

Formatted: Default Paragraph Font, Font: Times New Roman

Formatted: Font: Times New Roman, Font color: Black

Formatted: Default Paragraph Font, Font: Times New Roman

Formatted: Font: Times New Roman, Font color: Black

Formatted: Default Paragraph Font, Font: Times New Roman

Formatted: Font: Times New Roman, Font color: Black

1335 Environ. Res. Lett., 12(9), 094013. <https://doi.org/10.1088/1748-9326/aa8391>,
1336 2017.

1337 Reba, Michele, Benjamin Runkle, & Kosana Suvocarev. FLUXNET-CH4 US-HRC Humnoke Farm Rice Field –
1338 Field C. United States. <https://doi:10.18140/FLX/1669677>. 2020.

1339 Reichstein, M., Falge, E., Baldocchi, D., Papale, D., Aubinet, M., Bernhofer, P., Bernhofer, C., Buchmann, N.,
1340 Gilmanov, T., Granier, A., Grunwald, T., Havrankova, K., Ilvesniemi, H., Janous, D., Knohl, A., Laurila, T.,
1341 Lohila, A., Loustau, D., Matteucci, G., & Others. On the separation of net ecosystem exchange into
1342 assimilation and ecosystem respiration: review and improved algorithm. *Glob. Change Biol.*, 11(9), 1424–
1343 1439). <https://doi.org/10.1111/j.1365-2486.2005.001002.x>, 2005.

1344 Rey-Sanchez, Camilo, Daphne Szutu, Robert Shortt, Samuel D. Chamberlain, Joseph Verfaillie, & Dennis
1345 Baldocchi. FLUXNET-CH4 US-Bi1 Bouldin Island Alfalfa. United States. <https://doi:10.18140/FLX/1669666>.
1346 2020a.

1347 Rey-Sanchez, Camilo, Daphne Szutu, Kyle Hemes, Joseph Verfaillie, & Dennis Baldocchi. FLUXNET-CH4 US-
1348 Bi2 Bouldin Island corn. United States. <https://doi:10.18140/FLX/1669667>. 2020b.

1349 Richardson, A. D., Hollinger, D. Y., Burba, G. G., Davis, K. J., Flanagan, L. B., Katul, G. G., William Munger, J.,
1350 Ricciuto, D. M., Stoy, P. C., Suyker, A. E., Verma, S. B., & Wofsy, S. C. A multi-site analysis of random error
1351 in tower-based measurements of carbon and energy fluxes. *Agr. Forest Meteorol.*, 136(1), 1–18.
1352 <https://doi.org/10.1016/j.agrformet.2006.01.007>, 2006.

1353 Richardson, A. D., & Hollinger, D. Y. A method to estimate the additional uncertainty in gap-filled NEE resulting
1354 from long gaps in the CO2 flux record. *Agr. Forest Meteorol.*, 147(3), 199–208.
1355 <https://doi.org/10.1016/j.agrformet.2007.06.004>, 2007.

1356 Richardson, A. D., Mahecha, M. D., Falge, E., Kattge, J., Moffat, A. M., Papale, D., Reichstein, M., Stauch, V. J.,
1357 Braswell, B. H., Churkina, G., Kruijt, B., & Hollinger, D. Y. Statistical properties of random CO2 flux
1358 measurement uncertainty inferred from model residuals. *Agr. Forest Meteorol.*, 148(1), 38–50.
1359 <https://doi.org/10.1016/j.agrformet.2007.09.004>, 2008.

1360 Richardson, A. D., Aubinet, M., Barr, A. G., Hollinger, D. Y., Ibrom, A., Lasslop, G., & Reichstein, M.
1361 *Uncertainty quantification. Eddy Covariance: A Practical Guide to Measurement and Data Analysis.*
1362 (eds) Aubinet, M., Vesala, T., Papale, D., Springer Atmospheric Sciences, 2012.

1363 Richardson, A. D., Aubinet, M., Barr, A. G., Hollinger, D. Y., Ibrom, A., Lasslop, G., & Reichstein, M. *Uncertainty quantification. Eddy
1364 Covariance: A Practical Guide to Measurement and Data Analysis.* (eds) Aubinet, M., Vesala, T., Papale, D.,
1365 Springer Atmospheric Sciences, 2012.

1366 Richardson, Andrew D, & David Y Hollinger. FLUXNET-CH4 US-Ho1 Howland Forest (main tower). United
1367 States. <https://doi:10.18140/FLX/1669675>. 2020.

1368 Rinne, J., Riutta, T., Pihlatie, M., Aurela, M., Haapanala, S., Tuovinen, J.-P., Tuittila, E.-S., & Vesala, T. Annual
1369 cycle of methane emission from a boreal fen measured by the eddy covariance technique. *Tellus B*, 59(3), 449–
1370 457. <https://doi.org/10.1111/j.1600-0889.2007.00261.x>, 2007.

1371 Runkle, B. R. K., Suvočarev, K., Reba, M. L., Reavis, C. W., Smith, S. F., Chiu, Y.-L., & Fong, B. Methane
1372 Emission Reductions from the Alternate Wetting and Drying of Rice Fields Detected Using the Eddy
1373 Covariance Method. *Envir. Sci. Tech.*, 53(2), 671–681.
1374 <https://doi.org/10.1021/acs.est.8b05535>, 2019.

1375 Runkle, Benjamin, Michele Reba, & Kosana Suvocarev. FLUXNET-CH4 US-HRA Humnoke Farm Rice Field –
1376 Field A. United States. <https://doi:10.18140/FLX/1669676>. 2020.

1377 Ryu, Youngryel, Minseok Kang, & Jongho Kim. FLUXNET-CH4 KR-CRK Cheorwon Rice paddy. Korea,
1378 Republic of. <https://doi:10.18140/FLX/1669649>. 2020.

1379 Sachs, T., Giebel, M., Boike, J., & Kutzbach, L. Environmental controls on CH4 emission from polygonal tundra
1380 on the microsite scale in the Lena river delta, Siberia: CONTROLS ON TUNDRA CH4 FLUX AND
1381 SCALING. *Glob. Change Biol.*, 16(11) 3096 – 3110. <https://doi.org/10.1111/j.1365-2486.2010.02232.x>, 2010.

1382 Sachs, Torsten, Christian Wille, & Eric Larmanou. FLUXNET-CH4 DE-Dgw Dagowsee. Germany.
1383 <https://doi:10.18140/FLX/1669633>. 2020a.

1384 Sachs, Torsten, Christian Wille, Eric Larmanou, & Daniela Franz. FLUXNET-CH4 DE-Zrk Zarnekow. Germany.
1385 <https://doi:10.18140/FLX/1669636>. 2020b.

1386 Sakabe, Ayaka, Masayuki Itoh, Takashi Hirano, & Kitso Kusin. FLUXNET-CH4 ID-Pag Palangkaraya undrained
1387 forest. Indonesia. <https://doi:10.18140/FLX/1669643>. 2020.

1388 Saunio, M., Bousquet, P., Poulter, B., Peregon, A., Ciais, P., Canadell, J. G., Dlugokencky, E. J., Etiope, G.,
1389 Bastviken, D., Houweling, S., Janssens-Maenhout, G., Tubiello, F. N., Castaldi, S., Jackson, R. B., Alexe, M.,

Formatted: Default Paragraph Font, Font: Times New Roman

Formatted: Font: Times New Roman, Font color: Black

Formatted: Normal, Add space between paragraphs of the same style, Border: Top: (No border), Bottom: (No border), Left: (No border), Right: (No border), Between : (No border)

Formatted: Default Paragraph Font, Font: Times New Roman

Formatted: Font: Times New Roman, Font color: Black

Formatted: Normal, Add space between paragraphs of the same style, Border: Top: (No border), Bottom: (No border), Left: (No border), Right: (No border), Between : (No border)

Formatted: Default Paragraph Font, Font: Times New Roman

Formatted: Font: Times New Roman, Font color: Black

Formatted: Default Paragraph Font, Font: Times New Roman

Formatted: Font: Times New Roman, Font color: Black

Formatted: Default Paragraph Font, Font: Times New Roman

Formatted: Font: Times New Roman, Font color: Black

Formatted: Default Paragraph Font, Font: Times New Roman

Formatted: Font: Times New Roman, Font color: Black

Formatted: Normal, Add space between paragraphs of the same style, Border: Top: (No border), Bottom: (No border), Left: (No border), Right: (No border), Between : (No border)

Formatted: Default Paragraph Font, Font: Times New Roman

Formatted: Font: Times New Roman, Font color: Black

Formatted: Default Paragraph Font, Font: Times New Roman

Formatted: Font: Times New Roman, Font color: Black

Formatted: Font: Times New Roman, Font color: Black

Formatted ... [4]

Formatted ... [5]

Formatted: Font: Times New Roman, Font color: Black

Formatted ... [6]

1391 Arora, V. K., Beerling, D. J., Bergamaschi, P., Blake, D. R., & Others. The global methane budget 2000–2012.
 1392 Earth Syst. Sci. Data, 8, 697–751. <https://doi.org/10.5194/essd-8-697-2016>, 2016.

1393 Saunio, M., Stavert, A. R., Poulter, B., Bousquet, P., Canadell, J. G., Jackson, R. B., Raymond, P. A.,
 1394 Dlugokencky, E. J., Houweling, S., Patra, P. K., Ciais, P., Arora, V. K., Bastviken, D., Bergamaschi, P., Blake,
 1395 D. R., Brailsford, G., Bruhwiler, L., Carlson, K. M., Carrol, M., & Others. The Global Methane Budget 2000–
 1396 2017. Earth Syst. Sci. Data, 12, 1561–1623. [https://doi.org/10.5194/essd-12-
 1397 1561-2020](https://doi.org/10.5194/essd-12-1561-2020), 2020.

1398 Schafer, Karina. FLUXNET-CH4 US-MRM Marsh Resource Meadowlands Mitigation Bank. United States.
 1399 <https://doi:10.18140/FLX/1669684>. 2020.

1400 Schuur, E.A. FLUXNET-CH4 US-EML Eight Mile Lake Permafrost thaw gradient, Healy Alaska. United States.
 1401 <https://doi:10.18140/FLX/1669674>. 2020.

1402 Seyfferth, A. L., Bothfeld, F., Vargas, R., Stuckey, J. W., Wang, J., Kearns, K., Michael, H. A., Guimond, J., Yu,
 1403 X., & Sparks, D. L. Spatial and temporal heterogeneity of geochemical controls on carbon cycling in a tidal
 1404 salt marsh. Geochim. Cosmochim. Ac., 282, 1–18.
 1405 <https://doi.org/10.1016/j.gca.2020.05.013>, 2020.

1406 Shortt, Robert, Kyle Hemes, Daphne Szutu, Joseph Verfaillie, & Dennis Baldocchi. FLUXNET-CH4 US-Sne
 1407 Sherman Island Restored Wetland. United States. <https://doi:10.18140/FLX/1669693>. 2020.

1408 Sims, D. A., Rahman, A. F., Cordova, V. D., El-Masri, B. Z., Baldocchi, D. D., Flanagan, L. B., Goldstein, A. H.,
 1409 Hollinger, D. Y., Misson, L., Monson, R. K., Oechel, W. C., Schmid, H. P., Wofsy, S. C., & Xu, L. On the use
 1410 of MODIS EVI to assess gross primary productivity of North American ecosystems. J. Geophys. Res.-Biogeo.
 1411 111(G4). <https://doi.org/10.1029/2006jg000162>, 2006.

1412 Sonnentag, Oliver, & Manuel Helbig. FLUXNET-CH4 CA-SCB Scotty Creek Bog. Canada.
 1413 <https://doi:10.18140/FLX/1669613>. 2020a.

1414 Sonnentag, Oliver, & Manuel Helbig. FLUXNET-CH4 CA-SCC Scotty Creek Landscape. Canada. [https://
 1415 doi:10.18140/FLX/1669628](https://doi:10.18140/FLX/1669628). 2020b.

1416 Spahni, R., Wania, R., Neef, L., van Weele, M., Pison, I., Bousquet, P., Frankenberg, C., Foster, P. N., Joos, F.,
 1417 Prentice, I. C., & van Velthoven, P. Constraining global methane emissions and uptake by ecosystems. In
 1418 Biogeosciences, 8(6), 1643–1665. <https://doi.org/10.5194/bg-8-1643-2011>, 2011.

1419 Sparks, Jed P. FLUXNET-CH4 US-MAC MacArthur Agro-Ecology. United States.
 1420 <https://doi:10.18140/FLX/1669683>. 2020.

1421 Sturtevant, C. S., Ruddell, B. L., Knox, S. H., Verfaillie, J. G., Matthes, J. H., Oikawa, P. Y., & Baldocchi, D. D.
 1422 Identifying scale-emergent, nonlinear, asynchronous processes of wetland methane exchange. J. Geophys.
 1423 Res.-Biogeo., 121, 188–204. <https://doi.org/10.1002/2015JG003054>, 2016.

1424 Tagesson, T., Mölder, M., Mastepanov, M., Sigsgaard, C., Tamstorf, M. P., Lund, M., Falk, J. M., Lindroth, A.,
 1425 Christensen, T. R., & Ström, L. Land-atmosphere exchange of methane from soil thawing to soil freezing in a
 1426 high-Arctic wet tundra ecosystem. Glob. Change Biol., 18(6), 1928–1940. [https://doi.org/10.1111/j.1365-
 1427 2486.2012.02647.x](https://doi.org/10.1111/j.1365-2486.2012.02647.x), 2012.

1428 Tang, Angela Che Ing, Guan Xhuan Wong, Lulie Melling, Edward Baran Aeries, Joseph Wenceslaus Waili, Kevin
 1429 Kemudang Musin, Kim San Lo, & Frankie Kiew. FLUXNET-CH4 MY-MLM Maludam National Park.
 1430 Malaysia. <https://doi:10.18140/FLX/1669650>. 2020.

1431 Taoka, T., Iwata, H., Hirata, R., Takahashi, Y., Miyabara, Y., & Itoh, M. Environmental Controls on
 1432 Diffusive and Ebullitive Methane Emission at a Sub-Daily Time Scale in the Littoral Zone of a Mid-
 1433 Latitude Shallow Lake-Taoka, T., Iwata, H., Hirata, R., Takahashi, Y., Miyabara, Y., & Itoh, M.
 1434 Environmental Controls on Diffusive and Ebullitive Methane Emission at a Sub-Daily Time Scale in the
 1435 Littoral Zone of a Mid-Latitude Shallow Lake. J. Geophys. Res.-Biogeo., 125(9),
 1436 <https://doi.org/10.1029/2020JG005753>. 2020.

1437 Torn, Margaret, & Sigrid Dengel. FLUXNET-CH4 US-NGB NGEE Arctic Barrow. United States. [https://
 1438 doi:10.18140/FLX/1669687](https://doi:10.18140/FLX/1669687). 2020a.

1439 Torn, Margaret, & Sigrid Dengel. FLUXNET-CH4 US-NGC NGEE Arctic Council. United States.
 1440 <https://doi:10.18140/FLX/1669688>. 2020b.

1441 Treat, C. C., Anthony Bloom, A., & Marushchak, M. E. Nongrowing season methane emissions—a significant
 1442 component of annual emissions across northern ecosystems. Glob. Change Biol., 24(8), 3331–3343.
 1443 <https://doi.org/10.1111/gcb.14137>, 2018.

1444 Turetsky, M. R., Kotowska, A., Bubier, J., Dise, N. B., Crill, P., Hornibrook, E. R. C., Minkinen, K., Moore, T. R.,
 1445 Myers-Smith, I. H., Nykänen, H., Olefeldt, D., Rinne, J., Saarnio, S., Shurpali, N., Tuittila, E.-S., Waddington,

- Formatted:** Default Paragraph Font, Font: Times New Roman
- Formatted:** Font: Times New Roman, Font color: Black
- Formatted:** Default Paragraph Font, Font: Times New Roman
- Formatted:** Font: Times New Roman, Font color: Black
- Formatted:** Normal, Add space between paragraphs of the same style, Border: Top: (No border), Bottom: (No border), Left: (No border), Right: (No border), Between : (No border)
- Formatted:** Default Paragraph Font, Font: Times New Roman
- Formatted:** Font: Times New Roman, Font color: Black
- Formatted:** Normal, Add space between paragraphs of the same style, Border: Top: (No border), Bottom: (No border), Left: (No border), Right: (No border), Between : (No border)
- Formatted:** Default Paragraph Font, Font: Times New Roman
- Formatted:** Font: Times New Roman, Font color: Black
- Formatted:** Normal, Add space between paragraphs of the same style, Border: Top: (No border), Bottom: (No border), Left: (No border), Right: (No border), Between : (No border)
- Formatted:** Default Paragraph Font, Font: Times New Roman
- Formatted:** Font: Times New Roman, Font color: Black
- Formatted:** Default Paragraph Font, Font: Times New Roman
- Formatted:** Font: Times New Roman, Font color: Black
- Formatted:** Default Paragraph Font, Font: Times New Roman
- Formatted:** Default Paragraph Font, Font: Times New Roman
- Formatted:** Font: Times New Roman, Font color: Black
- Formatted:** Default Paragraph Font, Font: Times New Roman
- Formatted:** Default Paragraph Font, Font: Times New Roman
- Formatted:** Font: Times New Roman, Font color: Black
- Formatted:** Default Paragraph Font, Font: Times New Roman
- Formatted:** Default Paragraph Font, Font: Times New Roman
- Formatted:** Default Paragraph Font, Font: Times New Roman
- Formatted:** Font: Times New Roman, Font color: Black

1446 J. M., White, J. R., Wickland, K. P., & Wilmking, M. A synthesis of methane emissions from 71 northern,
1447 temperate, and subtropical wetlands. *Glob. Change Biol.*, 20(7), 2183–2197.
1448 <https://doi.org/10.1111/gcb.12580>, 2014.

1449 Ueyama, Masahito, Takashi Hirano, & Yasuhiro Kominami. FLUXNET-CH4 JP-BBY Bibai bog, Japan.
1450 <https://doi.org/10.18140/FLX/1669646>. 2020.

1451 Valach, Alex, Daphne Szutu, Elke Eichelmann, Sara Knox, Joseph Verfaillie, & Dennis Baldocchi. FLUXNET-CH4
1452 US-Tw1 Twitchell Wetland West Pond. United States. <https://doi.org/10.18140/FLX/1669696>. 2020a.

1453 Valach, Alex, Kuno Kasak, Daphne Szutu, Joseph Verfaillie, & Dennis Baldocchi. FLUXNET-CH4 US-Tw5 East
1454 Pond Wetland. United States. <https://doi.org/10.18140/FLX/1669699>. 2020b.

1455 Varlagin, Andrej. FLUXNET-CH4 RU-Fy2 Fyodorovskoye dry spruce. Russian Federation.
1456 <https://doi.org/10.18140/FLX/1669657>. 2020.

1457 Vazquez-Lule, Alma, & Rodrigo Vargas. FLUXNET-CH4 US-StJ St Jones Reserve. United States.
1458 <https://doi.org/10.18140/FLX/1669695>. 2020.

1459 [Vázquez-Lule, A., & Vargas, R. Biophysical drivers of net ecosystem and methane exchange across phenological
1460 phases in a tidal salt marsh. *Agricultural and Forest Meteorology*, 300, 108309.
1461 <https://doi.org/10.1016/j.agrformet.2020.108309>. 2021.](#)

1462 [Verma, S. B., Ullman, F. G., Billesbach, D., Clement, R. J., Kim, J., & Verry, E. S. Eddy correlation measurements
1463 of methane flux in a northern peatland ecosystem. *Bound. Lay. Meteorol.*, 58\(3\), 289–304.
1464 <https://doi.org/10.1007/BF02033829>.
1465 <https://doi.org/10.1007/BF02033829>, 1992.](#)

1465 Vesala, Timo, Eeva-Stiina Tuittila, Ivan Mammarella, & Pavel Alekseychik. FLUXNET-CH4 FI-Si2 Siikaneva-2
1466 Bog, Finland. <https://doi.org/10.18140/FLX/1669639>. 2020a.

1467 Vesala, Timo, Eeva-Stiina Tuittila, Ivan Mammarella, & Janne Rinne. FLUXNET-CH4 FI-Sii Siikaneva, Finland.
1468 <https://doi.org/10.18140/FLX/1669640>. 2020b.

1469 [Villarreal, S., Guevara, M., Alcaraz-Segura, D., Brunzell, N. A., Hayes, D., Loescher, H. W., & Vargas, R.
1470 Ecosystem functional diversity and the representativeness of environmental networks across the conterminous
1471 United States. *Agr. Forest Meteorol.*, 262, 423–433.
1472 <https://doi.org/10.1016/j.agrformet.2018.07.016>, 2018.](#)

1473 Villarreal, S., Guevara, M., Alcaraz-Segura, D., & Vargas, R. Optimizing an Environmental Observatory Network
1474 Design Using Publicly Available Data. *J. Geophys. Res.-Biogeo.*, 124(7), 1812–1826.
1475 <https://doi.org/10.1029/2018JG004714>, 2019.

1476 Vourlitis, George, Higo Dalmagro, Jose de S. Nogueira, Mark Johnson, & Paulo Arruda. FLUXNET-CH4 BR-Npw
1477 Northern Pantanal Wetland, Brazil. <https://doi.org/10.18140/FLX/1669368>. 2020.

1478 [Vuichard, N., & Papale, D. Filling the gaps in meteorological continuous data measured at FLUXNET sites with
1479 ERA-Interim reanalysis. *Earth Syst. Sci. Data*, 7\(2\), 157–171. <https://doi.org/10.5194/essd-7-157-2015>,
1480 <https://doi.org/10.5194/essd-7-157-2015>, 2015.](#)

1481 Weston, N. B., Dixon, R. E., & Joye, S. B. Ramifications of increased salinity in tidal freshwater sediments:
1482 Geochemistry and microbial pathways of organic matter mineralization. *J. Geophys. Res.*, 111(G1).
1483 <https://doi.org/10.1029/2005jg000071>, 2006.

1484 Weston, N. B., Vile, M. A., Neubauer, S. C., & Velinsky, D. J. Accelerated microbial organic matter mineralization
1485 following salt-water intrusion into tidal freshwater marsh soils. *Biogeochemistry*, 102, 135–151.
1486 <https://doi.org/10.1007/s10533-010-9427-4>, 2011.

1487 Wik, M., Crill, P. M., Varner, R. K., & Bastviken, D. Multiyear measurements of ebullitive methane flux from three
1488 subarctic lakes. *J. Geophys. Res.-Biogeo.* 118(3), 1307–1321.
1489 <https://doi.org/10.1002/jgrg.20103>, 2013.

1490 Windham-Myers, Lisamarie, Ellen Stuart-Haëntjens, Brian Bergamaschi, Sara Knox, Frank Anderson, & Kyle
1491 Nakatsuka. FLUXNET-CH4 US-Srr Suisun marsh - Rush Ranch. United States.
1492 <https://doi.org/10.18140/FLX/1669694>. 2020.

1493 Wohlfahrt, Georg, Albin Hammerle, & Lukas Hörtnagl. FLUXNET-CH4 AT-Neu Neustift, Austria.
1494 <https://doi.org/10.18140/FLX/1669365>. 2020.

1495 [Wutzler, T., Lucas-Moffat, A., Migliavacca, M., Knauer, J., Sickel, K., Šigut, L., Menzer, O., & Reichstein, M.
1496 Basic and extensive post-processing of eddy covariance flux data with REddyProc. *Biogeosciences*, 15, 5015–
1497 5030. <https://doi.org/10.5194/bg-2018-56-sc1>, 2018.](#)

1498 Xu, X., Riley, W. J., Koven, C. D., Billesbach, D. P., -W. Chang, R. Y., Commare, R., Euskirchen, E. S., Hartery,
1499 S., Harazono, Y., Iwata, H., McDonald, K. C., Miller, C. E., Oechel, W. C., Poulter, B., Raz-Yaseef, N.,
1500 Sweeney, C., Torn, M., Wofsy, S. C., Zhang, Z., & Zona, D. A multi-scale comparison of modeled and

Formatted: Default Paragraph Font, Font: Times New Roman

Formatted: Font: Times New Roman, Font color: Black

Formatted: Normal, Add space between paragraphs of the same style, Border: Top: (No border), Bottom: (No border), Left: (No border), Right: (No border), Between : (No border)

Formatted: Font: Times New Roman, Font color: Black

Formatted: Font: Times New Roman, Font color: Black

Formatted: Normal, Add space between paragraphs of the same style, Border: Top: (No border), Bottom: (No border), Left: (No border), Right: (No border), Between : (No border)

Formatted: Default Paragraph Font, Font: Times New Roman

Formatted: Font: Times New Roman, Font color: Black

Formatted: Default Paragraph Font, Font: Times New Roman

Formatted: Font: Times New Roman, Font color: Black

Formatted: Normal, Add space between paragraphs of the same style, Border: Top: (No border), Bottom: (No border), Left: (No border), Right: (No border), Between : (No border)

Formatted: Default Paragraph Font, Font: Times New Roman

Formatted: Font: Times New Roman, Font color: Black

Formatted: Default Paragraph Font, Font: Times New Roman

Formatted: Font: Times New Roman, Font color: Black

Formatted: Default Paragraph Font, Font: Times New Roman

Formatted: Font: Times New Roman, Font color: Black

Formatted: Default Paragraph Font, Font: Times New Roman

Formatted: Font: Times New Roman, Font color: Black

Formatted: Normal, Add space between paragraphs of the same style, Border: Top: (No border), Bottom: (No border), Left: (No border), Right: (No border), Between : (No border)

Formatted: Default Paragraph Font, Font: Times New Roman

Formatted: Font: Times New Roman, Font color: Black

1501 observed seasonal methane emissions in northern wetlands. *Biogeosciences*, 13(17), 5043–5056.
 1502 <https://doi.org/10.5194/bg-13-5043-2016>, 2016.

1503 Yvon-Durocher, G., Allen, A. P., Bastviken, D., Conrad, R., Gudasz, C., St-Pierre, A., Thanh-Duc, N., & del
 1504 Giorgio, P. A. Methane fluxes show consistent temperature dependence across microbial to ecosystem scales.
 1505 *Nature*, 507(7493), 488–491. <https://doi.org/10.1038/nature13164>, 2014.

1506 [Zhang, Z., Fluet-Choinard, E., Jensen, K., McDonald, K., Hugelius, G., Gumbrecht, T., Carrol, M., Prigent, C.,
 1507 Bartsch, A., & Poulter, B. Development of a global dataset of Wetland Area and Dynamics for Methane
 1508 Modeling \(WAD2M\) \[Data set\]. Zenodo. <http://doi.org/10.5281/zenodo.3998454>. 2020.](https://doi.org/10.5281/zenodo.3998454)

1509 [Zhang, Z., Fluet-Choinard, E., Jensen, K., McDonald, K., Hugelius, G., Gumbrecht, T., Carrol, M., Prigent, C.,
 1510 Bartsch, A., & Poulter, B. Development of a global dataset of Wetland Area and Dynamics for Methane
 1511 Modeling \(WAD2M\). *Earth Syst. Sci.* Zhang, Z., Fluet-Choinard, E., Jensen, K., McDonald, K., Hugelius, G.,
 1512 Gumbrecht, T., Carrol, M., Prigent, C., Bartsch, A., & Poulter, B. Development of a global dataset of Wetland
 1513 Area and Dynamics for Methane Modeling \(WAD2M\). In Review: *Earth Syst. Sci. Data*.
 1514 Data \[In press\]. 2021.](https://doi.org/10.5281/zenodo.3998454)

1515 [Zona, D., Gioli, B., Commane, R., Lindaas, J., Wofsy, S. C., Miller, C. E., Dinardo, S. J., Dengel, S., Sweeney, C.,
 1516 Karion, A., Chang, R. Y.-W., Henderson, J. M., Murphy, P. C., Goodrich, J. P., Moreaux, V., Liljedahl, A.,
 1517 Watts, J. D., Kimball, J. S., Lipson, D. A., & Oechel, W. C. Cold season emissions dominate the Arctic tundra
 1518 methane budget. *P. Natl. A. Sci. USA.*, 113\(1\), 40–45.
 1519 <https://doi.org/10.1073/pnas.1516017113>, 2016.](https://doi.org/10.1073/pnas.1516017113)

1520 [Zona, Donatella, & Walter C Oechel. FLUXNET-CH4 US-Atq Atqasuk. United States.
 1521 <https://doi.org/10.18140/FLX/1669663>. 2020a.](https://doi.org/10.18140/FLX/1669663)

1522 [Zona, Donatella, & Walter C Oechel. FLUXNET-CH4 US-Beo Barrow Environmental Observatory \(BEO\) tower.
 1523 United States. <https://doi.org/10.18140/FLX/1669664>. 2020b.](https://doi.org/10.18140/FLX/1669664)

1524 [Zona, Donatella, & Walter C Oechel. FLUXNET-CH4 US-Bes Barrow-Bes \(Biocomplexity Experiment South
 1525 tower\). United States. <https://doi.org/10.18140/FLX/1669665>. 2020c.](https://doi.org/10.18140/FLX/1669665)

1526 [Zona, Donatella, & Walter C Oechel. FLUXNET-CH4 US-Ivo Ivotuk. United States.
 1527 <https://doi.org/10.18140/FLX/1669679>. 2020d.](https://doi.org/10.18140/FLX/1669679)

Formatted: Default Paragraph Font, Font: Times New Roman

Formatted: Font: Times New Roman, Font color: Black

Formatted: Default Paragraph Font, Font: Times New Roman

Formatted: Font: Times New Roman

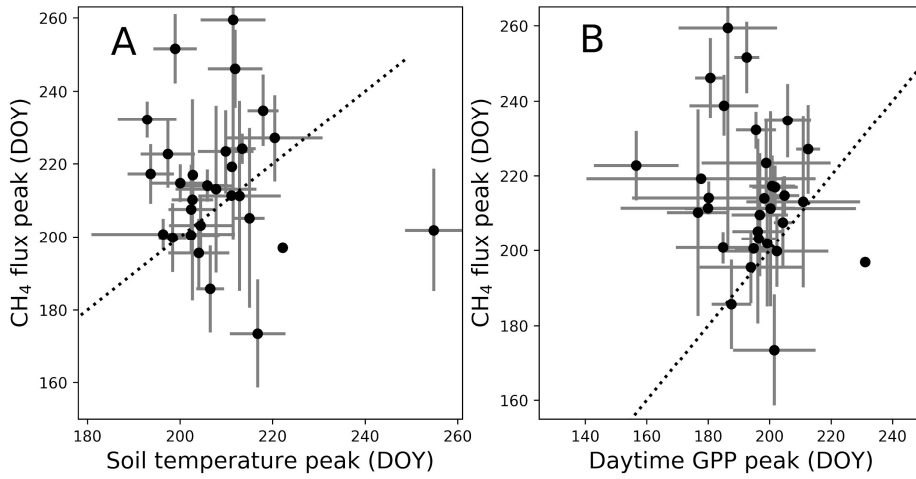
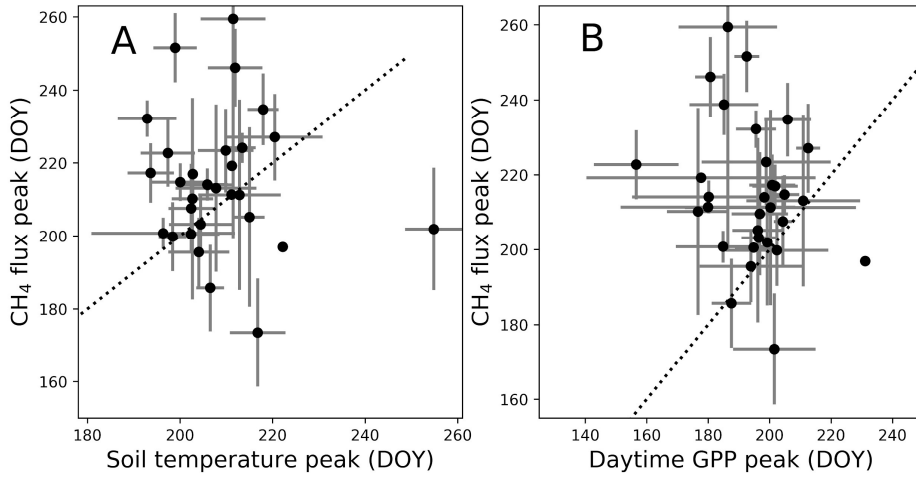
Formatted: Font: Times New Roman, Font color: Black

Formatted: Normal, Space After: 0 pt, Add space between paragraphs of the same style, Border: Top: (No border), Bottom: (No border), Left: (No border), Right: (No border), Between : (No border)

Formatted: Default Paragraph Font, Font: Times New Roman

Formatted: Font: Times New Roman, Font color: Black

Formatted: Add space between paragraphs of the same style



1534 Figure A1: Peak methane (CH₄) flux timing versus peak gross primary productivity (GPP) timing (A) and peak soil
1535 temperature timing by day of year (B). Points represent site average and error bars represent standard deviations. Dotted
1536 line represents 1:1 relationship.

1537 ▲

Formatted: Font: Arial, Font color: Auto

1538 **APPENDIX B**

1539

1540 **Table B1: Data variable names, descriptions, and units**

1541 **FLUXNET-CH4 Data Variables**

Formatted: Font: Times New Roman

1542 This webpage describes data variables and file formatting for the FLUXNET-CH4 Community Product.

1543 **1. Data Variable: Base names**

1544 Base names indicate fundamental quantities that are either measured or calculated/derived. They can also
1545 indicate quantified quality information.

1546 Table 1. Base names for data variables

<i>Variable</i>	<i>Description</i>	<i>Units</i>
TIMEKEEPING		
<u>T</u> <u>TIMESTAMP_STAR</u>	ISO timestamp start of averaging period, used in half-hourly data	YYYYMMDDHHMM
<u>TIMESTAMP_END</u>	ISO timestamp end of averaging period, used in half-hourly data	YYYYMMDDHHMM
<u>TIMESTAMP</u>	ISO timestamp used in daily aggregation files	YYYYMMDD
MET_RAD		
<u>SW_IN</u>	Shortwave radiation, incoming	W m ⁻²
<u>SW_OUT</u>	Shortwave radiation, outgoing	W m ⁻²
<u>LW_IN</u>	Longwave radiation, incoming	W m ⁻²
<u>LW_OUT</u>	Longwave radiation, outgoing	W m ⁻²

Formatted: Font: Times New Roman

Formatted: Font: Times New Roman

Formatted: Font: Times New Roman

Formatted Table

Formatted: Font: Times New Roman

Formatted: Font: Times New Roman

Formatted: Font: Times New Roman

Formatted: Font: Times New Roman

Formatted: Font: Times New Roman

Formatted: Font: Times New Roman

Formatted: Font: Times New Roman

<u>PPFD_IN</u>	Photosynthetic photon flux density, incoming	$\mu\text{molPhoton m}^{-2} \text{ s}^{-1}$	Formatted: Font: Times New Roman
<u>PPFD_OUT</u>	Photosynthetic photon flux density, outgoing	$\mu\text{molPhoton m}^{-2} \text{ s}^{-1}$	Formatted: Font: Times New Roman
<u>NETRAD</u>	Net radiation	W m^{-2}	Formatted: Font: Times New Roman
<u>MET_WIND</u>			Formatted: Font: Times New Roman
<u>USTAR</u>	Friction velocity	m s^{-1}	Formatted: Font: Times New Roman
<u>WD</u>	Wind direction	Decimal degrees	Formatted: Font: Times New Roman
<u>WS</u>	Wind speed	m s^{-1}	Formatted: Font: Times New Roman
<u>HEAT</u>			Formatted: Font: Times New Roman
<u>H</u>	Sensible heat turbulent flux (with storage term if provided by site PI)	W m^{-2}	Formatted: Font: Times New Roman
<u>LE</u>	Latent heat turbulent flux (with storage term if provided by site PI)	W m^{-2}	Formatted: Font: Times New Roman
<u>G</u>	Soil heat flux	W m^{-2}	Formatted: Font: Times New Roman
<u>MET_ATM</u>			Formatted: Font: Times New Roman
<u>PA</u>	Atmospheric pressure	kPa	Formatted: Font: Times New Roman
<u>TA</u>	Air temperature	deg C	Formatted: Font: Times New Roman

VPD	Vapor Pressure Deficit	hPa	Formatted: Font: Times New Roman
RH	Relative humidity, range 0-100	%	Formatted: Font: Times New Roman
			Formatted: Font: Times New Roman
MET_PRECIP			Formatted: Font: Times New Roman
P	Precipitation	mm	Formatted: Font: Times New Roman
			Formatted: Font: Times New Roman
PRODUCTS			Formatted: Font: Times New Roman
NEE	Net Ecosystem Exchange	$\mu\text{molCO}_2 \text{ m}^{-2} \text{ s}^{-1}$	Formatted: Font: Times New Roman
GPP	Gross primary productivity	$\mu\text{molCO}_2 \text{ m}^{-2} \text{ s}^{-1}$	Formatted: Font: Times New Roman
RECO	Ecosystem respiration	$\mu\text{molCO}_2 \text{ m}^{-2} \text{ s}^{-1}$	Formatted: Font: Times New Roman
			Formatted: Font: Times New Roman
GASES			
FCH4	Methane (CH4) turbulent flux (no storage correction)	$\text{nmolCH}_4 \text{ m}^{-2} \text{ s}^{-1}$	Formatted: Font: Times New Roman
			Formatted: Font: Times New Roman
MET_SOIL			Formatted: Font: Times New Roman
TS	Soil temperature	deg C	Formatted: Font: Times New Roman
WTD	Water table depth (negative values indicate below the surface)	m	Formatted: Font: Times New Roman
			Formatted: Font: Times New Roman

1548 **2. Data Variable: Qualifiers**

1549 Qualifiers are suffixes appended to variable base names that provide additional information about the
1550 variable. For example, the DT qualifier in the variable label GPP DT indicates that gross primary
1551 production (GPP) has been partitioned using the flux partitioning method from Lasslop et al. 2010.

1552 Multiple qualifiers can be added, and they must **follow the order in which they are presented here**.

1553 **2.1. Qualifiers: General**

1554 General qualifiers indicate additional information about a variable.

1555 · **F** : Variable has been gap-filled by the FLUXNET-CH4 team. Gaps in meteorological variables
1556 (including air temperature (TA), incoming shortwave (SW IN) and longwave (LW IN) radiation, vapor
1557 pressure deficit (VPD), pressure (PA), precipitation (P), and wind speed (WS)) were filled with ERA-
1558 Interim (ERA-I) reanalysis data (Vuichard and Papale 2015). Other variables were filled using the MDS
1559 approach in REdDyProc (see Delwiche et al. 2020 for more details).

1560 · **DT** : Variable acquired using the flux partitioning method from (Lasslop et al. 2010), with values
1561 estimated by fitting the light-response curve.

1562 · **NT** : Variable acquired using the flux partitioning method from (Reichstein et al. 2005), with values
1563 estimated from night-time data and extrapolated to day time.

1564 · **RANDUNC**: Random uncertainty introduced from several different sources including errors
1565 associated with the flux measurement system (gas analyzer, sonic anemometer, data acquisition system,
1566 flux calculations), errors associated with turbulent transport, and statistical errors relating to the location
1567 and activity of the sites of flux exchange (“footprint heterogeneity”) (Hollinger and Richardson 2005).

1568 · **ANNOPTLM** : Gap-filled variable using an artificial neural net routine from Matlab with the
1569 Levenberg-Marquardt algorithm as the training function, and parameters optimized across runs (more
1570 detail in (Sara Helen Knox et al. 2016; Sara H. Knox et al. 2019)).

1571 · **UNC** : Uncertainty introduced from ANNOPTLM gap-filling routine, as described in Knox et al.
1572 2016 and Knox et al. 2019.

1573 · **QC** : Reports quality checks on FCH4 gap-filled data (ANNOPTLM) based on length of data gap.
1574 1 = data gap shorter than 2 months, 3 = data gap exceeds 2 months which could lead to poor quality gap-
1575 filled data. Nondimensional.

1576

1577 **2.2. Qualifiers: Positional (V)**

1578 Positional qualifiers are used to indicate relative positions of observations at the site. For FLUXNET-CH4,
1579 positional qualifiers are used to distinguish soil temperature probes for sites with more than one probe.
1580 Probe depths for each positional qualifier per site are included in the metadata file included with data
1581 download and also in Table B6B7 of Delwiche et al. 2020. For sites where the original database file
1582 release in Ameriflux, AsiaFlux, or EuroFlux contains multiple probes at the same V depth, we average
1583 values and report only the average for each V position. The one exception to this is site US-UAF where
1584 the original positional qualifier from the data we downloaded from Ameriflux had different depths for the

Formatted: Font: Times New Roman

Formatted: Font: Times New Roman

Formatted: Font: Times New Roman

Formatted: Font: Times New Roman

Formatted: Font: Times New Roman

Formatted: Font: Times New Roman

Formatted: Font: Times New Roman

Formatted: Font: Times New Roman

Formatted: Font: Times New Roman

Formatted: Font: Times New Roman

Formatted: Font: Times New Roman

Formatted: Font: Times New Roman

Formatted: Font: Times New Roman

Formatted: Font: Times New Roman

Formatted: Font: Times New Roman

Formatted: Font: Times New Roman

Formatted: Font: Times New Roman

Formatted: Font: Times New Roman

Formatted: Font: Times New Roman

Formatted: Font: Times New Roman

Formatted: Font: Times New Roman

Formatted: Font: Times New Roman

Formatted: Font: Times New Roman

Formatted: Font: Times New Roman

1585 same qualifier. We still averaged the probe data, so _V qualifiers from US-UAF represent an average of
1586 more than one depth.

1587 3.0 Missing data

1588 Missing data are reported using -9999. Data for all days in a leap year are reported.

1589 4.0 References

1590 Hollinger, D. Y., and A. D. Richardson. 2005. "Uncertainty in Eddy Covariance Measurements and Its
1591 Application to Physiological Models." *Tree Physiology* 25 (7): 873–85.

1592 Knox, Sara Helen, Jaelyn Hatala Matthes, Cove Sturtevant, Patricia Y. Oikawa, Joseph Verfaillie, and
1593 Dennis Baldocchi. 2016. "Biophysical Controls on Interannual Variability in Ecosystem-Scale
1594 CO₂ and CH₄ Exchange in a California Rice Paddy." *Journal of Geophysical Research: Biogeosciences*.
1595 <https://doi.org/10.1002/2015jg003247>.

1596 Knox, Sara H., Robert B. Jackson, Benjamin Poulter, Gavin McNicol, Etienne Fluet-Chouinard, Zhen
1597 Zhang, Gustaf Hugelius, et al. 2019. "FLUXNET-CH₄ Synthesis Activity: Objectives, Observations,
1598 and Future Directions." *Bulletin of the American Meteorological Society* 100 (12): 2607–32.

1599 Lasslop, Gitta, Markus Reichstein, Dario Papale, Andrew D. Richardson, Almut Arneth, Alan Barr, Paul
1600 Stoy, and Georg Wohlfahrt. 2010. "Separation of Net Ecosystem Exchange into Assimilation and
1601 Respiration Using a Light Response Curve Approach: Critical Issues and Global Evaluation." *Global
1602 Change Biology*. <https://doi.org/10.1111/j.1365-2486.2009.02041.x>.

1603 Reichstein, Markus, Eva Falge, Dennis Baldocchi, Dario Papale, Marc Aubinet, Paul Berbigier, Christian
1604 Bernhofer, et al. 2005. "On the Separation of Net Ecosystem Exchange into Assimilation and
1605 Ecosystem Respiration: Review and Improved Algorithm." *Global Change Biology*.
1606 <https://doi.org/10.1111/j.1365-2486.2005.001002.x>.

1607 Vuichard, N., and D. Papale. 2015. "Filling the Gaps in Meteorological Continuous Data Measured at
1608 FLUXNET Sites with ERA-Interim Reanalysis." *Earth System Science Data*.
1609 <https://doi.org/10.5194/essd-7-157-2015>.

Formatted

... [10]

Formatted

... [11]

Formatted

... [12]

Formatted

... [13]

Formatted

... [14]

Formatted

... [15]

Font: Times New Roman

Page 54: [13] Formatted **Kyle Brook Delwiche** **4/13/2021 2:41:00 PM**

Font: Times New Roman

Page 54: [13] Formatted **Kyle Brook Delwiche** **4/13/2021 2:41:00 PM**

Font: Times New Roman

Page 54: [13] Formatted **Kyle Brook Delwiche** **4/13/2021 2:41:00 PM**

Font: Times New Roman

Page 54: [13] Formatted **Kyle Brook Delwiche** **4/13/2021 2:41:00 PM**

Font: Times New Roman

Page 54: [13] Formatted **Kyle Brook Delwiche** **4/13/2021 2:41:00 PM**

Font: Times New Roman

Page 54: [13] Formatted **Kyle Brook Delwiche** **4/13/2021 2:41:00 PM**

Font: Times New Roman

Page 54: [13] Formatted **Kyle Brook Delwiche** **4/13/2021 2:41:00 PM**

Font: Times New Roman

Page 54: [13] Formatted **Kyle Brook Delwiche** **4/13/2021 2:41:00 PM**

Font: Times New Roman

Page 54: [13] Formatted **Kyle Brook Delwiche** **4/13/2021 2:41:00 PM**

Font: Times New Roman

Page 54: [13] Formatted **Kyle Brook Delwiche** **4/13/2021 2:41:00 PM**

Font: Times New Roman

Page 54: [13] Formatted **Kyle Brook Delwiche** **4/13/2021 2:41:00 PM**

Font: Times New Roman

Page 54: [14] Formatted **Kyle Brook Delwiche** **4/13/2021 2:41:00 PM**

Font: Times New Roman

Page 54: [14] Formatted **Kyle Brook Delwiche** **4/13/2021 2:41:00 PM**

Font: Times New Roman

Page 54: [14] Formatted **Kyle Brook Delwiche** **4/13/2021 2:41:00 PM**

Font: Times New Roman

Page 54: [14] Formatted **Kyle Brook Delwiche** **4/13/2021 2:41:00 PM**

Font: Times New Roman

Page 54: [14] Formatted **Kyle Brook Delwiche** **4/13/2021 2:41:00 PM**

Font: Times New Roman

Page 54: [14] Formatted **Kyle Brook Delwiche** **4/13/2021 2:41:00 PM**

Font: Times New Roman

